ECO$_2$ project number: 265847

Deliverable 4.1: Potential impact of CCS leakage on marine communities
WP4; lead beneficiary: Plymouth Marine Laboratory

Potential impact of CCS leakage on marine communities

Ana M Queirós[1], Karl Norling[2,12], Teresa Amaro[2], Joana Nunes[1], Denise Cummings[1], Evgeny Yakushev[2], Kai Sorensen[2], Carolyn Harris[1], Malcom Woodward[1], Roberto Danovaro[3], Eugenio Rastelli[3], Elisabeth Alve[4], Cinzia De Vittor[5], Ana Karuza[5], Tamara Cibic[5], Marina Monti[5], Gianmarco Ingrosso[5], Daniela Fornasaro[5], Stanley Eugene Beaubien[6], Katja Guilini[7], Ann Vanreusel[7], Massimiliano Molari[8], Antje Boetius[8], Alban Ramette[8], Frank Wenzhöfer[8], Dirk de Beer[8], Miriam Weber[9], Stefanie Grünke[10], Nikolaus Bigalke[11], and Stephen Widdicombe[1]

[1]Plymouth Marine Laboratory, Prospect Place, Plymouth PL1 3 DH, United Kingdom

[2]Norwegian Institute for Water Research, Gaustadalléen 21, Oslo 0349, Norway

[3]Dept. of Life and Environmental Sciences, Polytechnic University of Marche, Via Brecce Bianche, 60131 Ancona, Italy

[4]Section of Geology and Geophysics, University of Oslo, Sem Sælands vei 1, Geologibygningen, Oslo 0371, Norway

[5]OGS (Istituto Nazionale di Oceanografia e Geofisica Sperimentale), Oceanographic Section, Via A. Piccard 54, 34151 Trieste, Italy

[6]Dipartimento di Scienze della Terra, Università di Roma "La Sapienza", P.le Aldo Moro 5, 00185 Roma, Italy

[7]Marine Biology Research Group, Ghent University, Krijgslaan 281-S8, Ghent, Belgium

[8]HGF-MPG Group for Deep Sea Ecology and Technology, Max Planck Institute for Marine Microbiology, Germany

[9]Hydra Institute for Marine Science, Elba Field Station, Italy

[10]Geophysical Institute, University of Bergen, Norway

[11]Marine biogeochemistry, Geomar, Kiel, Germany

[12]Department of Biological and Environmental Sciences, University of Gothenburg, Sweden

Deliverable 4.1: Potential impact of CCS leakage on marine communities
WP4; lead beneficiary: Plymouth Marine Laboratory

Contents

Deliverable 4.1: Potential impact of CCS leakage on marine communities
WP4; lead beneficiary: Plymouth Marine Laboratory

1. Executive summary

A primary aim for the ECO2 project was to determine the possible impacts of sub-seabed CO_2 leakage on marine communities and the ecosystem processes they support. In addition to the leakage of CO_2 it was also considered that the additional environmental risks associated with the displacement of high salinity, low oxygen reservoir formation water should also be explored. ECO2 (Work Package 4) addressed this issues using controlled laboratory exposure experiments and observations from a marine environment with naturally high levels of CO_2.

Modelling and experimental studies have shown that, due to the rapid dissolution of CO_2 into sediment porewaters and into the seawater immediately above the seafloor, the majority of biological impacts from CCS leakage are likely to be seen in benthic or epibenthic communities. At the centre of a leak large changes in carbonate chemistry can occur within the sediment, whilst further from the leak plumes of dense CO_2 enriched water can wash over the seabed. Consequently, although some information on pelagic systems is presented in this report, effort with the ECO2 project was primarily concentrated on the study of benthic habitats and communities.

Mesocosm experiments and observations at natural CO_2 seeps have confirmed that leakage from CCS has the potential to cause significant impacts and mortalities in benthic organisms leading to changes in community structure and a reduction in both biodiversity and ecosystem function. These community level impacts are driven by both the physiological response of organisms to high levels of CO_2 (see ECO deliverable D4.2 "The response and potential adaptation of marine species to CO_2 exposure associated with different potential CO_2 leakage scenarios" for a description of these responses) and the indirect effects of altering ecological drivers such as competition and predation. In addition, exposure to high salinity, low oxygen formation water can also have a significantly negative impact on marine communities and function.

Data from ECO2, and from other projects, has confirmed that the size and severity of the response of benthic communities to CO_2 exposure is strongly moderated by both the magnitude of the CO_2 dose and the duration of the exposure period. By combining this knowledge with the outputs of CO_2 dispersion models it should be possible to appreciate the spatial and temporal scales over which biological impacts are likely operate in the advent of leak.

In summary, this WP identified impacts on benthic communities by both CO_2 leakage scenarios and formation water release. These were observed not only at the biogeochemical level, but also in microbial communities, fauna and their behaviour. Whilst some information remains to be gathered, the results summarised in this report identified that the impacts of leakage of CO_2 on benthic ecosystems will be influenced by the scale and duration of the leak, and that potential effects will be

modulated by seasonality and hydrodynamics. These can act to mitigate impacts, or to exacerbate them, depending on the response measured. Some of this information generated by WP4.1 is entirely novel and lends support to the perspective the future monitoring work aimed at characterising potential impacts of CCS on benthic habitats should therefore consider this element of natural variability in natural systems. Without it, we are likely to fail to provide a true assessment of risk, impact and recovery.

2. Gathering data – methods and approaches

During the ECO2 project, a variety of methods and approaches have been used to assess the potential impacts of CCS leakage on the structure and function of marine communities. The use of these different approaches allows us to identify generic patterns and paradigms independent from the recognised, method specific weakness associated with single approach studies. Tightly controlled mesocosm based studies allow us to demonstrate cause and effect between specific environmental drivers (such as pH, hypoxia and salinity) and key biological responses. We have used a large mesocosm facility to examine the potential impacts of CCS leakage on typical NE European soft sediment biological communities and processes. In parallel to these experiments WP4 researchers have also studied natural CO_2 vents as analogues for the long-term impact of CO_2 leakage on shallow water and continental margin ecosystems, communities, species and their function. During joint campaigns with WP2 and WP3, changes in diversity and structure of marine communities along natural gradients from high CO_2 leakage to background levels have been analysed. By comparing mesocosm results with observations from field sites which are naturally exposed to elevated levels of CO_2 we can determine if experimental responses are seen in the more complex, natural, marine systems.

2.1 Mesocosm studies

A high CO_2 exposure system was built at the NIVA marine research station in Solbergstrand, Oslofjord, Norway. This was used to perform an exposure experiment (2012/2013) where 5 CO_2 concentration treatments were used (control (400 ppm), 1000, 2000, 5000 and 20000 ppm of CO_2), to investigate the impacts of a leakage from a CCs injection site or pipeline on benthic communities and processes. Sampling took place after 2 and 20 weeks of exposure, to identify potential short and medium term impacts, respectively. The severity and speed of impact on diversity and structure of micro-, meio- and macrobenthic communities were determined. Moreover, impacts on benthic ecosystem processes were also determined at each time-point by measuring changes in bioturbation activity (i.e. mixing of sediment particulates

by burrowing infauna), bio-irrigation (i.e. flushing of benthic sediment by burrowing fauna through burrow ventilation), and community respiration, all expected to reflect the physiological impact of environmental stressors. A variety of biogeochemical parameters and processes were also measured to identify potential changes in sedimentary nutrient and organic matter cycling. These included sedimentary pH profiles, fluxes of nutrients (PO_4, NH_4, SiO_4, NO_2, NO_3), and the rate of ammonia oxidation in the seawater and sediment, associated with experimental treatments. Seawater total alkalinity, total inorganic carbon, temperature, salinity, seawater and sedimentary pH were also monitored. Sedimentary properties including particle size distributions and porosity were also measured. To assess the impact of treatments on microbial activity, densities and organic matter composition and turnover, a new partner representing the Polytechnic University of Marche (UNIVPM) and lead by Prof Roberto Danovaro entered this WP free of costs. This group further measured viral abundance; total Prokaryotic abundance; relative importance of Bacteria and Archaea on total prokaryotic abundance; viral production; selective viral impact on Bacteria and Archaea; prokaryotic heterotrophic production; extracellular enzymatic activities; organic matter composition and turnover; and meta-genetic analysis of prokaryotic and metazoan benthic assemblages.

In response to recommendations from the 18 month project review, a second mesocosm experiment was devised to assess the short-term impacts of the release of hypoxic brine from formation waters during a sub-seabed CO_2 injection. The high CO_2 mesocosm system used in the first year was thus modified to accommodate this work, and this experiment ran in the end of summer 2013. Because we were interested in the effects of hypoxic brine, we also investigated, in parallel, the individual effects of hypoxia and high salinity on benthic biota and processes, to disentangle the potential contributions of each stressor to potential changes in the benthos. A fourth impact scenario was considered, in which tidal flushing of a brine plume by standard seawater was simulated (section 2.1.1), in light of the findings of the FP7 project QICS. This experiment therefore gauged five experimental treatments: control, high salinity (48 g/l NaCl), hypoxia (1.4 g/l O_2), mixed (48 g/l NaCl and 1.4 g/l O_2), and tidal(see section 2.1.2 for details). These exposures lasted 2 weeks.

To assess the impacts on benthic community structure and processes, the same endpoints were measured as had been for the high CO_2 experiment. Additional measurements were carried out for sedimentary sulphide and redox profiles.

2.1.1 Elevated CO_2 in the overlying water to simulate the impact of a plume of CO_2 enriched water

During the 3rd week of August 2012 (from the 13th to the 15th) sediments were collected in the Oslofjord (59°49.4788' N, 10°58.8595E), Norway, at 100m depth. Samples were collected using a KC Denmark 0.1m^2 box corer equipped with a liner, which allowed retrieving the sediment cores with minimal disturbance (fig.1a). Each box corer had an average penetration depth of ~40 cm. A total of 50 liners were collected and transferred to the benthic mesocosm system at the Marine Research Station, Norwegian Institute of Water Research, Solbergstrand, Norway. All cores were kept in complete immersion during transport and retrieval to the mesocosm, to prevent desiccation, and to minimise temperature changes. Once in the mesocosm, the liners were placed in a flow-through holding basin filled with seawater to a depth of 1 m for approximately 4 weeks, to allow organisms to acclimate to laboratorial conditions. A pipeline situated at 60 m in the adjacent fjord continuously supplied the holding basin with physically filtered, natural seawater (fig.1b).

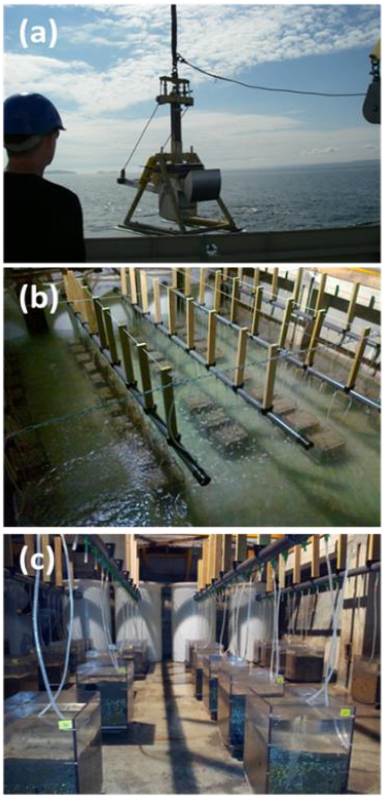

Figure 1: (a) K-C Denmark box corer deployment in the Oslofjord. (b) mesocosm acclimation of sediment liners (September 2012). (c) high CO_2 mesocosm setup (October 2012).

After acclimatization, the high CO_2 experiment was initiated, including 5 treatment levels (400 (control), 1000, 2000, 5000 and 20000 ppm of CO_2). The 50 liners were distributed randomly between treatments in equal numbers. Each liner was allocated to a treatment via constant supply of water from one of the five treatment seawater header tanks (fig.1c) at a flow rate of 120 mL.min^{-1}. The day light regime in the basing was approximately 8 hours

light: 16 hours dark, and temperature was allowed to follow ambient fluctuations. Sampling took place at the beginning of the experiments, prior to the beginning of the CO_2 exposures (T0); after 2 weeks (T1); and after 20 weeks (T2). These sampling points provided data on control conditions, the effects of a potential CO_2 short term leek, and those of a potential medium term leek, respectively. On each occasion, the liners were sampled for the parameters listed, using the methods below.

Impacts on macrofauna were determined from samples collected at all sampling points (T0, T1, T2, four liners per treatment). Two types of samples were collected from each liner to this end. A sub-core was collected to assess changes in diversity with depth within the sediment; and a second sample was acquired using all the sediment left in the liner after all other sampling had been carried out, to identify bulk changes in sedimentary macrofaunal comunities. In the first case, 10 cm diameter PVC corers were used to extrude a core approximatelyy 15 cm deep from each liner, which was sliced at 0–1, 1–3, 3–5, 5–10, 10–15 cm sediment layers. Each sediment layer was sieved through a 500 μm sieve, and each sample fixed in 10% buffered formaldeheyde until processing. The second macrofauna sediment sample was also sieved and fixed as above. In the lab, specimens were identified to the lowest taxonomical level possible, to estimate taxa abundances per m^2.

Impacts on meiofauna will be determined from four 10 ml sediment samples, collected at all sampling points (T0, T1, T2) from the first 5 cm sediment layer using a cut-off syringe, and pooled within each of four replicates per treatment.

Impacts on microbial communities are also being assessed. Three independent replicates of sediment samples form each liner were collected by hand coring (using Plexiglas tubes, 5.5 cm inside diameter) and sliced in 0-1; 1-3; 3-5; 5-10; 10-15 cm layers. For each layer, aliquots were collected and stored (-20°C) for subsequent analysis of viral and prokaryotic abundance (epifluorescence microscopy), organic matter composition (concentration of phytopigments, total lipids, carbohydrates and proteins) and metagenomic analysis of prokaryotic and metazoan benthic diversity (by means of 16S and 18S rRNA gene pyrosequencing). Incubations of sediment samples at in situ temperature for fluorometric

analysis of extracellular enzymatic activities (aminopeptidase, alkaline phosphatase and β-glucosidase) was conducted on the top sediment layer (0-1 cm). Sediment samples from the 0-1 and 10-15 cm layers were incubated at in situ temperature and stored (-20°C) until epifluorescence microscopy and genetic analyses for viral production and selective viral impact on Bacteria and Archaea. Prokaryotic heterotrophic production analysis was conducted on the 0-1 and 10-15 cm layers using the tritiated leucine incorporation method, (i.e. incubation of sediment samples at in situ temperature and subsequent storing of samples at +4°C until further analysis by liquid scintillation counting).

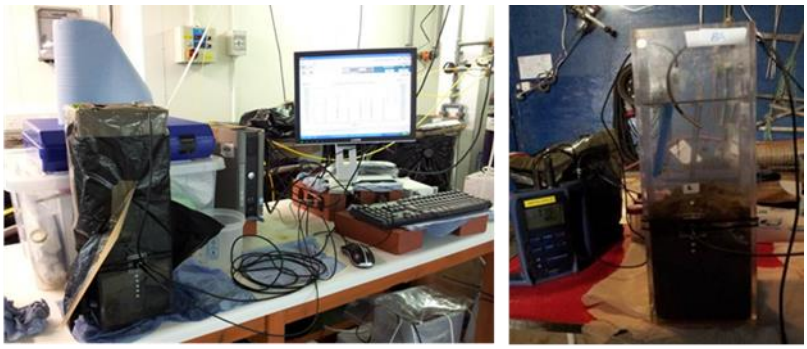

Figure 2: Acquisition of sedimentary pH profiles. Left: aquarium housing sediment and optical sensors (white), connected to a PC. Right: acquisition of otical pH profile using optical sensors at T2, showing temperature sensor (balck), and handhelp pH macroprobe.

To complement the biological datasets, the impact on a number of biogeochemical parameters and processes was quantified. ***Impacts on sedimentary pH profiles*** were determined by use of optical sensors (T1 and T2, Fig. 2, Queirós, Taylor et al. *in review*). Sediment cores (12x12 cm) were extruded from two replicate experimental units per treatment level onto tight fitting clear acrylic aquaria, within which optical pH sensors had been mounted. These cores were then allowed to equilibrate over 24 hours under the corresponding experimental seawater flow and CO_2 conditions, at the end of which pH profiles were acquired. pH was measured using Dual Lifetime Referencing based optical sensors, at cm intervals, and down to a depth of 5 cm within each core.Two cores were profiled per CO_2 treatment at T1 and T2.

Impacts on ammonia oxidation rates were measured following the method Kitidis et al. (2011) at T1 and T2. For this, 3-5 ml of the first cm of the sediment in each liner were sampled into six individual 10 ml Weathon glass serum bottles and filled with overlying treatment seawater. Each bottle was immediately sealed with a butyl rubber stopper under water, avoiding trapping of air bubbles. Three of these bottles were then injected with 100µL

of 100 mM stock solution of $NaClO_3$, and the remaining three bottles injected with 100 µL of 100 mM stock solution of allylthiourea. Additionally, six 10 ml Weathon glass serum bottles were filled with the seawater in each header tank and treated in the same way. All bottles were incubated in the dark within the mesocosm basin for approximately 20 hours, at known temperature, and subsequently frozen at -20^{o}C until processing. A 10 ml Weathon glass serum bottle was additionally filled with surface sediment from each liner to assess sediment porosity via dehydration. Ammonia oxidation rates in the sediment and seawater were subsequently calculated using the concentration of NO_2^- in the $NaClO_3$ samples, considering that in the allylthiourea treated samples, in each treatment. Allylthiourea and $NaClO_3$ are inhibitors of ammonia oxidation into nitrite and of nitrite into nitrate, respectively. NO_2^- concetrations were estimated using spectrophotometry, as described in Kitidis et al. (2011).

Impacts on nutrient fluxes (PO_4, NH_4, SiO_4, NO_2, NO_3) were measured at T0, T1 and T2. To this end, 50ml samples of seawater from each inlet and liner pair were collected on three occasions to cover the night night cycle, at each time point (T0, T1 and T2). The concentration of each nutrient in each sample was estimated using a nutrient auto-analyser (Branne & Luebbe, AAIII) and standard methods (Brewer and Riley 1965; Mantoura and Woodward 1983; Kirkwood 1989; Zhang and Chi 2002; Grasshoff, Kremling et al. 2009). Fluxes were calculated using the equation in Widdicombe and Needham (2007) considering the difference in concentration between paired inlet and liner samples.

Sediment granulometry and organic content were determined at all time-points (T0, T1 and T2) from 10 ml sediment samples collected from the first 5cm of sediment layer of each of four replicates per treatment, using a cut-off syringe. Particle size distributions were estimated using a Beckman Coulter LS laser particle size analyser. Organic content is to be determined as in Buchanan (1984).

Fluxes of oxygen, alkalinity TIC and manganese were measured using a flow-through technique at T2 (Schaanning et al., 2008). A lid was placed on top of each box to eliminate gas exchange with the atmosphere. With the use of a multichannel peristaltic pump with separated tubes from the respective header tanks to each tank, a flow through system was

rebuilt. When the rate of the water flow through the tanks was stabilized, concentrations of dissolved oxygen, pH, total Mn, alkalinity and TIC were measured. We measured concentrations of dissolved oxyegen (with a Clark electrode and with Winkler technique(Hansen, 1999), pH (with Metrohm 380 pH meter), total Mn with spectrophotometric technigue (Grashoff et al., 1999), alkalinity and TIC as recommended in (Dickson et al., 2007).

Impacts on bioturbation (i.e. the biogenic mixing of sedimentary particulates) were measured at T1 and T2. This process can be used to assess the overall activity of faunal organisms, resulting from the displacement of materials during feeding, scavenging and burrow construction. Bioturbation was quantified by use of a fluorescent sediment tracer adequate to the sediment type used in this experiment (i.e. luminophores, fig. 4.3a) and 2D UV imaging. These well established methods consist in the addition of luminophores (Mahaut and Graf 1987) to sediments containing a community or species of interest in situ or under laboratory conditions (Gerino, Aller et al. 1998; Solan, Wigham et al. 2004), followed by an incubation period and subsequent retrieval. A profile of the tracer distribution with sediment depth can then be visualised at a cross-section of the sediment (e.g. liner wall, Fig. 3a,b), and the bioturbation activity of the species present quantified from this in a number of ways.

Two sets of data were acquired at each time-point: whole liner measurements (all liners, Fig. 3a); and additional measurements were carried out using UV time-lapse photography in the cores extruded for pH profiling (two replicates per treatment level, Fig 3b and c). In the first case, we added 0.15g.cm^{-2} of homogenised luminophores to the sediment surface within each

liner, making up a luminophore surface of approximately 0.02 m^2 (Figure 3a),

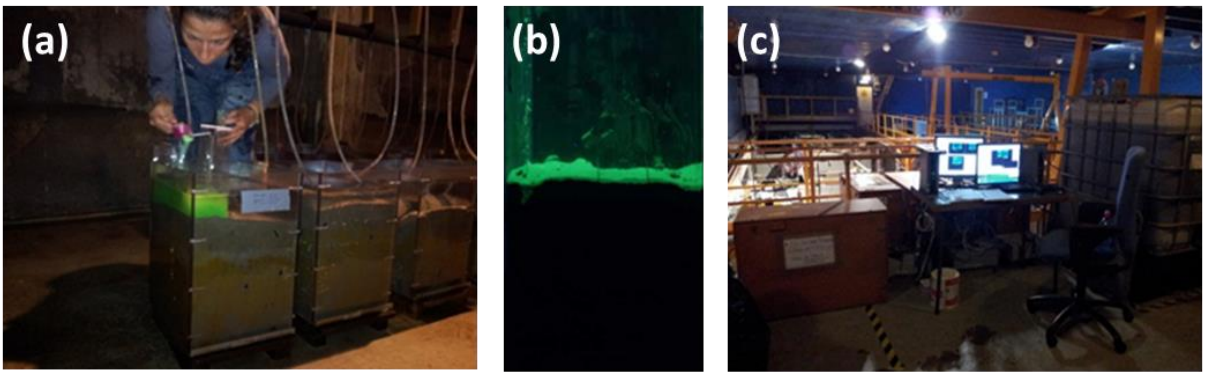

Figure 3: Measuring bioturbation. (a) laying luminophores for whole liner bioturbation assessment. (b) a sediment core used for time-lapse bioturbation assessment, under UV light. (c) the time-lapse setup for 5 CO_2 treatments, showing imaging boxes and PC setup.

covering approximately 25% of the liner surface area. At this stage, all circulation was interrupted to allow the tracer to settle. The tracer formed a layer approximately 0.3 cm thick within one hour, after which time the re-circulation in each liner was re-initiated. One side of each of four liners per CO_2 treatment was photographed under UV light at this point, to define initial conditions for the bioturbation transport models used subsequently (section 3.6). For imaging, we used a modification of the camera setup in Schiffers, Teal et al. (2011); i.e. an imaging black box was lowered onto each liner, housing the individual liner at one end, for each photograph. Two 8W UV-A lights, fixed onto the inside of the box and powered externally, stimulated luminophore excitation, enabling the tracing of the fluorescent luminophore particles against the dark background sediment. Images were captured using a digital SLR camera (Canon EOS 500D; 15.1 MP; pixel size≈ 100µm), which had been fixed at the opposing end of the imaging box, at 90 cm from the wall of the visualised liner. Cameras were set to use 10 seconds exposure, f=5.6, ISO=100, and were remotely controlled via a PC using time-lapse software (GB Timelapse, V 3.6.1). Images were captured in RGB format and stored using JPEG compression. At the end of 48 hours, the same side of each liner was photographed again to estimate bioturbation profles.

For the time-lapse bioturbation incubations, we extruded 12 x 12 x 20 cm cores used for pH profiling (as above) onto clear acrylic aquaria, at the end of each time-point, insuring that at least 3.0 L of overlying exposure water was retained above the sediment. Each aquarium was transferred into a second type of imaging black box, following the setup in Schiffers, Teal et

al. (2011), the inside of which was illuminated by an 8W UV-A light. Inside, each core was supplied with seawater from the corresponding exposure water system using a peristaltic pump system (Watson Marlow) to generate a flow through. The flow was set to 20 mL.min^{-1}, one sixth of the flow in the experimental exposure liners given the relatively smaller surface area of these cores, and therefore maintaining a similar water residence time. After 24 hours, 0.15g.cm-^{2} of the same luminophores were gently added to the surface of each core as before, raising the sediment-water interface by approximately 0.3 cm. This marked the beginning of a two day observation of community bioturbation behaviour, during which one of the walls of each core was photographed continuously, using fluorescent time-lapse photography at hourly intervals, which started one hour after the addition of the tracer (Figure 3b and c). Camera and software setups used were the same as described above. At the end of the 48 hours, all of the cores were sieved over a 500 μm round mesh, retaining all macrofauna which was fixed in 10% buffered formaldeheyde, and stained with rose Bengal until processing.

All images were analysed using custom-made standardized scripts modified from Queirós (2010), which enable the extraction of the location of the flurescent luminophoes in each image in relation to the linearized sediment water interface, and thus the reconstruction of luminophore profiles within the sediment. We used the whole liner data to quantify bioturbation by estimation of maximum bioturbation depth. We also fitted the observed luminophore profiles to the biodiffusion transport model (Guinasso and Schink 1975) to quantify the biodiffusion coefficient, an indicator of bioturbation intentsity and thus activity.We used the time-lapse data to estimate the same parameters and model coefficients, and to fit the Shiffers model that describes bioturbation as a on random-walk process (Schiffers, Teal et al. 2011).

Impacts on bio-irrigation**,** i.e. sediment flushing by burrowing fauna, were quantified, as this process has important effects on sedimentary biogeochemistry (Kristensen, Penha-Lopes et al. 2012) and can also be used to assess the overall condition of the infuanal communities. In summary, we used a chamber setup (Fig. 4) to incubate four liners per treatment, at T0, T1 and T2. To each liner, we added the innert tracer NaBr to make up a concentration of 10M, considering the exact volume of water in each liner. Each liner was incubated over four hours under controlled flow conditions (5 rpm, Figure 4), during which no circulation to and from the main seawater system was allowed. Water samples were collected at hourly intervals to determine variation of tracer concentrations over time. 50 ml water samples were immediately filtered (GF/F), and frozen at -20^{o}C until processing. Concentrations will be determined via spectrophotometric methods sensu Presley and Claypool (1971).

Figure 4: Bio-irrigation measurement chamber setup.

Seawater total alkalinity and total inorganic carbon were monitored in each header tank and in liners, once a week, using the methods in Dixson, Munday et al. (2010). Sewater temperature, pH, salinity and oxygen, were monitored twice a week in each liner, and in header tanks, using macro probes. Table I illustrates environmental parameters measured in the water overlying each liner throughout the 20 week experiment, providing mean ± sd for each parameter estimated across replicate liners.

Table I: Experimental conditions in water overlying sediments during the high CO_2 experiment (rows 1-5, section 2.1.1), and the formation water experiment (rows 6-10, section 2.1.2). Nominal stressor treatments in the first column, and the associated geochemical impacts illustrated in the pH, salinity and oxygen columns.

Treatment	Temperature	Salinity	pH	Oxygen
400 ppm	8.89 +/-2.35	33.82 +/-0.52	8.05 +/-0.06	7.31 +/-0.35
1000 ppm	8.75 +/-1.61	33.82 +/-0.52	7.68 +/-0.10	7.34 +/-0.33
2000 ppm	8.70 +/-1.65	33.82 +/-0.52	7.47 +/-0.11	7.34 +/-0.32
5000 ppm	8.75 +/-1.54	33.82 +/-0.52	7.06 +/-0.08	7.26 +/-0.33
20000 ppm	8.79 +/-2.3	33.81 +/-0.52	6.58 +/-0.06	7.23 +/-0.35
Control	12.3 +/-1.6	33.9 +/-0.3	8.0 +/-0.1	7.8 +/-0.5
Hypoxic	13.1 +/-1.6	33.9 +/-0.1	7.9 +/-0.1	3 +/-1.3

Hypersaline	12.5 +/-1.8	48.2 +/-1.2	7.9 +/-0.1	7.2 +/-0.5
Mixed	12.9 +/-1.8	48.0 +/-1.3	7.8 +/-0.1	2.7 +/-0.1
Tidal	12.7 +/-1.8	41.6 +/-8.5	7.85 +/-0.1	4.25 +/-2.2

2.1.2 The ECO2 hypoxic brine "Formation water" experiment

Sediment cores (32 x 27 x 40 cm, 0.9 m^2 surface area) were collected on the 13th -14th of August 2013 from Oslofjord (Norway, 59^{o}49.4788' N 10^{o}58.859' W, 100 m depth) using a KC Denmark 0.1m^2 box-corer. All cores were returned to the laboratory within 8 hours of collection, at the Marine Research Station, Norwegian Institute of Water Research, Solbergstrand, Norway. On arrival, the liners were distributed randomly within the experimental basin where they were immediately submerged in a common flow through bath of physically filtered seawater collected locally from Oslofjord (approx. 60 m depth) for 19 days. T0 was set as the control sampling point, lasting between the 3rd and the 10th of September 2013. Experimental exposures ran between the 11th of September and the 7th of October 2013 (T1), when the last sediment core was sampled. During these 3 ½ weeks, 20 liners were exposed to the five experimental treatment levels described above, generated and maintained as batch water in 4 individual 16m^3 basins. High salinity was achieved by raising the salinity of control seawater to 48 g/L using 99% NaCl (GCRiebber) in line with a conservative estimate of the levels estimated for formation fluids in the Southern Viking Grabben (MA 2003). Hypoxia was achieved by bubbling of N_2 gas in the batch basins containing control seawater, via an adapted Walchem system. Oxygen was lowered to 1.4 g/L. The tidal treatment was simulated by flushing of a header tank that was supplied with water from the mixed treatment with control water, twice a day (9AM-3PM, and 9PM-3AM of each experimental day). At each time point, samples were collected to determine a range of environmental responses for all of the endpoints described above for the high CO_2 experiment (section 2.1 and 2.1.1), using the same methods.

In this experiment, ***sedimentary pH profiles*** were acquired using glass microelectrodes (Cai and Reimers 1993) and macroprobes (Metrohm 380 pH meter). These were acquired on slicing of the sediment cores to quantify possible effects on the vertical distribution of macrofauna, as before (section 2.1.1) ***Sedimentary sulphide and redox profiles*** were

acquired simultaneously, also using macroprobes (Radiometer En, silver chloride electrode filled with potassium chloride solution, which is suitable as a reference electrode). The experimental conditions observed in the liners are summarized in Table I, and in figure 5, below. In addition, ***distributions of phosphate, ammonia, nitrate, dissolved manganese (Mn^{2+}) and dissolved iron (Fe^{2+}), and alkalinity in the pore water*** were measured in 10 cm cores at the end of experiment, on the 10th of October 2013. We calculated the DIC and saturations of calcite and aragonite as a functions of pH and alaklinity with the CO2SYS excel sheet (http://cdiac.ornl.gov/ftp/co2sys/).

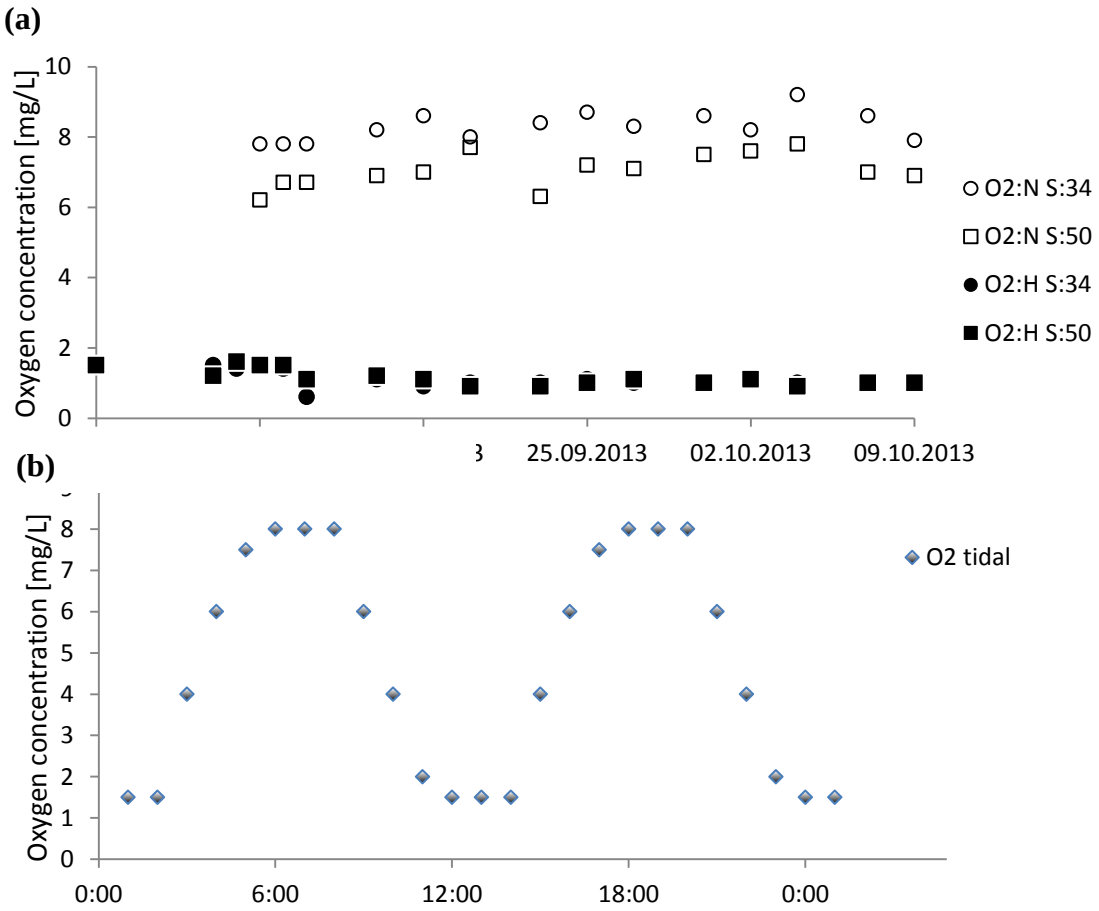

Figure 5: Oxygen concentration in the header tank seawater (a) and in the tidal treatment seawater mixing basin (b) during the formation water experiment (section 2.1.2). a) shows the difference between oxygen concentration in the control (open circles) and the high salinity treatment (open squares), and that in the hypoxic (filled circles) and mixed treatments (filled squares).b) show the by-daily tidal regime imposed in the "tidal treatment", illustrating the oscillation of oxygen concentration between conditions during the flushing of the high salinity and hypoxic plume by control water (normoxic conditions, high tide), and when no flushing of the high salinity and hypoxic plume was simulated (low tide).

2.2 Field observations at a natural CO_2 seeps

Several field campaigns were carried out in natural CO_2 vents at the Panarea island, part of Aeolian islands, as natural analogues. The Aeolian Islands are located in the south-eastern Tyrrhenian Sea, north of the town of Messina, in Sicily, Italy. They are the visible part of the mainly submarine Aeolian volcanic structure (Beccaluva et al. 1982). Panarea is a small 3.3 km^2 island and its nearest neighbor is Stromboli Island with its active volcano. The release of CO_2 from the seabed in Panarea, visible by gas emissions, is mostly controlled by the NE-orientated faults (Gabbianelli et al. 1933). The gas contains mostly of CO_2 (Calanchi et al. 1995).

Gas emissions at the Panarea site are present in moderate flows and also in strong fumaroles. Emissions are found in rocky, sandy and seagrass areas. The underwater habitats are a patchwork of sand slopes and seagrass meadows. Close to the island and also between the small islands, rocky habitats are dominant. Explorative dives have confirmed that some areas are influenced by thermal fluids and / or sulfur precipitations. Those with pure CO_2 venting have been selected as field sites for the study of CO_2 effects in this project. Where gas emissions occur, reduced pH in the seawater was detected (pH range 7.4 to 8.1; pCO_2 range 360 to 3000 ppm, Figure 6), corresponding to a low to intermediate CO_2 treatment in the mesocosm experiments.

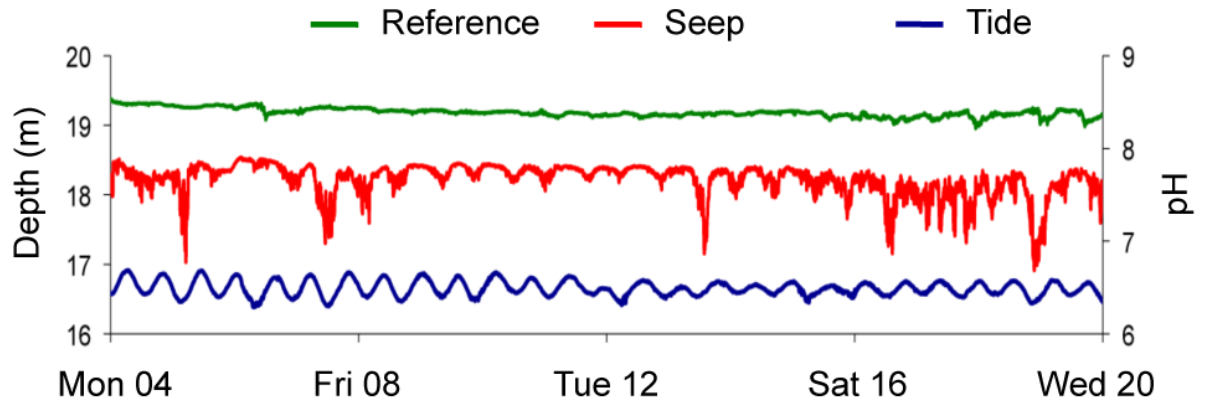

Figure 6: pH and pressure (tide) data measured in situ with RBR sensors (RBR-Datalogger XR-420 D; RBR, Ottawa, Canada, www.rbr-global.com). RBRs were positioned at St. B2 (Reference) and St B1 (seep: HighCO_2), 2 cm above the sediment surface, and they collected measurements in continuo for two weeks. At the same time and location the "Handheld" microsensor instrument recorded data for pCO_2 (Microelectrodes Inc., USA), temperature (Pt100; UST Umweltsensortechnik GmbH, Geschwenda, Germany), pH and oxygen (data not show).

Deliverable 4.1: Potential impact of CCS leakage on marine communities
WP4; lead beneficiary: Plymouth Marine Laboratory

After an initial sampling campaign in the summer of 2011, two CO_2-impacted and one background site had been identified as suitable sampling sites for functional long-term investigations of the microbial and meiofaunal community affected by CO_2 emissions: "HighCO_2" (St. B1), "LowCO_2" (St. B3) and "Ref" (St. B2). Stations B1 and B2 (referred to as the control sites), were chosen also for water column characterization. The same sites were re-visited for biological and geochemical sampling. Furthermore, OGS and UniRoma1-CERI collected waters samples for chemical and biological analyses along a transect crossing a vents area between Bottaro and Lisca Bianca Isles (LB transect). In this area, gas emissions characterized by H_2S smell were also detected.

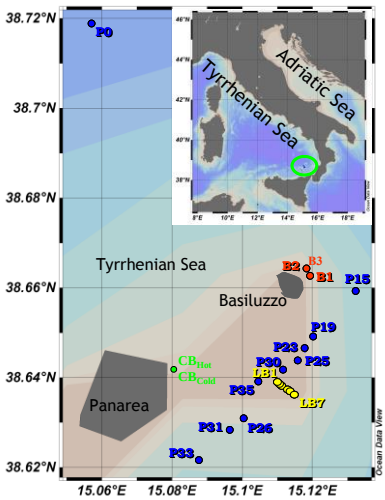

Figure 7: Position of stations sampled off of Panarea during Eurofleets, in the summer of 2011 (P= PACO2 stations – long transect, B= Basiluzzo stations, CB=CB stations, LB=LB stations – short transect).

In addition, in the summer of 2011, under the framework of the 'Eurofleets' Project (call 2010), an oceanographic survey (PaCO2) was carried out onboard the R/V Urania, off the coast of Panarea Island. Detailed profiles conducted in deep water sites, impossible from the small boats normally used at Panarea test site, have allowed for a complete characterization of the water column along a transect cutting the submerged seamount where the bulk of previously known gas leakage points occur (McGinnis et al. 2011). During the cruise, OGS and UniRoma1-CERI carried out chemical and biological analyses in the water column and set up an experiment to evaluate the intensity and impact of viral production and decay on

prokaryotes along a CO_2 gradient. The indicative position of the stations sampled during the different campaigns are reported in figure 7.

In October 2012, May 2013, and May 2014 further research within the framework of WP2, WP3 and WP4 was conducted. Two more sites, characterized by very different sediment temperatures across a distance of approx. 1 m, were included in the study (CB-HOT, CB-COLD). A summary of site conditions is given in Tables II and III. Details about the methods used in Table II can be found in Annex I.

Table II: Main characteristics of the three sedimentary sampling sites at Basiluzzo Island (Panarea Island, Italy). Observations were made during field trip ECO2-3 (June, 2012) by divers (*)..

	"HighCO$_2$" St. B1	**"LowCO$_2$" St. B3**	**"Ref." St. B2**
Coordinates	N 38°39.749' E 15°07.123'	N 38°39.820' E 15°07.137'	N 38°39.827' E 15°07.118'
Water depth*	14-15 m	21 m	14-16 m
Temperature[1]	19°C	19°C	19°C
Gas emission[2]	Yes (CO_2 98%)	Yes (CO_2 97%)	no
Area*	10 × 20 m	2 areas, each 3.5 × 5 m	10 × 10 m
Substrate[3]	fine-medium sand	fine-medium sand	fine-medium sand
Seagrass*	*Posidonia oceanica*	*Posidonia oceanica*	*Posidonia oceanica*
Seagrass Epibionts*	hydrozoa & bryozoa, but also calcareous	hydrozoa & bryozoa, but also calcareous	calcareous, but also hydrozoa & bryozoa

[1]bottom water temperature was measured with SeaGuard CTD (AADI, Norway)
[2]CO_2 concentrations were determined via gas chromatography
[3]Subrate type was assess via physical separation through sieving

Table III: Main characteristics of the two sedimentary sampling sites close to Panarea Island (Italy). Observations were made during field trip ECO2-6, ECO2-7 and ECO2-9 (October, 2012, May 2013 and May 2014).

	"CB-HOT"	**"CB-COLD"**
Coordinates	N 38°38.536' E 15°04.714'	N 38°38.536' E 15°04.714'
Water depth	11.9 m	11.9 m
Temperature	40 ± 5 °C	19 ± 2 °C
Gas emission	No bubbles	No bubbles
Thermal waters leakage	Yes, enriched in CO_2 (5-11 mg /m^3 s flux)	No
Area	1 × 1 m	1 × 1 m
Substrate	fine-medium sand	fine-medium sand
Seagrass	*Posidonia oceanica*	*Posidonia oceanica*

In the latter campaign, the general ***physical-chemical properties of the water column*** were determined with a CTD SeaBird 19 probe. This unit was equipped with sensors for temperature, conductivity, pressure, fluorescence, pH, and dissolved oxygen. ***Water samples*** were collected at discrete depths with Niskin bottles for an accurate characterization of the marine carbonate system (pCO_2, pH, A_T, DIC), chemical properties related to natural seabed CO_2 leakage (H_2S, nutrients) and planktonic communities. The rates of prokaryotic carbon production and the exoenzymatic activities have also been examined.

The headspace technique was used for the quantification of ***seawater pCO_2 (***Capasso and Inguaggiato, 1998), whereas the ***pH and total alkalinity*** was determined following the standard operating procedures (SOP 3b, SOP 6a, SOP 6b) described in Dickson et al., 2007. ***Hydrogen sulphide concentrations*** were estimated spectrophotometrically according to Fonselius et al. (1999). A Bran+Luebbe Autoanalyzer 3 was used for the colorimetrical ***analysis of nutrients*** (nitrite, NO_2, nitrate, NO_3, ammonium, NH_4, phosphate, PO_4 and silicic acid, H_4SiO_4) as reported by Hansen and Koroleff (1999).

Viral abundances were determined from formalin-fixed samples which were immediately stored in liquid nitrogen (-80°C) until processing. Samples for the analysis of ***prokaryotic abundance*** were preserved in buffered formalin, stored at 4 °C and processed within a week.

Viruses and prokaryotes were enumerated in epifluorescence microscopy. Water samples for the estimate of ***viral production and decay*** were incubated at *in situ* temperature, as well as the incubations with antibiotics to determine the burst size and lysogenic prokaryotic fraction.

Prokaryotic heterotrophic production analysis in seawater was conducted using the tritiated leucine incorporation method, (i.e. incubation of water samples at *in situ* temperature, extraction using the microcentrifugation method and subsequent storage of samples at +4°C until the analysis of the activity by liquid scintillation counting).

Extracellular enzymatic activities (aminopeptidase, alkaline phosphatase, β-glucosidase and lipase) were determined using fluorometric analysis of hydrolisis rate of water samples incubated at *in situ* temperature.

Abundance and species composition of Phytoplankton and Microzooplankton were estimated according to the Utermöhl's method (1958).

Virtually undisturbed sediment cores were collected by scuba divers and subsampled for the analyses of abiotic parameters (sediment grain-size, Total Organic Carbon and Total Notrogen, Biopolymeric Carbon) and benthic communities (microphytobenthos and meiofauna) and both primary production and prokaryotic heterotrophic production.

Sediment grain-size analyses were performed using a Malvern Multisizer 2000S analyzer.

Total Organic Carbon and Nitrogen were determined using a CHNO-S elemental analyzer mod. ECS 4010 (Costech, Italy) according to the methods of Pella and Colombo (1973) and Sharp (1974).

Biopolymeric carbon (BPC, sensu Fichez, 1991) was rquantified as the sum of the carbon equivalents of carbohydrates, proteins and lipids. Two different carbohydrate (CHO) fractions were analysed on lyophilized sediment samples following Blasutto et al. (2005). ***The carbohydrate fraction*** was measured spectrophotometrically using the phenol-sulphuric acid assay following Dubois et al., (1956), modified by Gerchacov & Hatcher (1972).

Proteins were determined according to Hartree (1972) modified by Rice (1982).

Total lipids were extracted from lyophilized sediment samples by direct elution with chloroform and methanol (1:2 v/v) following the procedure of Bligh and Dyer (1959) and analysed according to Marsh and Wenstein (1966).

To estimate the ***impacts on Microphytobenthos***, the surface sediment layer was collected in triplicates and fixed with 4% formaldehyde/filtered sea water. Only cells containing pigments were counted and identified to the genus and, when possible, to the species level under an inverted light microscope.

Some associated processes were measured. ***Primary production (PP)*** was estimated using the ^{14}C incubation method (i.e. incubation of sediment samples *in situ* and subsequent storing of samples at +4°C until further analysis by liquid scintillation counting).

Prokaryotic heterotrophic production in surface sediment was measured using the the tritiated leucine incorporation method (i.e. incubation of sediment samples *in situ* and subsequent storage of samples at +4°C until further analysis by liquid scintillation counting).

PAR measurements were performed at the beginning and at the end of all incubations.

3. Response of specific ecosystem components to leakage from CCS

3.1 Macrofauna

3.1.1 High CO_2 mesocosm experiment

The macrofauna data from this experiment is still being processed by NIVA. Therefore, there is no preliminary information available at this stage, about the impact of the formation water treatments on macrofauna community structure. Some information about the level of activity of these communities can, however, be derived from section 3.6.1, as bioturbation activity and depth can be used a proxies for individual fitness..

3.1.2 Formation water leakage mesocosm experiment

The macrofauna data from this experiment is still being processed by NIVA. Therefore, there is no preliminary information available at this stage, about the impact of the formation water treatments on macrofauna community structure. Some information about the level of activity of these communities can, however, be derived from section 3.6.2, as bioturbation activity and depth can be used a proxies for individual fitness.

3.1.3 Natural seeps

Macrofauna found at the Panarea sites during the field campaign in 2012 was composed of relatively small organisms, occuring in low densities (0-10 cm, CO_2 seep St.B1: 1884 ± 1306 ind.m^{-2}, CO_2 seep st. B3: 509 ± 392 ind.m^{-2}, control site St. B2: 2063 ± 792 ind.m^{-2}). Densities at the CO_2 seep site St. B3 were significantly lower than those at both other sites. Although diversity did not differ, the macrofauna composition at both CO_2 seep sites differed from the control site based on the occurrence of more oligochaetes and amphipods, and less polychaetes and gastropods at the seep sites. The macrofaunal organisms are currently being identified to the lowest possible taxonomic level.

3.2 Meiofauna

3.2.1 High CO_2 mesocosm experiment

Sample processing is ongoing, having suffered significant delays associated with sample shipment between Norway (NIVA) and the UK (PML). No preliminary findings are thus available.

3.2.2 Formation water leakage mesocosm experiment

Meiofauna sample processing is ongoing, having suffered significant delays associated with sample shipment between Norway (NIVA) and the UK PML). No preliminary findings are thus available.

3.2.3 Natural seeps

The results from the 2012 meiofaunal samples indicated density differences in sediments and on seagrass shoots under the influence of CO_2 seepage. Total meiofauna densities were significantly higher in the control sediments at St. B2 compared to the CO_2 seep sediments at St. B1 and B3 (1340 ± 176 ind.10cm^{-2} vs. 384 ± 201 ind.10cm^{-2}, respectively), while in the seagrass shoots, the opposite was true (169 ± 53 ind.10cm^{-3} vs. 467 ± 217 ind.cm^{-3}, respectively, figure 8). From the sediment samples collected in 2013, similar trends emerge. Where CO_2 seepage occurs, densities are highest in the first two centimeter of sediment, showing a steep decline with depth, while at the background site, a more gradual decline with depth was observed. This pattern is also reflected by the nematode biomass, which was also significantly reduced at the CO_2-impacted site (27 ± 15 µg dwt 10cm^{-2} versus 152 ± 55 µg dwt 10cm^{-2}; 2012). In the sediments, nematode species composition differed between CO_2-impacted sites and a non-impacted background site for both 2011, 2012 and 2013. This was not observed in meiofaunal taxonomical composition. The nematode species composition also differed between the two different seepage sites in 2011 and 2012, but not in 2013. In the most severe CO_2-impacted site differences were also observed in nematode species composition between the three consecutive years, caused by the shifting abundance of one particular species, i.e. *Calomicrolaimus compridus*. This species dominated (average ranging from 20 - 26%) in 2011 and 2013, in equal contributions to 2 other species, and dominated communities in 2012 with 84 ± 7%. Nematode species richness was significantly lower in the

CO_2-impacted sites compared to the non-impacted sites, for all three consecutive years (averages of 9 - 12; 12 - 17 and 29 – 32 species for the station B1, B3 and B2, respectively). Similar trends were found when comparing the diversity index ES (51). In the seagrass (leafs and shoots), no significant effects of CO_2 were detected on the taxonomical composition of meiofauna assemblages. There are more results to follow on the potential effect of acidified porewater on the physiology (respiration rates) of the meiobenthos.

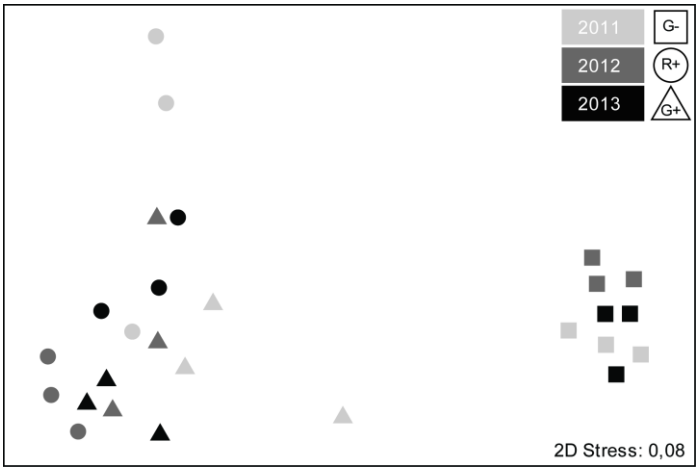

Figure 8: non-metric Multi-Dimensional Scaling plot illustrating the dissimilarity between samples based on nematode densities (standardised). Note the clear dissimilarity between the nematode assemblages found at Control st.B2 (=G-) and both CO_2 seep st.B1 (=R+) and CO_2 seep st.B3 (=G+)

3.3 Microbes

3.3.1 High CO_2 mesocosm experiment

Results obtained for the top 1 cm layer of the sediments show that the prokaryotic abundance in the controls increased during the entire experiment (Fig.9). Conversely, all the acidified systems, independently on the level of acidification, showed values of prokaryotic abundance comparable or lower than the control at T0. However, the prokaryotic abundance in the CO_2-treated systems reached values comparable to the control after the long-term acidification.

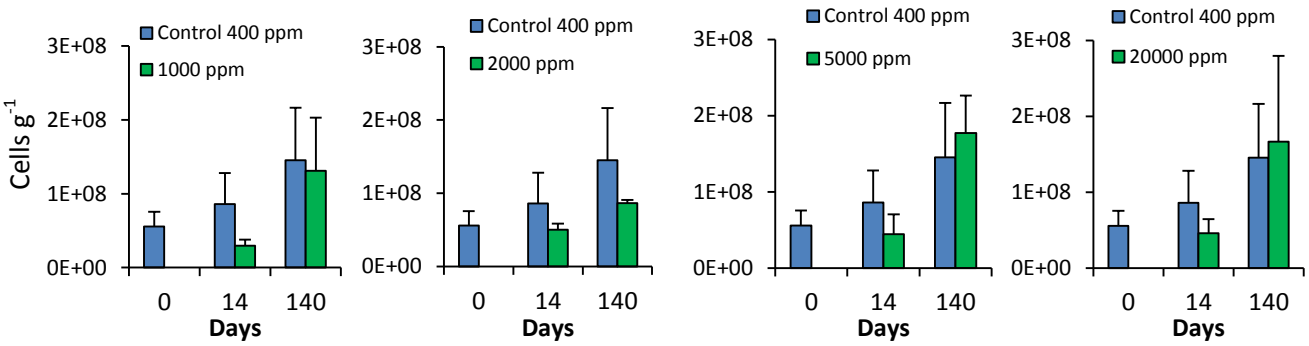

Figure 9: Prokaryotic abundance in the 0-1 cm sediment layer

The temporal trends in viral abundance (Figure 10) differed from those of the prokaryotes, both in the controls and in the treatments. Indeed, viral abundance decreased in the controls at T1 and increased again at T2, at values almost identical to those at T0. The acidified systems showed trends similar to the control at T1, but, at T2, viruses did not reach the same abundance determined at T0.

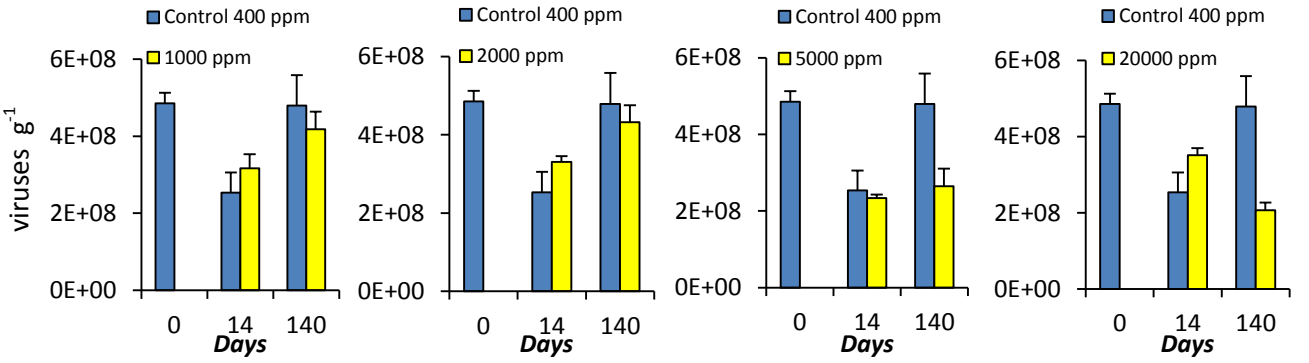

Figure 10: Viral abundance in the 0-1 cm sediment layer.

Given the increasing trend in prokaryotic abundance and the decrease or steady value of viral abundance over time, the virus-to-bacterium ratio (VBR) decreased over time (Figure 11), with the lowest values displayed at the end of the experiment (T2), both in the untreated and in the acidified systems. However, in the controls, the VBR reached this low value already at T1, while in the treatments this decrease was less evident or even not significant at T1.

This suggests that the lowering of the pH can alter the natural trends of the variations in viral and prokaryotic abundances, due to the different response of viruses and prokaryotes to the acidification. In particular, prokaryotes seem to be negatively affected more than viruses after

a short-term acidification treatment, independently of the level of acidification. On the contrary, the levels of acidification determine different responses in the long-term period, with the lowest VBR resulting in the two extreme acidification conditions (5000 and 20000 ppm), the 1000 and 2000 ppm treatment being otherwise similar to the control.

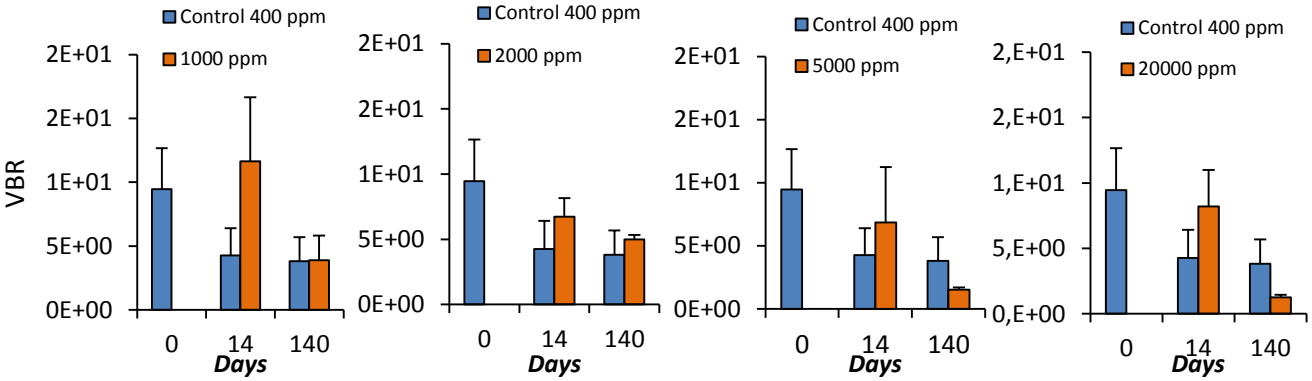

Figure 11: Virus-Bacteria ratio in the 0-1 cm sediment layer

The rates of viral production showed the highest peak in the control at T1 (Figure 12), decreasing then at T2, but still more than 3 times higher than at T0. This trend did not result from any of the acidified system, with viral production rates generally lower than the control, with the exception of the most acidified samples at T2. During some specific time intervals, viral production in the acidified systems appeared to be inhibited, with resulting values extremely low or below the detection limit.

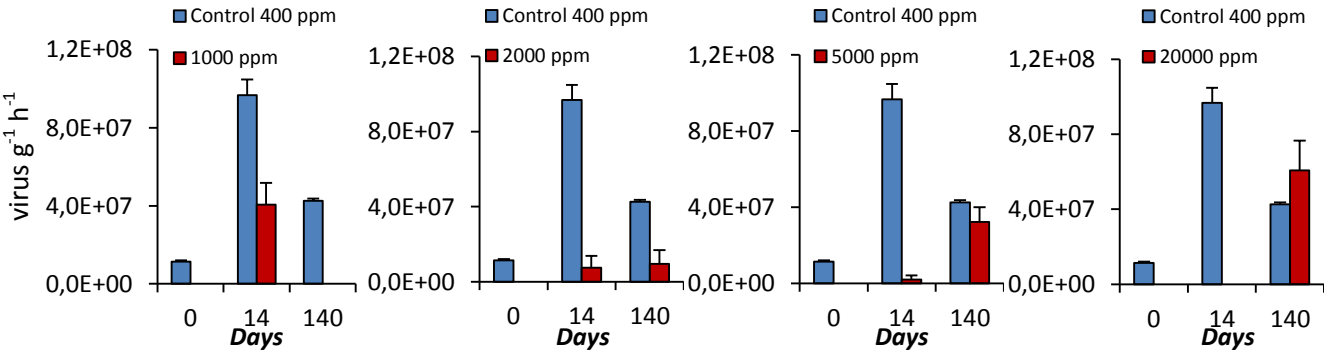

Figure 12: Viral production in the 0-1 cm sediment layer.

In the control systems, the prokaryotic heterotrophic carbon production did not change significantly after the first two weeks of the experiment (Figure 13), while it significantly

decreased at T2. The decrease in prokaryotic heterotrophic production at T2 was reported also in the acidified systems; however, in all of the acidified systems, this decrease was evident at T1 already.

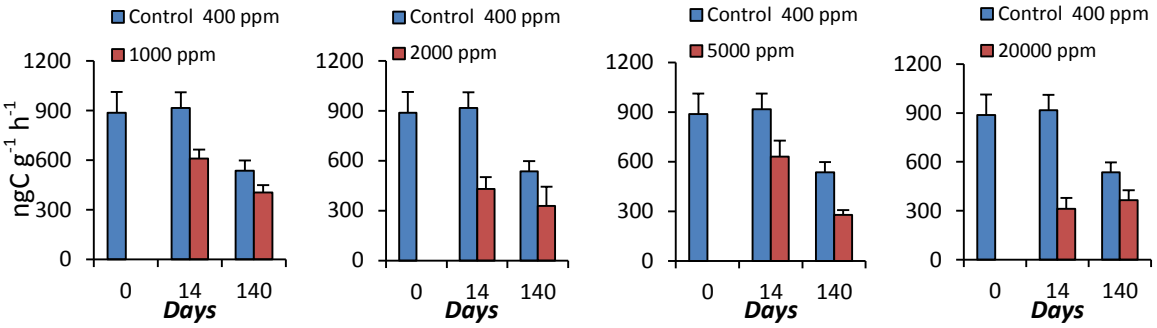

Figure 13: Prokaryotic heterotrophic production in the 0-1 sediment layer.

All of the enzymatic activities decreased over time in all of the systems, including controls (Figures 14a, 14b and 14c). As already noticed for the decreasing trends in prokaryotic heterotrophic carbon production, also the rates of extracellular enzymatic degradation of protein, lipids and carbohydrates did not change significantly after the first two weeks of the experiment (T1), while a significant decrease was evident at T2. Notably, in all of the acidified systems, the reduced rates of the extracellular enzymatic degradation of the organic matter was evident at T1 already.

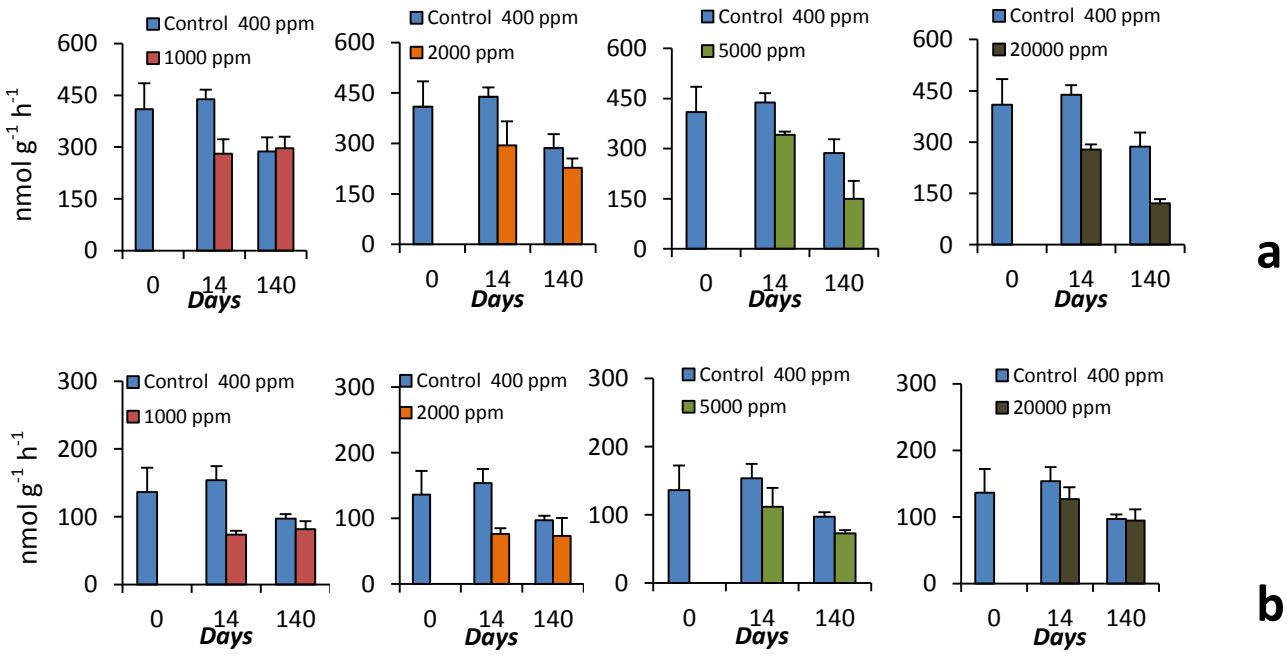

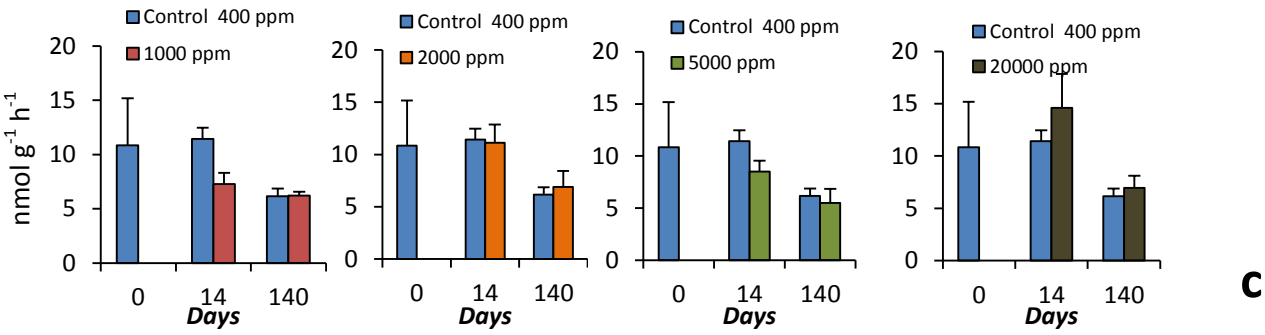

Figure 14: Extracellular enzymatic activities in the 0-1 cm sediment layer; a) Aminopeptidase; b) Alkaline phosphatase; c) Beta-Glucosidase.

The values of biopolymeric carbon (defined as the carbon equivalents of proteins, carbohydrates and lipids assuming as a conversion factor 0.49, 0.40 and 0.75 respectively) did not show significant trends of increase or decrease in concentration over time (Figure 15). Moreover, the protein-to-carbohydrate ratio did not change significantly during the 20 weeks of the experiment, also suggesting that the availability and quality of food resources was not limiting the activity and metabolism of the microbial compartment during the experiment.

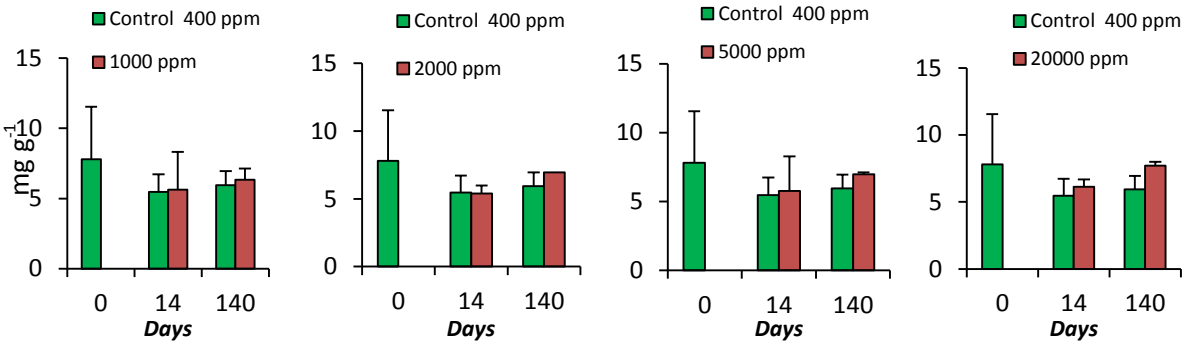

Figure 15: Biopolymeric Carbon concentration in the 0-1 cm sediment layer.

3.3.2 Formation water leakage mesocosm experiment

Microbial samples from this experiment are still being processed, and there are therefore no preliminary results, at this stage.

3.3.3 Natural seeps

3.3.3.1 Microphytobenthos

Comparing the three sampling periods, the highest microphytobenthic abundances in the Basiluzzo site were reached in October 2012, both in the red vent (B1) and in the grey vent (B3). Intermediate abundance values were observed in May 2013 while the lowest ones were obtained in June 2012. The highest microphytobenthic densities were consistently recorded at St. B1, with its absolute maximum in October 2012 (20045 ± 2344 cells cm^{-2}), about four times higher than the abundance observed at the reference site (B2). Differences in the microalgal densities between St. B2 and St. B3 were not so marked. Only in October 2012 the abundances in the reference site (B2) and in the grey vent (B3) considerably differed, but in June 2012 and in May 2013 the microalgal numbers were comparable, indicating that at St. B3 there is no clear influence of the CO_2 emission on the development of the microphytobenthic community. In fact, the absolute minimum was not detected at the reference site (B2) but at St. B3 in June 2012 (1617 ± 177 cells cm^{-2}, figure 16a).

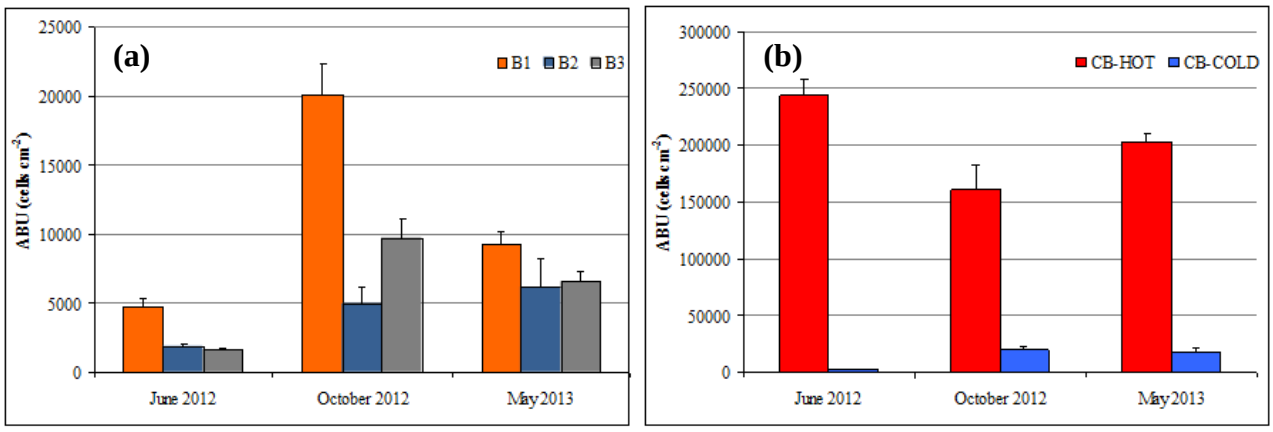

Figure 16: a) Total abundance of the microphytobenthic community in the Basiluzzo site. **b)** Total abundance of the microphytobenthic community at the hot and cold part of St. CB.

On the contrary, very remarkable differences in the values of microphytobenthic abundance were recorded between the cold and hot part of St. CB during all three sampling periods. In June 2012 values in St. CB-HOT reached 243361 ± 14384 cells cm^{-2} and were almost 100 times higher compared to those observed at St. CB-COLD (2510 ± 29 cells cm^{-2}). Even though the difference in total densities was much lower in October 2012 and May 2013, in

both periods the microphytobenthos abundance at the St. CB-HOT was still about 10 times higher compared to that at St. CB-COLD (Figure 16b). Taking into account the total values of microphytobenthic abundance only, St. CB-COLD can be considered reasonably comparable to the St. B1.

At all sites the microalgal community was mainly composed of different pennate diatoms. At St. CB-HOT the predominant genus was *Navicula* sp. and *Navicula* cf. *cancellata* alone exceeded 30% of the total abundance compared to the nearby St. CB-COLD, where its abundance was negligible.

3.3.3.2 Bacteria

In the water column and on the seagrass leaves, the bacterial community structure did not show any significant differences between the sites investigated. Conversely bacterial community analyses of recovered sediments confirmed the previously detected difference between the CO_2-impacted sites and the background site without seepage (Figure 17a). The analysis of similarity of the molecular fingerprinting results (ARISA) also confirmed the presence of significant different bacterial communities inhabiting the three sites investigated (ANOSIM: $R = 0.919$, $p<0.001$), and these differences were constant over all investigating period (2011-2012). Further both the number of OTUs and diversity index (Simpson's evenness) provide evidence of reduction of the bacterial diversity in seep sites compared to the background site. The results of pyrosequencing (454 MPTS) confirmed that the seabed CO_2 emissions are responsible for a change in the bacterial community structure, already visible at Phylum level. CO_2 sensitive taxa belonged to phyla Proteobacteria (e.g. γ- and δ-proteobacteria), Bacteroidetes (e.g. Flavobacteriales), Cyanobacteria, and Chloroflexi. Overall, CO_2 effects explained up to 60% of the variance in community composition. Both OTU richness and evenness were reduced at CO_2-impacted vs the reference site (Figure 17b). Despite these change in bacterial community structure and diversity, both total prokaryotic abundance and active fraction of Bacteria (as detected by CARD-FISH) were not affected by different environmental setting characterizing CO_2-seep sites and background site, indicating that CO_2-sensitive types are replaced by taxa tolerant of high CO_2. Although the effect of CO_2 seabed leakage on bacterial extracellular enzymatic activities has been observed, the differences responses of enzymes (beta-glucosidase, chitobiase, aminopeptidase and esterase)

in CO_2-impacted and non-impacted sites suggest a non-uniform response of whole bacterial metabolism (organic matter degradation) and the presence of functional groups differentially affected by CO_2 emissions. Ongoing analyses are investigating the identity of high CO_2-tolerant bacterial types and their functional role. The results from the transplantation experiments, to assess the short and middle CO_2 leakage effect on bacterial assemblages, are currently under processing as well.

Overall these preliminary results show that at Basiluzzo CO_2-impacted sites the CO_2 leakage is responsible of shift in bacterial diversity and increase of benthic diatoms (Table IV), the latter as response of enhance of nutrient availability (i.e. silicate and iron; see 3.5.3.2). However any relevant change both in active bacterial population size and in organic matter degradation rates suggest that not all bacterial taxa present at background CO_2 levels were able to profit from this higher microphytobenthic biomass, maybe due to the acidification of the site, and therefore that bacterial functions between the sites are more or less retained.

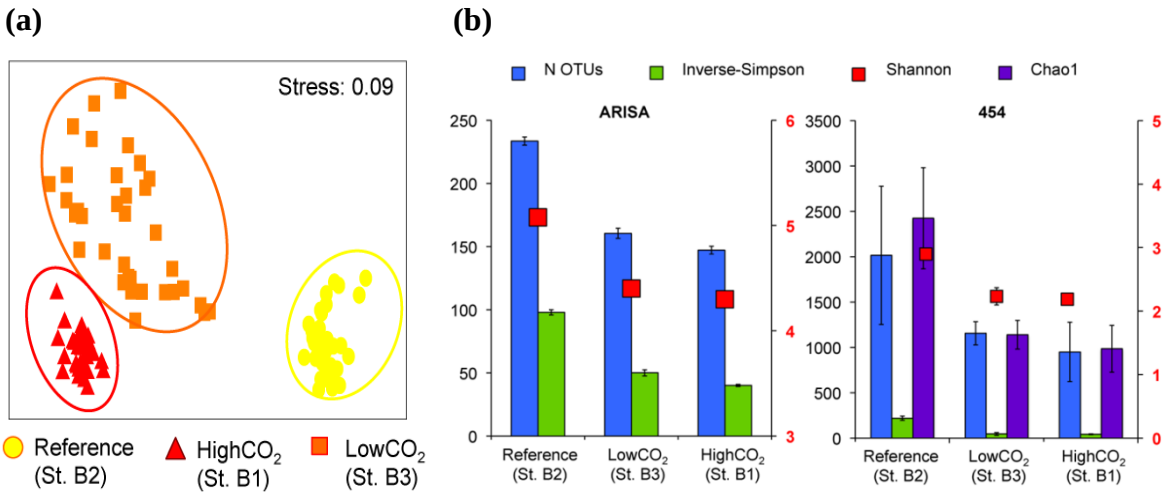

Figure 17: Difference in bacterial community communities between sites investigated. **a)** nMDS ordination, based on Bray-Curtis similarity, carried out on the results of high-resolution fingerprinting technique (ARISA).**b)** Richness, diversity and evenness indices calculated from fingerprinting (ARISA) and pyrosequencing (454 MPTS) data-set.

3.3.3.3 Microbe mediated processes

In October 2012, preliminary estimates of some functional parameters, i.e. Primary Production (PP) and Prokaryotic C Production (PCP), were carried out nearby Panarea Island which was characterised by the emission of hot gas from the coarse sand sediments (St. CB).

Primary production rates were six times higher in the hot part of the site (42.88 ± 5.75 mg C m^{-2} h^{-1}) than in the cold one (7.16 ± 0.13 mg C m^{-2} h^{-1}). The photosynthetic rate generally strongly depends upon the microphytobenthic abundance and in fact the microalgal density was more than 8 times higher in the hot part compared to the abundance in the cold part of the site.

Prokaryotic C Production rates were comparable between the two parts of St. CB: 0.112 ± 0.011 µg Cdry h^{-1} (St. CB- COLD) and 0.113 ± 0.001 µg Cdry h^{-1} (St. CB-HOT). In May 2013 PP and PCP were estimated in Basiluzzo at St. B1, St. B2 and St. B3. The highest PP was estimated at St. B1 (8.39 ± 1.98 mg C m^{-2} h^{-1}), a similar value was obtained at St. B2 (7.54 ± 1.43 mg C m^{-2} h^{-1}) while the lowest photosynthetic rate was measured at St. B3 (4.36 ± 0.62 mg C m^{-2} h^{-1}). Although measurements were carried out in two different periods, PP rates obtained at St. B2 and B3 were comparable to the one observed at the cold part of St. CB. However, considering the total microphytobenthic abundance (almost twice in the cold part of St. CB compared to that at St. B1) the microalgal community seemed to be more photosynthetically active in May than in October.

The highest Prokaryotic C Production rate was measured at St. B1 (0.276 ± 0.030 µg Cdry h^{-1}) while the lowest at the reference site (0.110 ± 0.019 µg Cdry h^{-1}), with a value comparable with St. CB. The third site (B3) was characterised by an intermediate PCP rate (0.185 ± 0.028 µg Cdry h^{-1}).

For what concerns microphytobenthos, there is no clear influence of the CO_2 emission on the development of the microphytobenthic community, since according to the vent different results were obtained. However, the elevated abundances of microalgae inhabiting the sediments of St. CB-HOT suggest that the combined effect of higher CO_2 concentration and high temperatures could exert a stimulatory effect on this community which seems also very active as shown by the elevated primary production rates.

For what concerns the prokaryotic heterotrophic production, both the high CO_2 concentration (St. B1 and B3) and its combined effect with elevated temperatures (St. CB-HOT) seems to not exert clear effects on such prokaryotic activities since the rates measured at vents are rather comparable with those of control sites (St. B2 and CB-COLD, respectively).

3.4 Seagrasses

At the Panarea site, studies on ecological aspects of CO_2 effects on the seagrass *Posidonia oceanica* included the Leaf Area Index (LAI), photosynthetic rate, weight of calcareous epibionts, abundance and diversity of epibionts and grazing indications on the leaves. Under the influence of CO_2, the determined LAI was smaller, but the epibiont abundance and diversity were higher as compared to a background site without seepage. Grazing marks by the sea urchin *Paracentrotus lividus* were less and by the fish *Sarpa salpa* were more abundant at the impacted sites.

The seagrass leaf area index was reduced at the two CO_2-impacted sites. At the non-impacted site**,** the seagrass *Posidonia oceanica* has ca. twice the leaf area per square meter. Preliminary grazing data showed that the overall grazing was reduced at the highest impacted site. Grazing of seagrass might be altered with less impact of echinoderms but more impacts from fish. Grazing marks by the sea urchin *Paracentrotus lividus* were less abundant, but more grazing marks by the fish *Sarpa salpa* were more frequently observed at the CO_2-seep sites. The epifauna studies of the upper seagrass leaves revealed that *Coralliacea* algae were not missing, contrary to expectation, but were less abundant, whereas thalleous, gelatinous and filamentous algae were more frequently observed at the CO_2-impacted sites**,** c.f. controls. The hydrozoan**s** *Sertullariidae*, *Plumulariidae* and *Aglaopheniidae* were more abundant**,** and *Campanulariida*e was present**,** at the impacted site but not at the non-impacted site. The bryozoans *Lichenopora* and *Microporella* were more abundant**,** whereas *Celleporina* and *Chorizopora* were less abundant at the CO_2-impactet sites. *Cellepor*a, *Collarina*, *Fenestrulina* and *Tubulipora* were only present at the seep site. The abundance of the ascidiacea genus *Botyllus* was seven times higher at the impacted site. This indicates a shift in the species community. Overall the study showed that the abundance and taxonomic groups is increased at the CO_2-impacted site (Table IV). The weight of calcareous epibionts on the first ten centimeters of the leaves was ca. two and a half times higher than at the reference site. This indicates that the growth of specific calcareous species seems to be favored at the seep sites.

The experiment on the net photosynthetic rate of the lowest 10 centimeters of the leaves revealed that this function is not impacted by the surrounding water CO_2. The same positive

rate in oxygen production was measured at both sites. That was also the case when the leaves were exposed to the water of the respective other site.

Table IV: Synthesis of CO_2 leakage effects on benthic communities at Panarea (Basiluzzo rock island sites).

	Abundance	**Biomass**	**Community Composition**	**Species Diversity**	**Activity**
Microphyto-benthos (diatoms)	Yes[1]	–	Yes	–	No
Bacteria	No	No	Yes	Yes	Yes
Meiofauna	Yes	Yes	Yes	Yes	–
Macrofauna	Yes[2]	–	Yes	No	–
Seagrass (*Posidonia oceanica*)	No	Yes[3]	na	na	No
Epibionts	Yes	Yes	Yes	Yes	na

[1] markedly at St. B1
[2] only at St. B3
[3] Leaf Area Index (LAI)
– = data currently under processing
na = data not available

3.5 Biogeochemistry

3.5.1 High CO_2 mesocosm experiment

3.5.1.1 Sedimentary pH profiles

The sediment in the liners was characterized as mud, having a mud content 95.12 ± 3.35 % (mean ± sd), and sediment porosity within the first cm horizon was 71.25 ± 15.76%. The corresponding pH profiles are given in figure 18, below. Sediments were more acidic (i.e. lower pH profiles) at 20 weeks than at 2 weeks, except in control cores. As expected, pH was

higher at the sediment water surface than at depth, except in the highests CO_2 treatments, at T1 (2 weeks). Differences between the experimental treatments were clear with regard to sedimentary pH profiles, indicating that the increase in CO_2 concentration in the overlying water could disturb carbonate chemistry down to 5 cm within the sediment. The degree of departure from the control profiles increased with increased CO_2 concentration in the overlying water, and the duration of the exposures. This effect may have significant consequence for organisms inhabiting these sediments, and associated ecosystem processes. Indeed, burrowing fauna have been found to surface in response to short-term drop in pH (Murray, Widdicombe et al. 2013). This was also observed here (see section 3.6.1), as burrowing depth and bioturbation activity both decreased significantly with CO_2 increase (fig.23), but only at 20 weeks. Thus, the experimental treatments used here to simulate a CO_2 leak at the seabed, were found to modify sedimentary conditions. These apprently small changes appeared to cause or at least be linked to changes in macrofauna behaviour within the sediment at 20 weeks, that are consistent with physiological stress (Section3.6.1), but not at 2 weeks. It is thus likely that prolongued (though not short term) changes induced by exposures to a CO_2 leak may have discernable, negative consequences for benthic communities and processes. These effects are further explored int he subsequent sections (but see section 3.6.1).

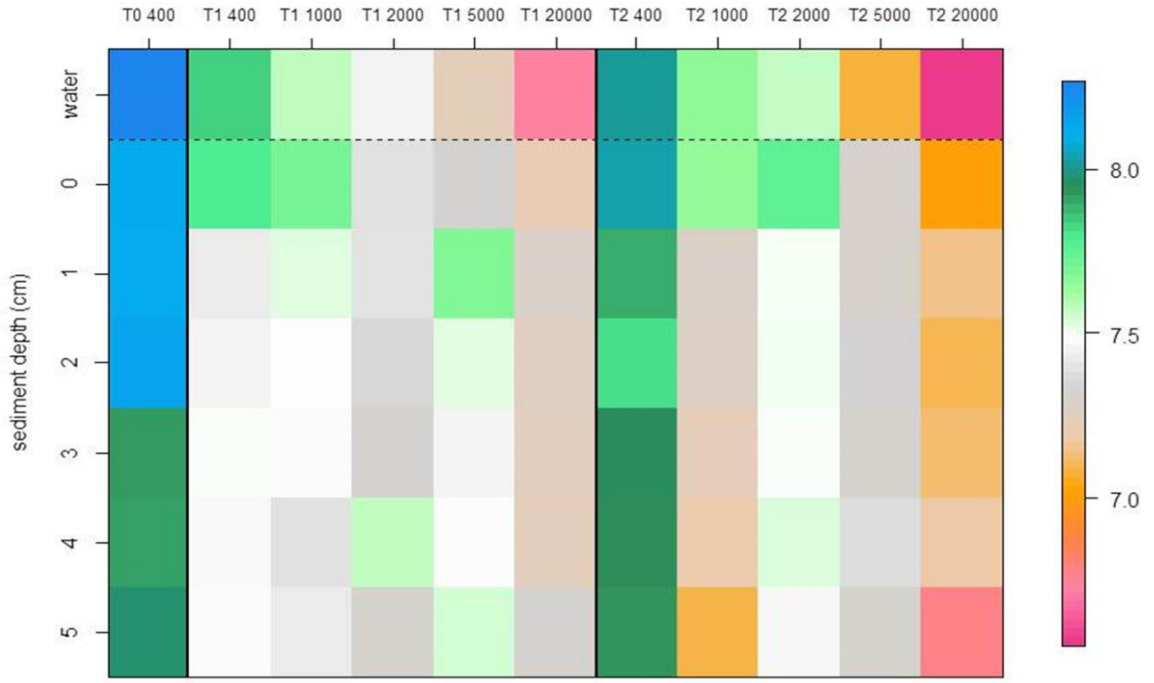

Figure 18: mean sedimentary pH profiles, measured and averaged over two sediment cores at T0, T1 (two weeks) and T2 (20 weeks) during the high CO_2 experiment (leakage experiment). Corresponding CO_2 nominal treatments are highlighted in the yy axis (400 to 20000 ppm, section 3.5.1.1).

3.5.1.2 Nutrient fluxes

Fluxes of ammonia, nitrite, nitrate, phosphate and silicate measured during the high CO_2 experiment are illustrated in figure 19 a-e, below. Large variability in fluxes was observed within treatments, particularly in fluxes measured after 2 weeks of exposure, leading to error

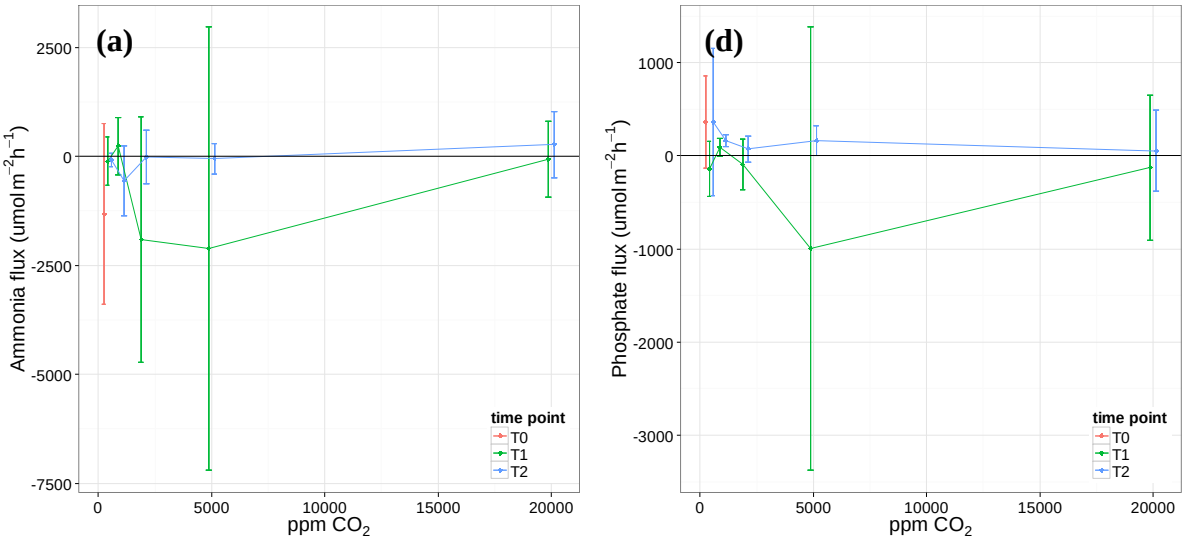

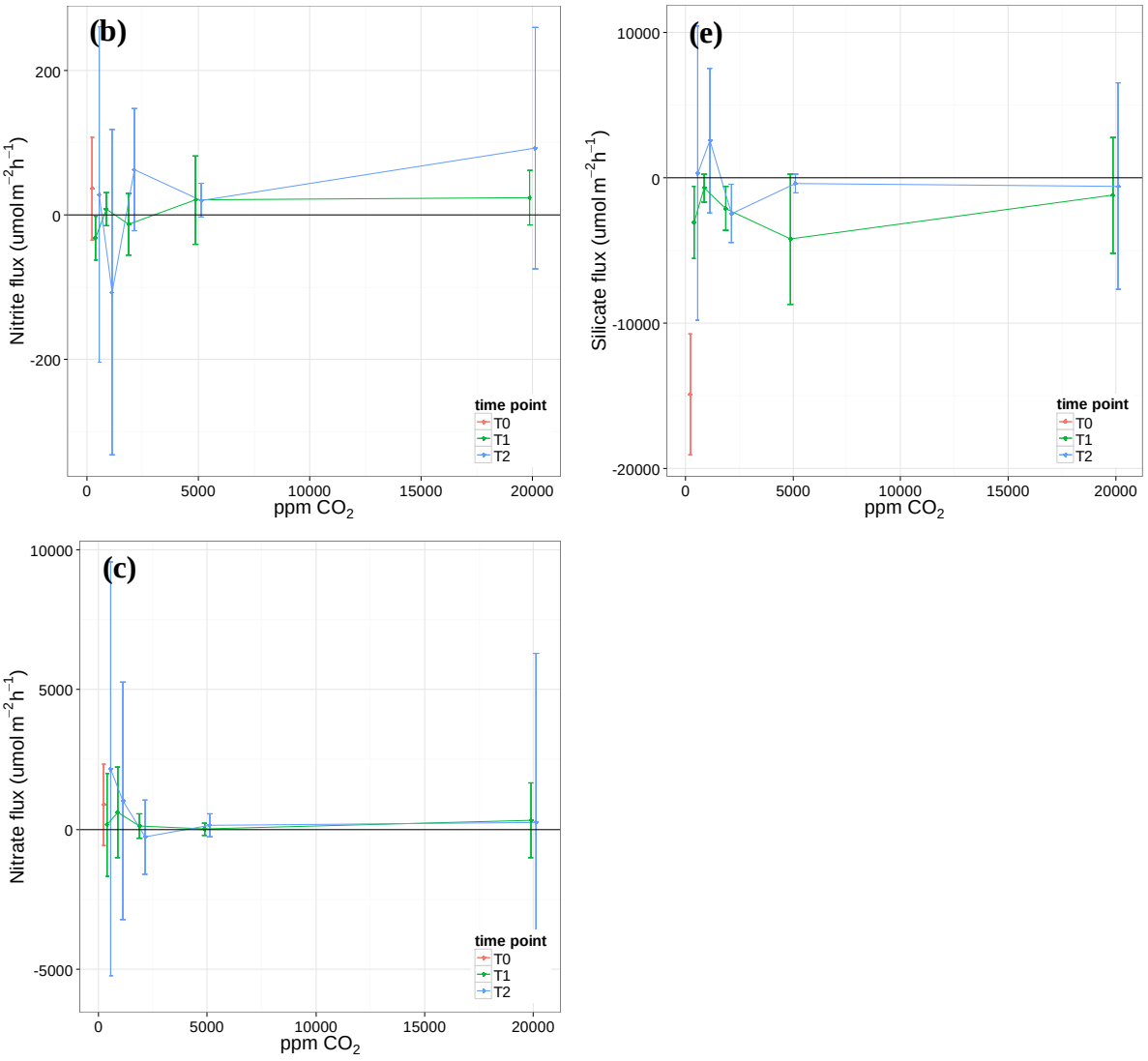

Figure 19: Fluxes of Ammonia (a), Nitrite (b), Nitrate (c), Phosphate (d) and Silicate (e) measured during the high CO_2 mesocosm experiment (section 3.5.2.1).

bars that predominantly overlapped zero, particularly for nutrients involved in the nitrogen cycle (Figure 19a-c). The preliminary data are now being assessed to determine the cause of variability and whether there are problems with specific samples, but similar results were identified in at the natural seeps (section 3.5.3.1).

The analysis of the phosphate and silicate fluxes does not render any clear patterns of impact of CO_2 levels at either 2 or 20 weeks (Figure 19). However, the decrease in phosphate uptake (towards phosphate release) observed at T1 with increased CO_2 levels matches the short-term

impacts of CO_2 measured by Widdicombe and Needham (2007). This pattern was not observed at 20 weeks, as was also found by Widdicombe, Dashfield et al. (2009). The same studies didn't find short or medium effects of increased CO_2 levels on silicate fluxes in muddy sediments, as also seen here.
Please see section 3.6.1 for overall system analysis.

3.5.1.3 Ammonia oxidation in the water and sediments

Nitrite levels in seawater and sediments in ATU and $NaClO_3$ treated samples are summarized in figure 15. ATU and $NaClO_3$ are inhibitors of NH_3^- and NO_2^- oxidation, respectively, playing an important role in the fixation of nitrogen. All values measured were well above the detection limit of the instrument, which was 0.005 and 0.009 µmol NO_2^- L^{-1}, for seawater and sediment samples, respectively (Kitidis, Laverock et al. 2011).

Two factors may have confounded our results. Some variability was observed between treatments, indicating the need for use of higher replication in future work. Additionally, some nitrite was available when the oxidation of NH_3^- to NO_2^- was inhibited in ATU treated samples. This was particularly visible at two weeks, in the control sediment samples, and at twenty weeks in the control seawater samples collected from the header tanks (Figure 20). Possible alternative sources of nitrite in these samples are the reduction of nitrate to nitrite (de-nitrification) and the anaerobic oxidation of ammonia, both of which are anaerobic processes. Seawater in both the header tanks and liners was normoxic in all CO_2 treatments (Table I). However, it is possible that during the ammonia oxidation incubations, which lasted approximately 24 hours, oxygen may have become depleted within the incubation vials, triggering these other pathways. For example, nitrate was high in the header tank seawater in control conditions at twenty weeks (raw nutrient flux data, not shown), so de-nitrifcation may have been stimulated by possible exhaustion of oxygen and abundance of substrate (nitrate),

Deliverable 4.1: Potential impact of CCS leakage on marine communities
WP4; lead beneficiary: Plymouth Marine Laboratory

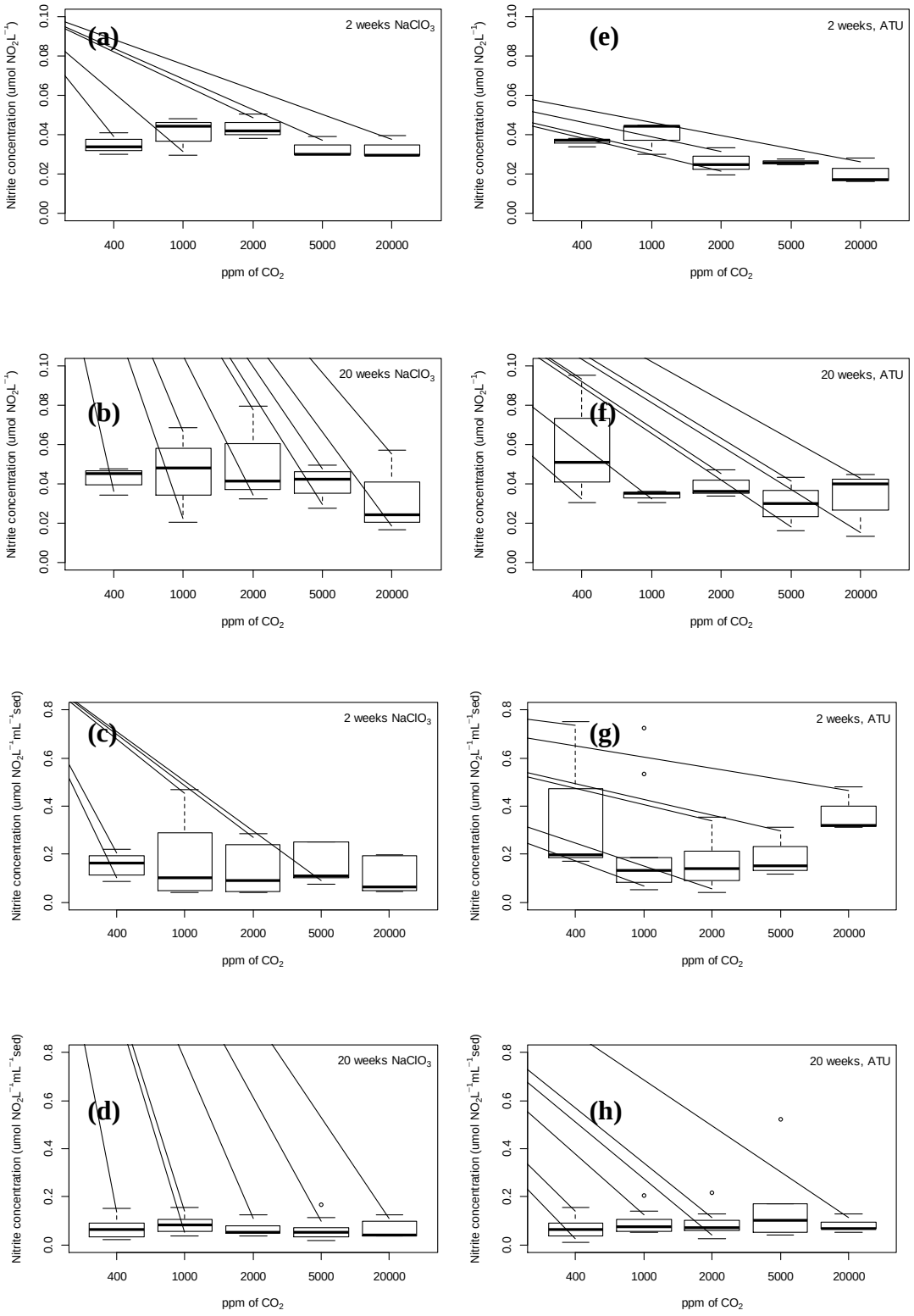

Figure 20: Nitrite concentration measurements in seawater (a,b,e and f) and sediment (c,d,g and h) used to estimate ammonia oxidation rates during the high CO_2 experiment (section 3.5.1.3).

explaining the peak in nitrite in the ATU treated control seawater samples at the end of our incubations in fig. 20.

Ammonia oxidation rate estimates for the seawater and sediment are summarized in figure 21a and b, below. The range of values measured are in in line with Kitidis, Laverock et al. (2011) which measured rates associated with CO_2 disturbances in three distinct ecosystems. Ammonia oxidation rates with negative values indicate higher availability of Nitrite in ATU than in $NaClO_3$ treated samples (fig.15), as discussed above. Contrary to the standing paradigm (Beman, Chow et al. 2011; Kitidis, Laverock et al. 2011), we found that ammonia oxidation in the water column did not appear to decrease with increased CO_2. Rather, it appeared to be stimulated above 1000 ppm CO_2 in relation to control conditions (fig. 21a), where the rates were near zero. At two weeks of exposure, ammonia oxidation rates above 1000 ppm of CO_2 were consistently statistically different for zero across seawater samples and treatments, while at lower CO_2 levels, they were not. This interpretation could not be corroborated by the nutrient flux data, which was highly variable. At twenty weeks, this change was not observed, but this result may be a reflection of possible seasonality in microbial activity (winter months), as sedimentary nitrite was low also in control conditions at this stage (fig.21b), consistent with the findings in section 3.3.1. It is also possible that at twenty weeks, such results may be confounded by the high values of nitrite we measured in the ATU treated sediment samples (fig.20h), which may have resulted from other biogeochemical pathways.

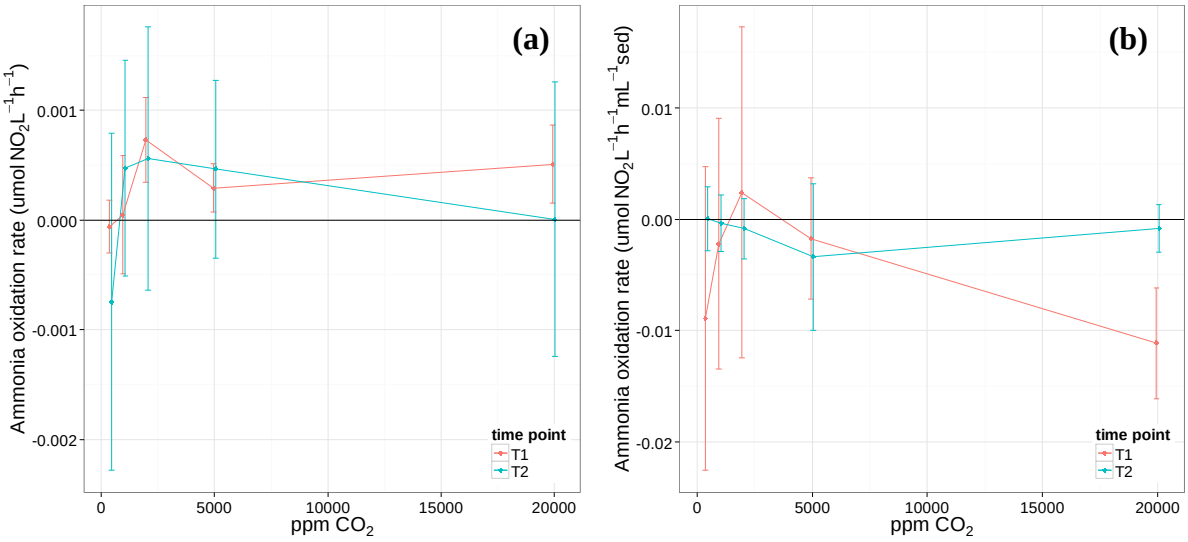

Figure 21: Ammonia oxidation rates in the seawater (a) and sediments (b), estimated during the high CO_2 experiment (section 3.5.1.3).

In the sediment, and in agreement with other studies, ammonia oxidation did not appear to change in relation to CO_2, being low and not statistically different from zero in any of the treatments, at 2 or 20 weeks of exposure (Figure 21b). So overall, sedimentary ammonia oxidation did not appear to be significantly impacted by our CO_2 treatments, and the short and medium-term exposures (T1 and T2). Covnersely, seawater ammonia oxidation rates appeared to be stimulated above 1000 ppm of CO_2 in comparison with the control data, in which rates were variable, and overall close to zero. This result suggests that a possible effect of CO_2 on ammonia oxidation could occur even after short term exposures (T1, 2 weeks), and that this type of leakage scenario has the potential to significantly impact seawater nitrogen cycling. However, this potential finding could not be confirmed by the nutrient flux data, which exhibited high variability. The lack of observed long term effects of exposure to CO_2 on ammonia oxidation may have been played down in this experiment by variability associated with possible seasonality in microbial activity (see section 3.3.1). Future studies examining the effects the length of exposure duration in the context of CCS leakage should thus take this element of natural variability into account.

3.5.1.4 Sediment-water fluxes of dissolved oxygen, dissolved manganese, total alkalinity, TIC and H+

The fluxes rates in the overlying water measured during the high CO_2 experiment at T2 are shown in figure 22, below. No measurements were successful at the other time-points.

Sediment Oxygen Consumption (SOC) values for the control experiment (3.3 mmol O_2 m^{-2} d^{-1} in electrode measurement, and 3.9 mmol O_2 m^{-2} d^{-1}in Winkler measurements,), Figure 22 a and b) were lower than those determined in the field at that time (approx.9.6 ± 7.7 mmol O_2 m^{-2} d^{-1} (n=2). That is a reasonable value, since the sediment in these experiments had been isolated from a natural input of organic matter for 20 weeks, at this point. Both electrode and Winkler estimates showed that SOC decreased with increasingly acidic conditions.

Calculated on the base of pH, sediment consumption of H+ (fig. 22, actually an apparent sediment consumption of H+, because sediment –water exchange is one of factor affecting sediment water H+) indicated that the direction of this "flux" changes in the most acidic conditions (pH=6,6): This may be due to carbonate dissolution in the sediments.

The flux of Mn was variable. Some liners exhibited much higher fluxes of manganese from the sediment to the overlying water than others. This can testify to a patchiness of this flux, that can be influenced by the micro scale features, i.e. presence of Mn nodules or bioirrigation effects. Subsurface pore water often has high concentrations of dissolved, divalent manganese. Under well oxygenated bottom water, upwards diffusing Mn^{2+} will normally be trapped by oxidation and precipitation within the sediment, near the sediment-water interface. However, a random disturbance of this Mn cycling, e.g. by bioturbation, can easily produce occasional leakage of dissolved Mn into the overlying water. We cannot explain the efflux of Mn from the sediment in the most acidic conditions. TA consumption increased with decreased pH and no significant effect was measured in seawater TIC in relation to CO_2 treatments.

(b)

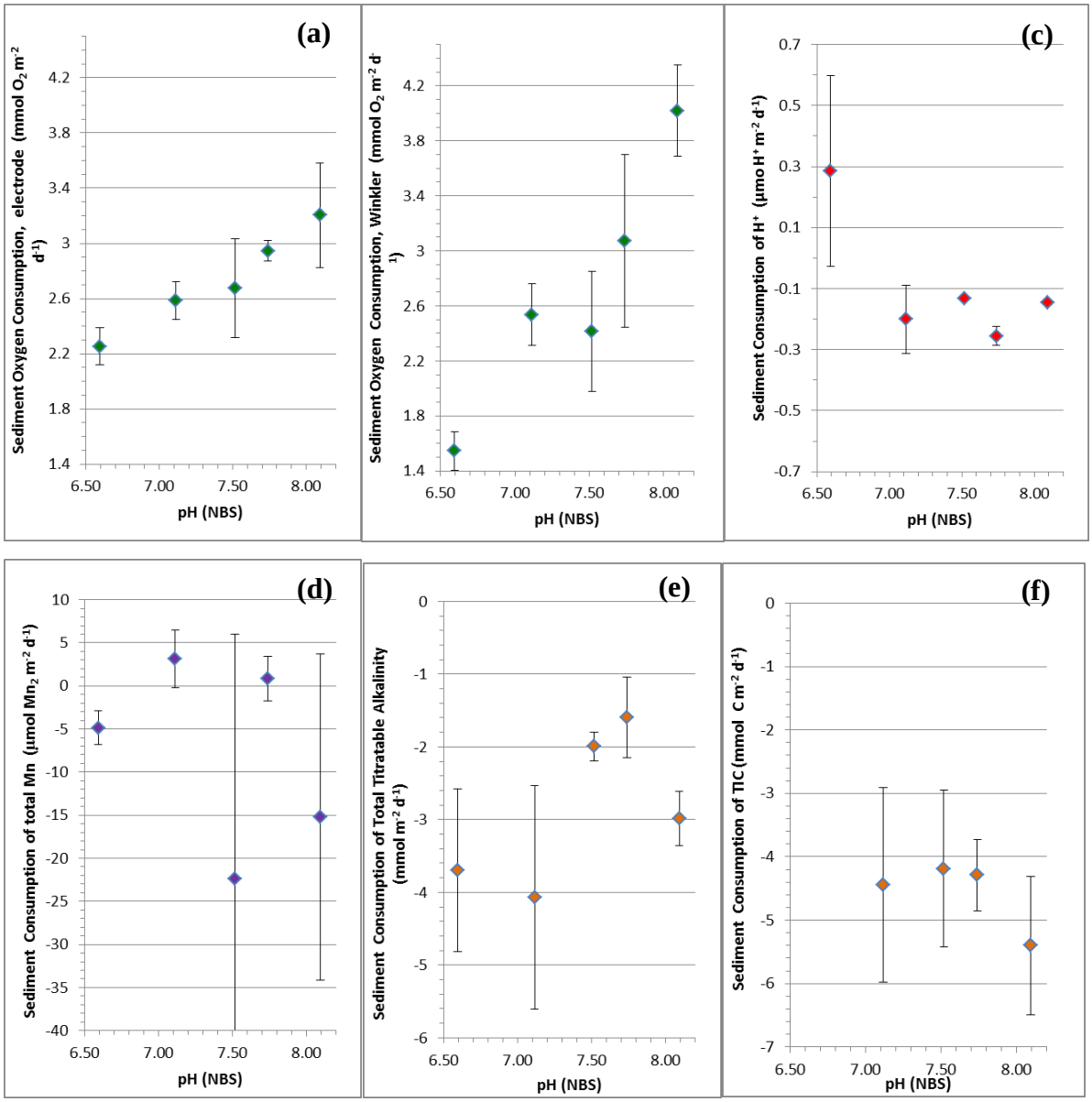

Figure 22: Oxygen and carbonate chemistry in the water column at T2. Sediment Oxygen Consumption measured in tanks using Clark electrode (a) and Winkler (b) techniques (see 2.1.1 for methods). Sediment Consumption of H+ (c), total Mn(d), Total Titratable Alkalinity (e) and total inorganic carbon (f) measured in tanks at T2.

3.5.2 Formation water leakage mesocosm experiment

3.5.2.1 sedimentary pore-water oxygen, pH, sulphide, redox, alkalinity, phosphate, nitrate + nitrite, ammonia, manganese (II) , iron (II), DIC, Ω_{Ar} and Ω_{Ca} profiles

The sediment in the liners was characterized as mud, having a mud content of 95.36 ± 1.64 % (mean ± sd), and sediment porosity within the first cm horizon was 78.89 ± 6.85% (mean ± sd). The corresponding profiles for pH, sulphide (pS) and redox (Eh) are given below, at the begining of the experiment (T0, figure17 a-c), and at the end (T1, Figure 23 d-e). In control conditions, sedimentary pH varied btween 8 and 7.6 units. At the end of the experiment, high salinity treatments (high salinity and mixed treatements) had pH profiles that were more acidic overall. This effect can impact burrowing fauna, which have been found to surface in response to short-term drop in pH (Murray, Widdicombe et al. 2013). Indeed, shallower burrowing depth was observed in fauna exposed to the high salinity treatment (section 3.6.2, fig.35b). Treatments with low oxygen (hypoxic and mixed treatments) had shallower redox transition depths overall (Figure 23f). This effect may also have impacted burrowing fauna, which tends to concentrate above the redox transition to avoid the formation of H_2S (Aller 1982; Birchenough, Parker et al. 2012). This effect was indeed observed, as bioturbation depth was also shallower in the hypoxic and mixed treatments in relation to the controls (section 3.6.2, fig. 35b). The hypoxic treatment did indeed have the highest concentration of sulphide (fig.23e).Thus, the experimental treatments used here to simulate a short term exposure (2 weeks) to formation water released through CO_2 injection into sub-seabed reservoirs, were found to modify sedimentary conditions.

The maximum oxygen penetration depth (10 mm) was found in the Control and Hypersaline treatments (Annex II, Fig. A1), when dissolved oxygen (DO) concentrations in the water were 125-160 µM. Minimum DO penetration was observed in the Mixed and and Hypoxic treatments (3 mm), with DO content in the bottom water of around 30-40 µM. The Tidal treatment induced and intermediate penetration depth of about 7 mm. The depth of DO penetration doesn't seem to depend on salinity. See annex II for DO plots.

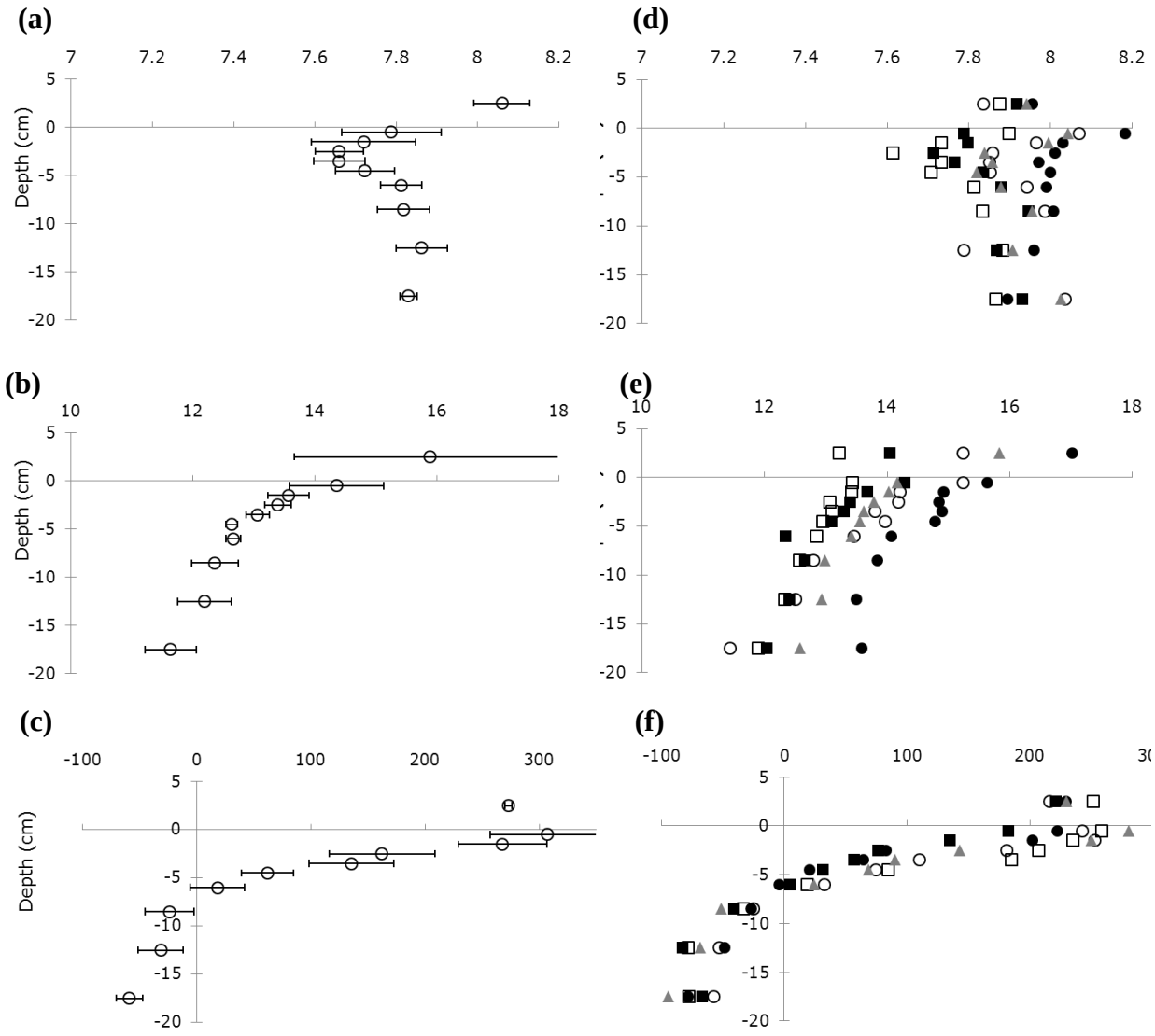

Figure 23: Profiles of pH (-log$_{10}$[H$^+$] ,a and d), sulphide (-log$_{10}$[H$_2$S total], b and e), and redox (mV, c and f) within the sediment (depth, cm), estimated during the formation water experiment at T0 (left) and T1 (right, section 3.5.2.1). Symbols represent control (○), high salinity (□), hypoxia (●), mixed (■), and tidal treatments (▲) . All values are averaged over measurements carried out in the four replicate sediment cores used to assess the vertical distribution of fauna (section 3.1.2).

Phosphate was characterized by concentrations 2-5 µM in the upper 12 cm of the water column and its distribution was of irregular character (at least with the sampling resolution used, Annex II, Fig. A2 for all plots). The upper layer of the sediment was enriched with nitrate (up to 40 µM). Its concentration then decreased, but remained high (5 µM) even in anoxic conditions. This can be probably explained by an oxidation of ammonia during sampling and storage of the samples. The concentrations of ammonia generally increased

from low values up to 80-120 mm in the deepest layer 10-15 cm. The distribution of Mn^{2+} was characterized by a maximum (50-130 µM) in the layer 3-5 cm. Concentrations of Fe^{2+} had a general tendency of an increase in the deeper layers > (to about 50 -70 µM). Alkalinity was in the limits 5200-6400 µM with a tendency of an increase with depth. The values of DIC were in the limits 5200-6400. The upper 2 centimetres of the pore water was oversaturated for both calcite and aragonite, while in the deeper layer (5-15 cm) the pore water was close to saturation or undersaturated for aragonite (Figure A2, Annex II).

In general, a clear connection between the experimental treatments and the profiles for alkalinity, phosphate, nitrate+nitrite, ammonia, manganese (II) , iron (II), DIC, Ω_{Ar} and Ω_{Ca} was not evident (Annex II). However, the more typical pattern of a replacement of nitrate with ammonia in the deeper layer, a maximum of Mn^{2+} followed by a maximum of Fe^{2+} was found in the Control treatments but not others. The classical increase of alkalinity with sediment depth was most pronounced under hypersaline conditions.

The apprently small observed changes in sedimentaty bigeochemical profiles appeared to cause or at least be linked to changes in macrofauna behaviour within the sediment, that are consistent with physiological stress (3.6.2) It is thus likely that such changes induced by even short term exposures to stressors associated with the release of formation water may have discernable, negative consequences for burrowing communities (see section 3.6.2). These effects may be directly linked to the increase in salinity and decrease in oxygen simulated here, or to the consequential measured effects on pore-water profiles.

3.5.2.2 Nutrient fluxes

The experimental treatments had a significant effect on nutrient fluxes. The main finding is that the natural variability observed in nutrient fluxes in the controls (Figure 24) was limited in the other treatments, although different stressors appeared to drive different nutrients in various ways. The high variability observed in the controls somewhat limits the statistical approaches we were able to use, and so focus is drawn to particular cases in which the nutrient fluxes appeared to be consistently driven in a specific direction, between treatments. Of particular interest is the case that the single-stressor treatments (hypoxic and high salinity)

appear to cause directional changes in the nitrogen cycle, but multi-stressor treatments (mixed and tidal) appeared to cause change that was not directly a sum of the former. The combination of the two individual stressors (hypoxia and high salinity) on the microbes mediating nutrient cycling, or on the fauna impacting those processes (e.g. bioturbation, excretion), was thus greater than that expected from the sum of the individual stressor impacts. These effects were observable when all the nutrient data were pooled together (Figure 25), and the liners from the multi-stressor treatments exhibited the greatest departure (overall) from the other treatments.

Nitrite fluxes varied the most in control conditions, where the highest rates of both production and uptake in the sediment were measured. Variance was the lowest in both hypoxic and high salinity treatments, where the values were concentrated around zero. It appears that in these treatments, pathways associated with nitrite production and uptake in the sediment may have thus been balanced (fig.24b). Conversely, nitrite was high in liners and low in header tank seawater in the tidal treatment, indicating the presence of a marked and consistent flux from the sediment into the water column in the liners, which was not present in other treatments (i.e. negative flux, fig.24b one-way Analysis of Variance: R^2= 44.55% and $p< 0.05$). This result suggests that the tidal treatment may have stimulated nitrite production within the sediment.

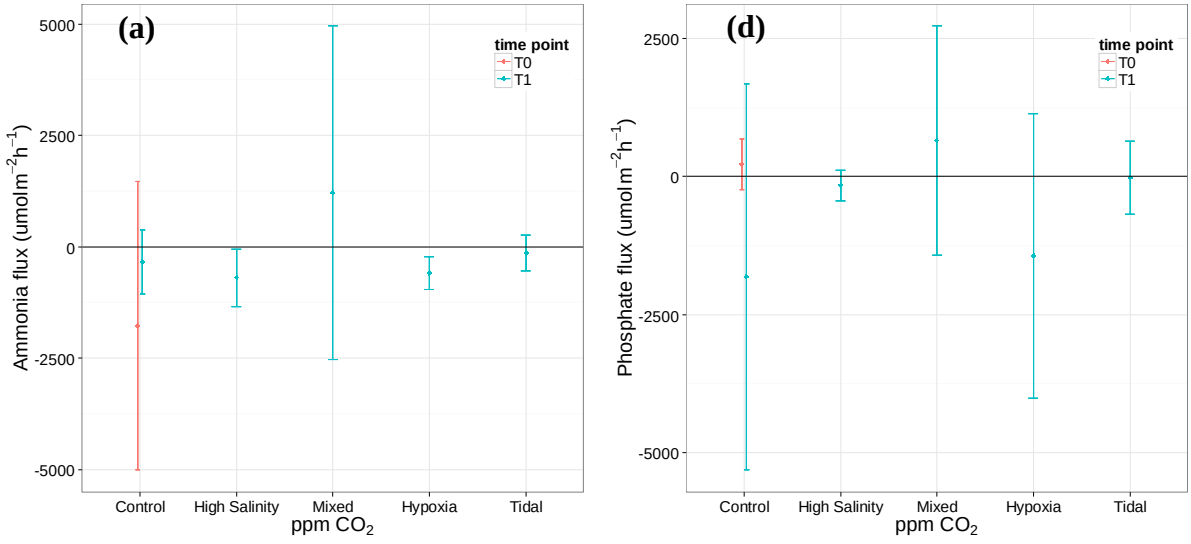

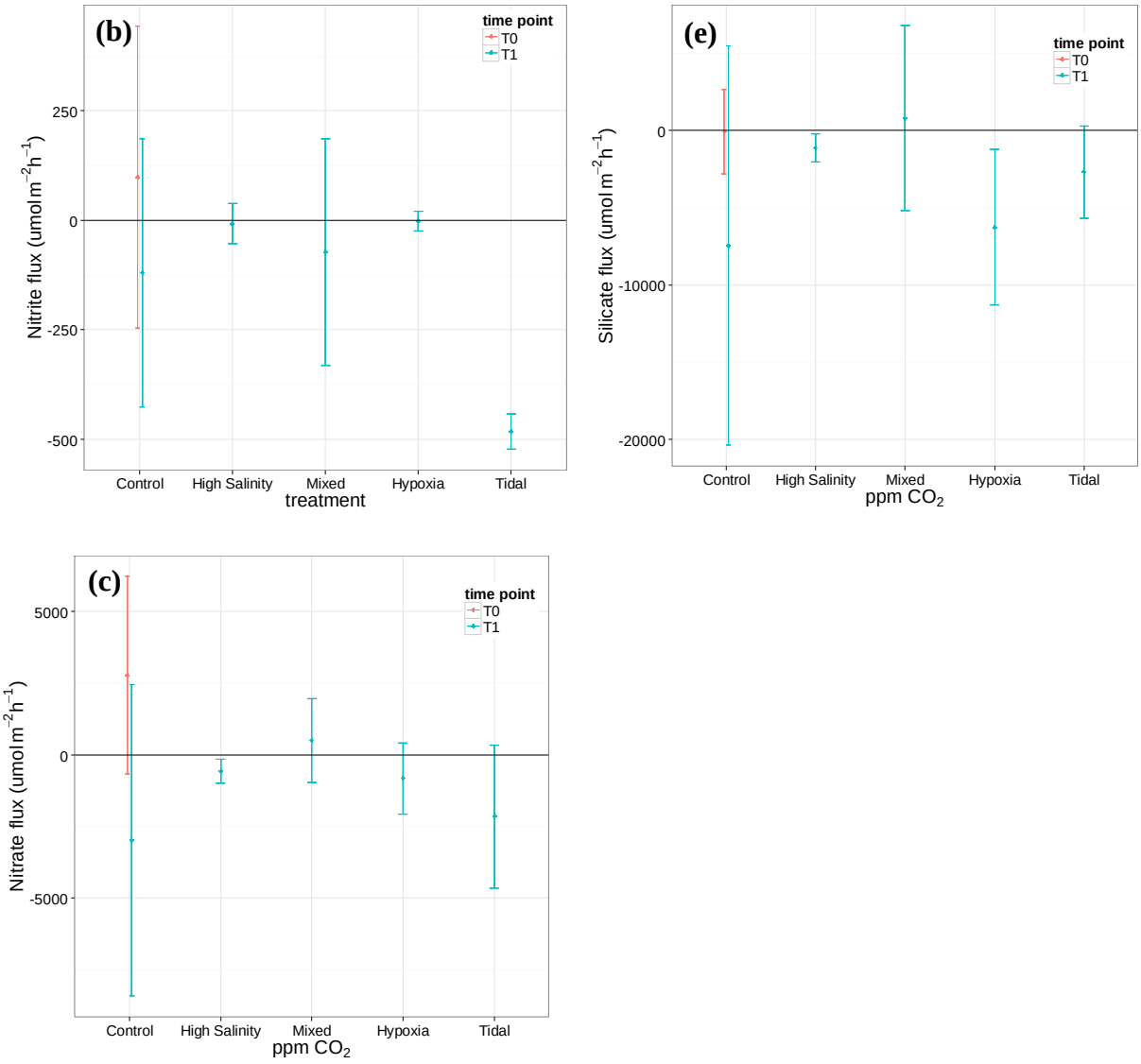

Figure 24: Fluxes of Ammonia (a), Nitrite (b), Nitrate (c), Phosphate (d) and Silicate (e) measured during the formation water experiment (section 3.5.2.2).

Ammonia fluxes were not significantly impacted by experimental treatments statistically. (fig.24a). However, production of ammonia from the sediment (negative flux) was consistently observed in the hypoxic treatment (to a less extent also in the high salinity treatment). The spike in sedimentary nitrite observed in the ATU treated samples from the hypoxic treatment (see section 3.5.2.3) suggests that denitrification may have been stimulated by hypoxia, reducing nitrate to nitrite and eventually to ammonia in this treatment. Thus, hypoxia appeared to stimulate denitrification, in relation to the controls.

Nitrate fluxes were not statistically significantly affected by experimental treatments overall, with variance observed between replicates, particularly in control conditions, leading to error bars that overlapped with zero (fig.24c). There was a suggestion of production of nitrate within the sediment in the tidal treatment, as was observed with nitrite (fig.24c). Consistency, across analyses, was observed in the high salinity treatments, where release of nitrate from the sediment was consistently observed (negative fluxes observed in all samples, fig. 24c). This finding is consistent with a high and significant ammonia oxidation rate observed in surficial sediments in the high salinity treatment (see section 3.5.2.3, fig.27b), suggesting that sedimentary nitrification (at least at the sediment water interface) was stimulated by high salinity, departing from the results observed in control conditions (i.e. ammonia oxidation was not consistently observed in the controls).

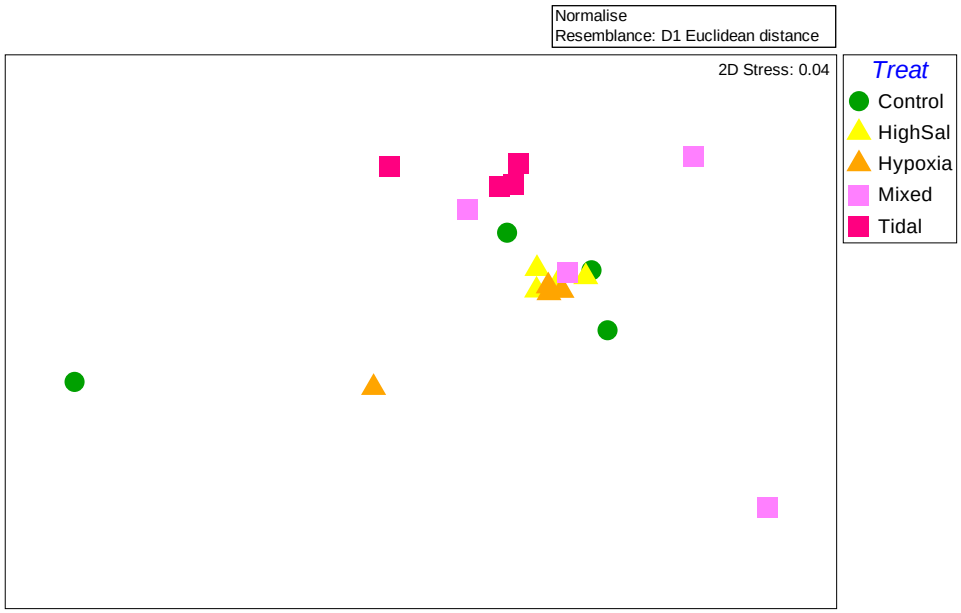

Figure 25: non-linear Multi-Dimensional Scalling plot illustrating the dissimilarity (Euclidean distance) between samples based on all (normalised) nutrient fluxes together. Note how the multi-stressor treatments (mixed and tidal) exhibit the overall greatest departure from the other treatments, except for controls.

Phosphate and silicate fluxes exhibited similar patterns of impact by experimental treatments, but these were not statistically significantly different from the controls, overall. Release of phosphates from sediments did not increase in low oxygen in relation to the controls (negative flux, fig.24d), contrary to the expectation that iron oxy-hydroxides (important in the adsorption of phosphate) would be converted to iron sulphides in low oxygen conditions (Krom and Berner 1980). This result may be a consequence of the high variability observed

in the controls, or a consequence of oxygen availability not changing markedly between the two treatments within sediments (not measured). A flux of silicate from the sediments was consistently observed in the hypoxic treatment (and to an extent in the high salinity treatment). Silicate in sediments is required by the growth of diatoms and some foraminifera, and the release of silicate from muddy sediments is typically dominated by the regeneration of biogenic silica from accumulated organic material, consequentially from dead and decaying diatoms and hypoxia intolerant, silicated foraminifera (Marinelli 1992; Platon, Sen Gupta et al. 2005; Widdicombe and Needham 2007). As such, it is suggested that the observed flux of silicate may be indicative of increased mortality of benthic diatoms or forams under hypoxic conditions. There is plenty of evidence in the literature to suggest that foraminifera communities can be highly sensitive to consistent reductions in bottom water oxygen (Alve and Nagy 1990). Analysis of alkalinity data in these treatments will aid this interpretation, as silica tends to dissolve in high alkalinity.

In summary, the short term chemical changes imposed by the experimental treatments that simulated formation water release caused discernable impacts in the flux of nutrients between the sediment and seawater, in relation to control conditions. These results are corroborated by the results of the ammonia oxidation analysis and bioturbation (sections 3.5.2.3 and 3.6.2). In summary, hypoxia stimulated denitrification and an increase in silicate fluxes, and high salinity stimulated ammonia oxidation, in relation to control conditions. These changes are likely to have significant implications for benthic-pelagic coupling in impacted ecosystems. The duration of these impacts, and recovery from them, would thus depend on the ability of the local hydrodynamic regime to disperse/ dissolve formation water plumes. The tidal and mixed treatments caused variable responses that could not be easily interpreted across the various datasets, but see section3.6.2, which suggests that these systems exhibited, overall, the greatest change from the controls.

3.5.2.3 Ammonia oxidation in the water and sediments

Nitrite levels in seawater and sediments in ATU and $NaClO_3$ treated samples are summarized in figure 26. We used ATU and $NaClO_3$ in the same way as in the high CO_2 experiment,

because they inhibit NH_3^- and NO_2^- oxidation, respectively, impacting the fixation of nitrogen. All values measured were above the detection limit of the instrument, which was 0.005 and 0.009 µmol NO_2^- L^{-1}, for seawater and sediment samples, respectively (Kitidis, Laverock et al. 2011).

Ammonia oxidation rate estimates for seawater and sediments are provided in figure 27 a and b, respectively. These rates were variable in control replicates, and thus averaged around zero, in both sediment and seawater samples. Negative rate estimates indicate that nitrite concentration was higher in ATU treated samples (where ammonia oxidation is inhibited, figure 26 c and d) than in those treated with $NaClO_3$ (in which oxidation of nitrite to nitrate is inhibited, figure 26 a and b). We found that in both sediment and seawater, hypoxia and high salinity appeared to have inverse effects on ammonia oxidation rates. I.e. hypoxia caused negative oxidation rates, which were more consistently measured in the sediment samples (fig.27 b). This result appeared to be driven by a marked spike in nitrite in all ATU treated sediment samples, suggesting that this effect was consistent across replicates (fig.26c). The parallel observation of increased production of ammonia in the sediment in the hypoxic treatment (section 3.5.2.2) indicates that this nitrite concentration is probably a result of a stimulation of denitrification in relation to control conditions (fig. 24a and fig.26c). Conversely, high salinity appeared to cause a consistent increase of ammonia oxidation rates in relation to controls, that was statistically different from zero in the sediment samples, but more variable in seawater samples (fig. 27b). This result is driven by high values of nitrite measured in the $NaClO_3$ but not ATU treated sediment samples (fig.26 a and c), consistent with a statistically significant flux of nitrate from the sediment into the water column (negative flux, fig. 24c). Together these result point towards the stimulation of nitrification pathways in relation to controls, caused by high salinity. This positive effect appeared to be dominant with regard to ammonia oxidation in the seawater when the two stressors were combined (mixed treatment, fig. 24a), while for sedimentary communities, this effect was not observed, suggesting a difference in the microbial communities driving these pathways in the sediment and seawater. The effect of hypoxia or high salinity in single and the multi-stressor mixed treatment on ammonia oxidation were however not observed the seawater and

sediments exposed to the tidal treatment, suggesting that tidal variability may enable the recovery/ or limit the overall impacts of these stressors on microbial communities.

So in summary, the short term exposures of these microbial communities to hypoxia and high salinitiy associated with formation waters caused marked effects on ammonia oxidation. Analysed in conjuction with the nutrient flux measurements (section 3.5.2.2), this experiment suggests that even short term exposures to formation water can significantly impact nitrogen cycling in both sediment and seawater. However, these effects appeared to be to an extent mitigated by tidal flushing. Hence, an understanding of hydrodynamic conditions (i.e. bottom currents) near plume sites may be an important component of quantifying the potential impact of formation water release in a CCS risk assessment.

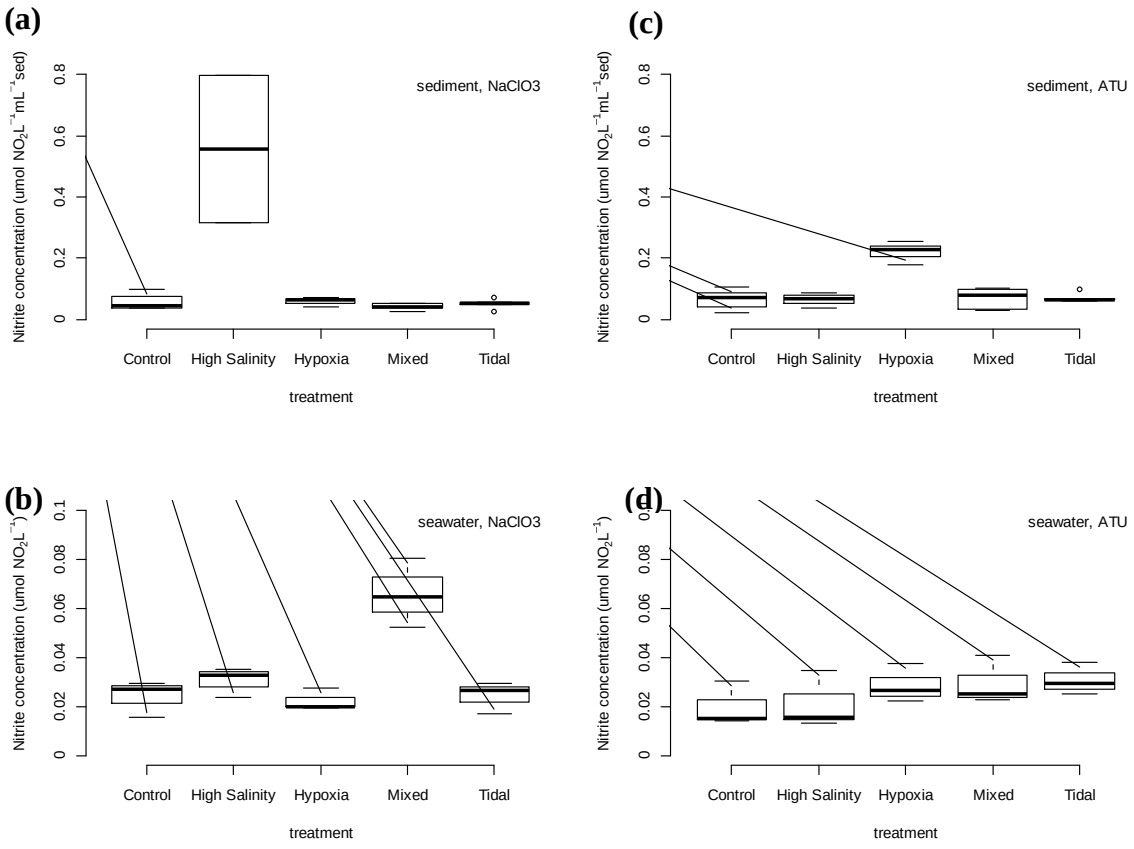

Figure 26: Nitrite concentration measurements in $NaClO_3$ treated sediment and seawater samples (a and b, respectively), and in ATU treated sediment and seawater samples (c and d, respectively), used to estimate ammonia oxidation rates at the end of the formation water experiment (section 3.5.2.3).

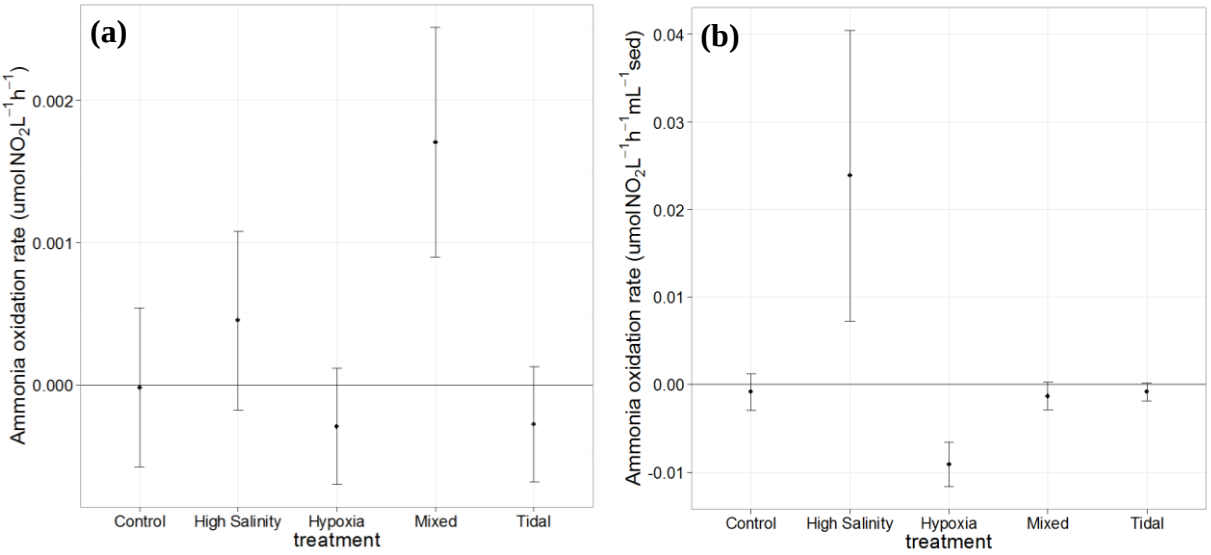

Figure 27: Ammonia oxidation rates in the seawater (a) and sediments (b), estimated during the formation water experiment (section 3.5.2.3).

3.5.3 Natural seeps

3.5.3.1 Water column

The Panarea sites at Basiluzzo rock Island exhibited specific biogeochemical properties. The analysis carried out by GEOMAR of videos acquired at bottom of CO_2-impacted sites showed that CO_2 vents were characterized by an average bubble size of 1.14 cm (radius range: 0.94 – 1.30 cm) and gas-flow of 11.1 ml sec^{-1} (range: 9.2 – 15.3 ml sec^{-1}).

CTD data on water column stratification and pH were by OGS/UniRoma1used to decide the location and depth of discrete water sampling for various chemical and biological analyses. Among chemical parameters studied, data on seawater carbonate system (pCO_2 and dissolved inorganic carbon, i.e. DIC), silicate and hydrogen sulphide appear the most relevant to identify CO_2 the presence of seeps. The greatest impact occurred at St. B1 during June 2012 campaign, when the strongest water column stratification was present. The leaking CO_2 was therefore less rapidly diluted in the bottom waters, resulting in the increase of seawater pCO_2 and DIC values, and a decrease in pH. Measured inorganic nutrients did not show a significant correlation with CO_2 leakage points, with the exception of silica. This may leach

due to reactions between the acidified waters and the shallow sediments, or due to co-migration of silica-charged waters together with the CO_2, and silica exhibited a very similar distribution in the water column to that of pCO_2 and pH.

Along the transect between Bottaro and Lisca Bianca Isles (LB transect), data on the carbonate system, nutrients, basic aqueous chemistry, allowed the identification of three main anomalous areas, with one on either side and one above the mount itself. In correspondence of this geothermal spring, hydrogen sulphide concentration as well as the partial pressure of CO_2 (max = 11020.1 µatm) exhibited very high values. These results clearly evidence the presence of gas leakage from the seabed at this point, which can influence the water column chemistry. In particular, in the same water mass, an extraordinary acidification was detected (pHT min = 6.680) in association with undersaturation of the aragonite ($\Omega_{Aragonite} < 1$) (Figure 28)

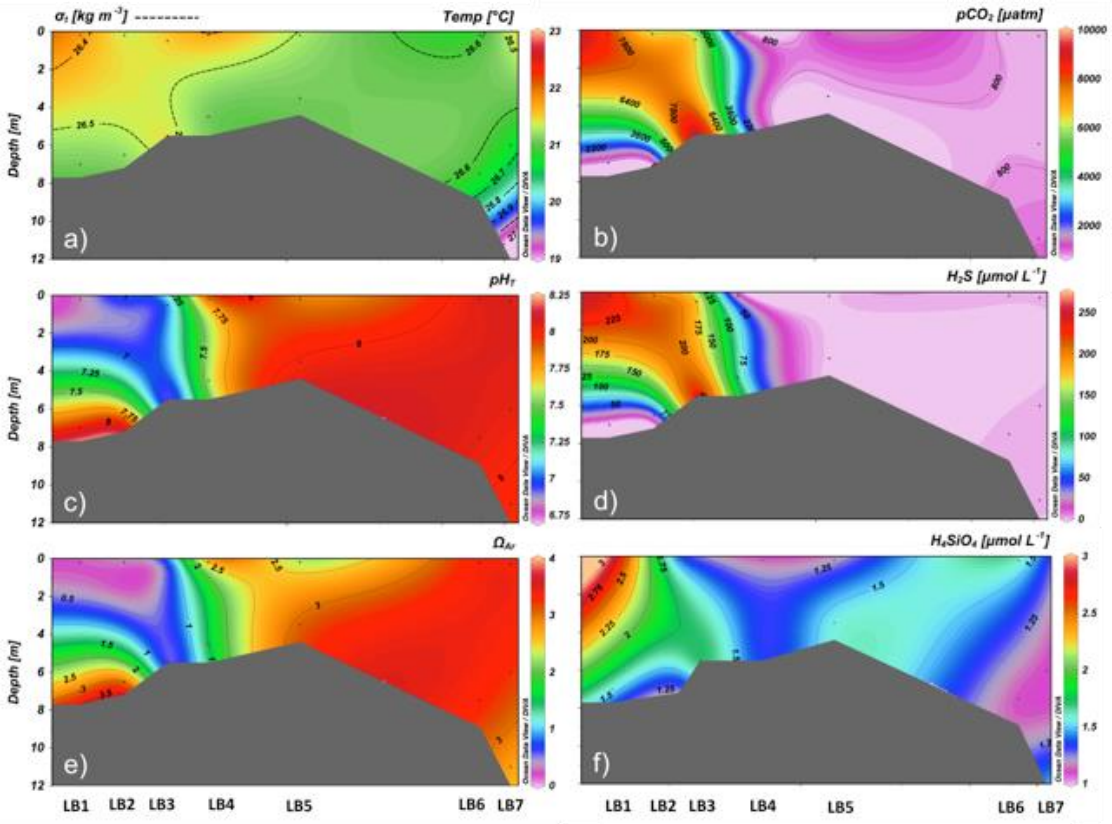

Figure 28: Contour plot of seawater (a) temperature - density anomaly (σt – dashed isolines), (b) partial pressure of CO_2 (pCO_2), (c) pH at total scale (pHT), (d) hydrogen sulphide, (e) aragonite saturation state (ΩAr), and (f) silicic acid, along the transect between Bottaro and Lisca Bianca Isles (section 3.5.3.1).

Such extreme seawater acidity represents the typical condition of the CO_2 vents in this area and it could easily lead the dissolution of calcareous shells or skeletons of calcifying organisms.

The high increase of the silicates concentration observed in correspondence with the hydrothermal vents probably as a consequence of the turbulence induced by the seepage of gas bubbles which transport upwards the interstitial water enriched in silicates.

Despite the occurrence of this significant leakage-related trend, the other measured nutrients did not exhibit similar variation in relation to the presence of the vents (i.e. ammonium and phosphate might be expected to increase together with the silicates). The reason for this discrepancy is under investigation, but this was also observed in the mesocosm experiments (section 3.5.1).

3.5.3.2 Sediments

The effect of CO_2 seabed emissions was clearly visible on pore water chemistry, and concurrent pH reduction, increase of DIC and, alkalinity, reduction of and $\Omega_{calcite}$ (<1), and enhanced of chemical weathering (high concentration of iron, manganese and silicate) were observed along sediment profiles in CO_2-impacted sites (Figure 29).

At St. B3, all these parameters exhibited high variability and, on average, they had intermediate values compared to those measured at other CO_2-seep (St. B1) and at the reference site (St. B2). This suggests a weaker or less constant CO_2 flow at St. B3 than at St. B1. Conversely, the concentration of nutrients (ammonia, nitrite, nitrate and phosphate) in pore waters did not vary significantly between CO_2-impacted sites and non-impacted sites.

Coarse sand was the dominant fraction in all three sites (from 40% to 60%), with variable contributions of fine and medium fractions. Mean grain size was somewhat higher at the reference site (average 775±37 µm in 2012 and 699±12 µm in 2013; ANOVA, $p<0.0001$) compared to Grey-CO_2-seep (658±88 µm in 2012 and 640±16 µm in 2013) and Red-CO_2-seep (508±87 µm in 2012 and 548±20 µm in 2013). The differences in granulometry between the sites concerned mainly the medium and coarse sand fractions, thus there was no significant difference in porosity between Background and CO_2-seep sites (values of ca 50%).

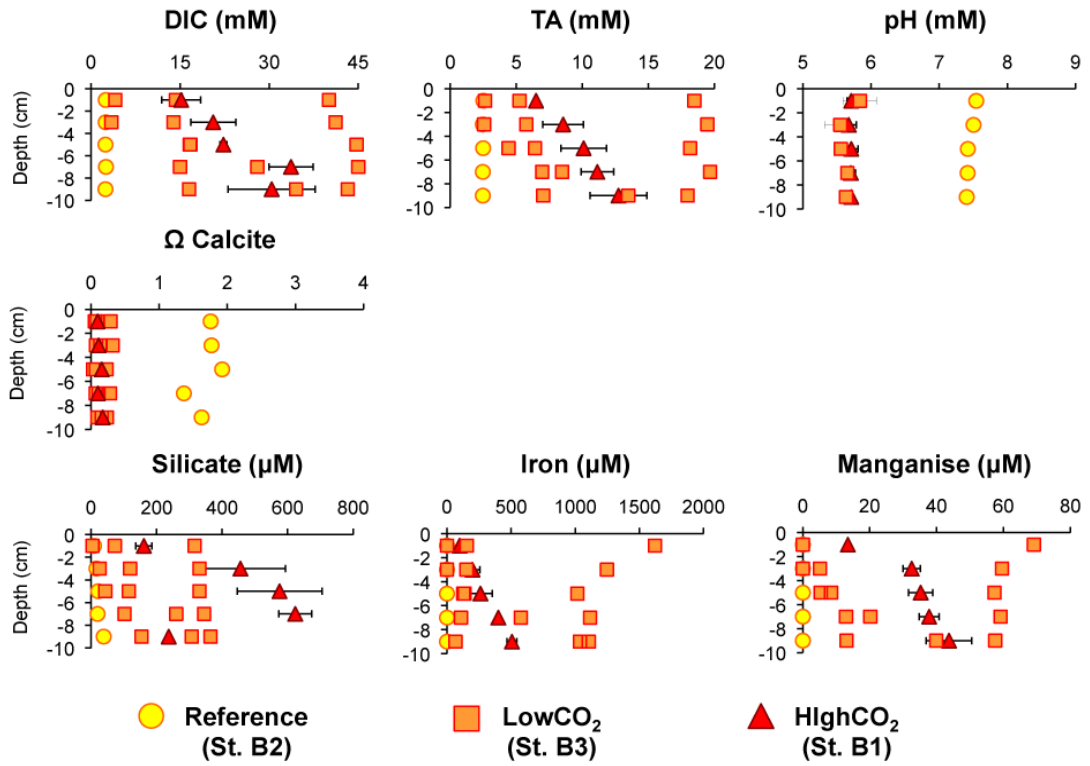

Figure 29: Sediment profiles for DIC (dissolved inorganic carbon), TA (total alkalinity), pH and concentration of silicate, iron and manganese are showed. Pore-water samples were obtained with the help of the TUBO device and by using Rhizons MOM (19.21.21F, mean pore size 0.15 µm; Rhizosphere Research Products, Wageningen, Netherlands) attached to 10 mL-syringes (for more sampling and analytical details please see cruise report ECO2-3). If sample's replicates had a variability of less than 25%, then the average and standard deviation are reported. Otherwise, all replicate profiles are plotted.

Sediment porosity was found to be ca 50% in all sites investigated, with no variation observed along sediments profiles. Sediment samples were also analysed for phytopigment content (chlorophyll-a and phaeopigment) and total organic matter (TOM). In all sedimentary layers analysed, the amount of chlorophyll-a in the sediment was significant higher at High CO_2-seep (8.7±3.5 µg.g^{-1} dwt) compared to the Reference and Low CO_2-seep sites (1.2±0.4 µg.g^{-1} dwt and 2.0±0.8 µg.g^{-1} dwt, respectively; ANOVA, $p<0.0001$). We observed also significant differences in phaeopigment content (ANOVA, $p<0.0001$), which decreased significantly from sediments of HighCO_2-seep to those of LowCO_2-seep and the reference site. TOM exhibited higher variably than phytopigments in the sediments investigated, and sediments of the High CO_2-seep sediments had a TOM content significantly higher compared

to LowCO$_2$-seep and Reference sediments (1.2±0.5 % vs. 0.7±0.3 % and 0.7±0.6 %, respectively).

In the sites investigated in October 2012 and May 2013, the grain size of the sediments was dominated by coarse and medium sand (sand generally > 80-90 %); gravel contributed from 0.4 to 21 % while mud was negligible (always lower than 0.4%).

The distribution of total carbon (TC), organic carbon (TOC) and total nitrogen (TN) is quite variable both among the stations and the campaigns (Figure 30). Very high TC values characterized the October 2012 campaign showing a maximum > 2 mg C g^{-1} at station B2 where the minimum of TN concentration was detected. TOC constituted from 47% to 96% of the TC reaching the highest percentage at the hot part of the CB station. In May 2013, a general decrease of concentrations (both of carbon and nitrogen) characterized all the sampled stations with values up to 2- and 9-fold lower for carbon and nitrogen, respectively. These differences could be ascribable to the variation of the sediment grain size and to the changes in the benthic biomass.

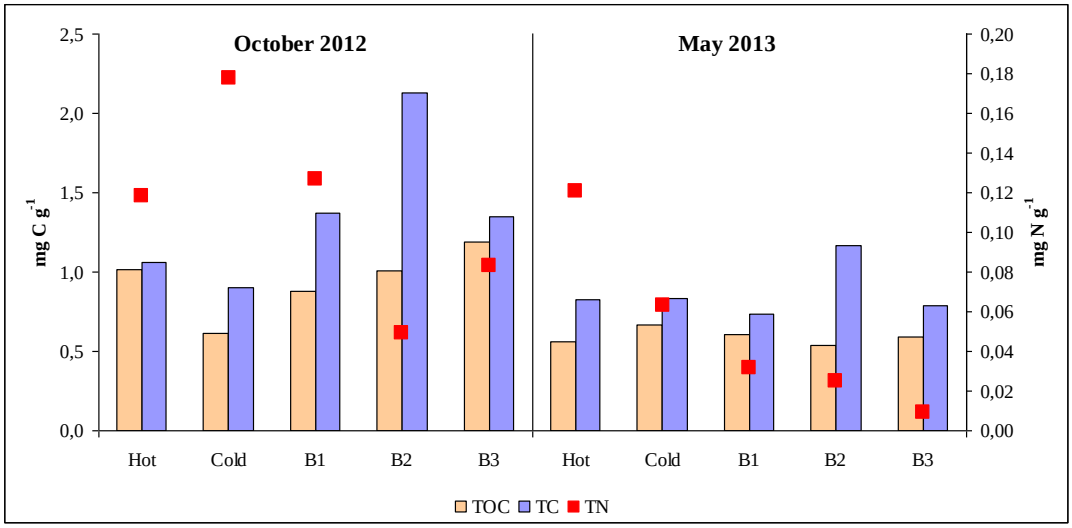

Figure 30: TC (Total Carbon), TOC (Total Organic Carbon) and TN (Total Nitrogen) concentrations in the sediment sampling in the studied area in October 2012 and May 2013 campaigns.

A similar trend was observed also in the biopolymeric carbon (BPC) content of sediments from the same campaigns (Figure 31). In October 2012, the total content of BPC was relatively low (~ 260 µg C g^{-1}) at the reference site (St. B2) and the cold part of CB station,

while approximately 2-fold higher concentrations were detected at the two CO_2 impacted stations (B1 and B3) and at CB-HOT station. Lipids were the dominant fraction of the BPC pool, followed, with the only exception of station CB-COLD, by proteins. EDTA extractable carbohydrates were generally lower while water soluble carbohydrates were not detectable.

Both lipid and protein contents were 2-fold higher in hot sediments than in cold ones. This variability could be attributed to the elevated densities of microalgae in the hot site. A similar trend was observed also at Basiluzzo site with the higher values measured at the CO_2 impacted stations in respect to the control site but without the same correspondences with the benthic communities.

During the May 2013 campaign, the BPC concentrations dropped off reaching values lower than 200 µg C g^{-1} at all the stations. Similarly to the pattern observed in TOC, the higher decrease was detected at stations CB-HOT, B1 and B3 and it was attributable to a drastic reduction of lipid contents.

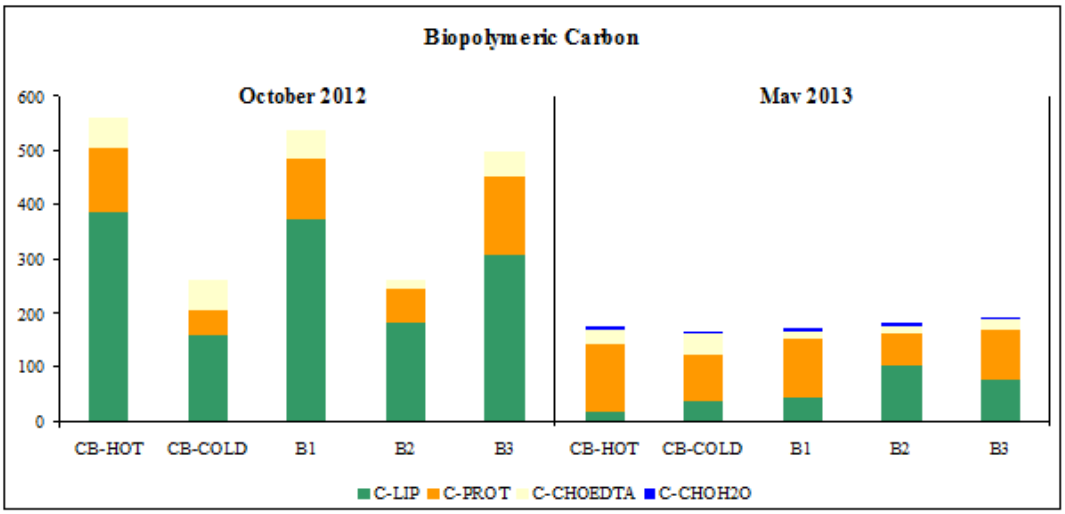

Figure 31: Biopolimeric Carbon concentration during the October 2012 and May 2013 campaigns as sum of protein (C-PRT), lipids (C-LIP), EDTA extractable carbohydrates (C-CHOEDTA) and water soluble carbohydrates (C-$CHOH_2O$).

3.6 Bioturbation and bio-irrigation

Bioturbation (i.e. the biogenic mixing of sedimentary particulates resulting from the displacement of materials during faunal feeding, scavenging and burrow construction) and bio-irrigation (flushing of burrows by burrowing fauna) can be used to assed the overall activity of faunal organisms. This is because metabolically challenging environments, such as

those imposed by environmental stressors, can lead to overall changes in individual activity, as a consequence of survival strategies. In such environments, species are required either the ability to re-locate energetic resources to cope with modified physiological pressures (Brown, Gillooly et al. 2004; Pörtner and Farrell 2008) or the ability to adapt (Somero 2010; Hoffmann and Sgrò 2011). Because of the duration of the experiments carried out in this project, our results fall into the first category. In this case, organisms that are physiologically impacted by environmental stressors will either require more resources (i.e. food) to sustain a possible higher energetic cost of living associated with stress response pathways (Thomsen, Casties et al. 2013), or they may be able counteract the deleterious effects of stressors via metabolic depression (Pörtner, Langenbuch et al. 2004). In the first case, and increase in individual activity would be expected, while in the second case, a reduction in activity would be more likely, and these should thus be observable in changes in bioturbation and bio-irrigation of burrowing macrofauna, which result from the overall activities of these organisms. The effect in either process at the community level, as measured here, will likely depend on which species are present, their vulnerability, and their abundances.

The bio-irrigation samples are still in process, and so this section focuses on the analysis of the bioturbation data. We have yet to finalise the estimation of bioturbation via fitting of the random-walk model to the time-lapse data, which will enrich the conclusions of this section. Nevertheless, we provide information about the impact of the experiments on bioturbation depth and biodiffusion, two key aspects of bioturbation as a process that can be used as proxies for the occurrence of physiological stress associated with environmental conditions (section 2.1.1).

3.6.1 High CO_2 mesocosm experiment

Analysis of the macrofauna communities at 2 weeks of exposure (T1) indicated that there was no apparent difference in the communities exposed to different CO_2 treatments (section 3.1.1, TBC). At 20 weeks, however, the average abundance in the bioturbation time-lapse cores was higher than in the highest CO_2 treatment (3680 ± 491 ind.m^{-2} c.f. 3159 ± 49 ind.m^{-2}, mean ± sd), with the values in the other three treatments fluctuating between the two. This suggests that mortality at 20000 ppm of CO_2 may have been higher than in controls. This effect on

community structure is visible when macrofaunal community biodiversity measurements taken on these cores (number of species, Margalef species richness index, Pielou's evenness index, Shannon and Simpson's diversity indices) are considered together to establish the similarity between communities exposed to the different treatments (Euclidean distance based on normalized diversity measurements, calculated on untransformed community abundance data). Indeed, the corresponding nMDS plot of the dissimilarity between these communities (fig.32, below) illustrates the control and 1000 ppm communities clustering together, with distance to these increasing as the CO_2 concentration increased. This result indicates a change in these communities after 20 weeks of exposure to the CO_2 treatments, which had a bearing on the bioturbation measurements carried out.

We focus here on the bioturbation measurements carried out on the whole liners (section 2.1.1), while the bioturbation data from the time-lapse incubations is still being processed. The results are presented in figure 33, below. We found that the biodiffusion coefficient, an indicator of the intensity of bioturbation, did not change in response to the CO_2 treatments at 2 weeks (T1, one way Analysis of variance, R^2=9.7%, $p>0.10$), but decreased significantly with increased CO_2 levels in the seawater at 20 weeks (T2, fig. 33a, one way Analysis of variance, R^2=30.64%, $p< 0.10$). This result suggests that after 20 weeks, the fauna was less active in the sediment as CO_2 increased, while at 2 weeks the intensity of bioturbation was variable, but not statistically related to the CO_2 treatments.

In addition, we found a significant effect of the CO_2 treatments on maximum bioturbation depth. Maximum bioturbation depth became significantly shallower as CO_2 increased at 20 weeks (T2, fig. 33b, generalized least squares model fit allowing for heterogeneous variances between CO_2 treatments, p=0.05), but not at 2 weeks (T1, fig. 33b, generalized least squares

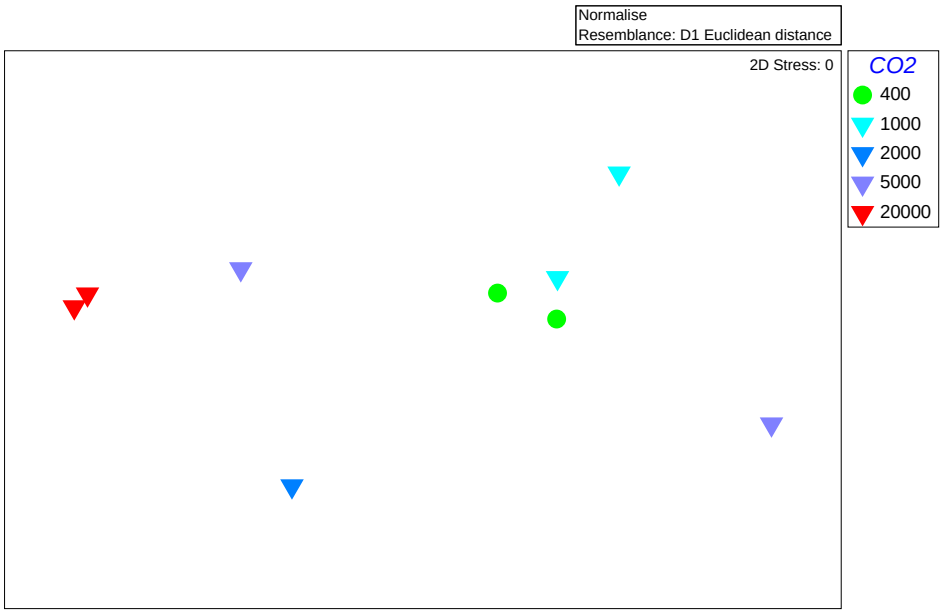

Figure 32: non-metric Multi-Dimensional Scaling plot illustrating the dissimilarity (Euclidean distance) between samples based on diversity measurements (normalised) taken on the communities at 20 weeks of exposure to high CO_2 treatments. Note how the higher CO_2 concentrations exhibit overall greatest departure from the control treatment (section 3.6.1).

model fit allowing for heterogeneous variances between CO_2 treatments, $p>0.10$). A lack of effect on bioturbation depth at 2 weeks of exposure indicates that the organisms did not try to re-position themselves vertically within the sediment in response to short-term CO_2 exposure, but that this effect was visible at 20 weeks. Shallow burrowing depth is a common response of bioturbators to stressors (Pearson and Rosenberg 1978; Marsden and Bressington 2009; Queirós, Hiddink et al. 2011) and so it is possible that the fauna may not have been significantly impacted by CO_2 in a short term exposure (T1) but that the continuous exposure to high CO_2 may have led to more profound physiological stress, in the long run (T2).

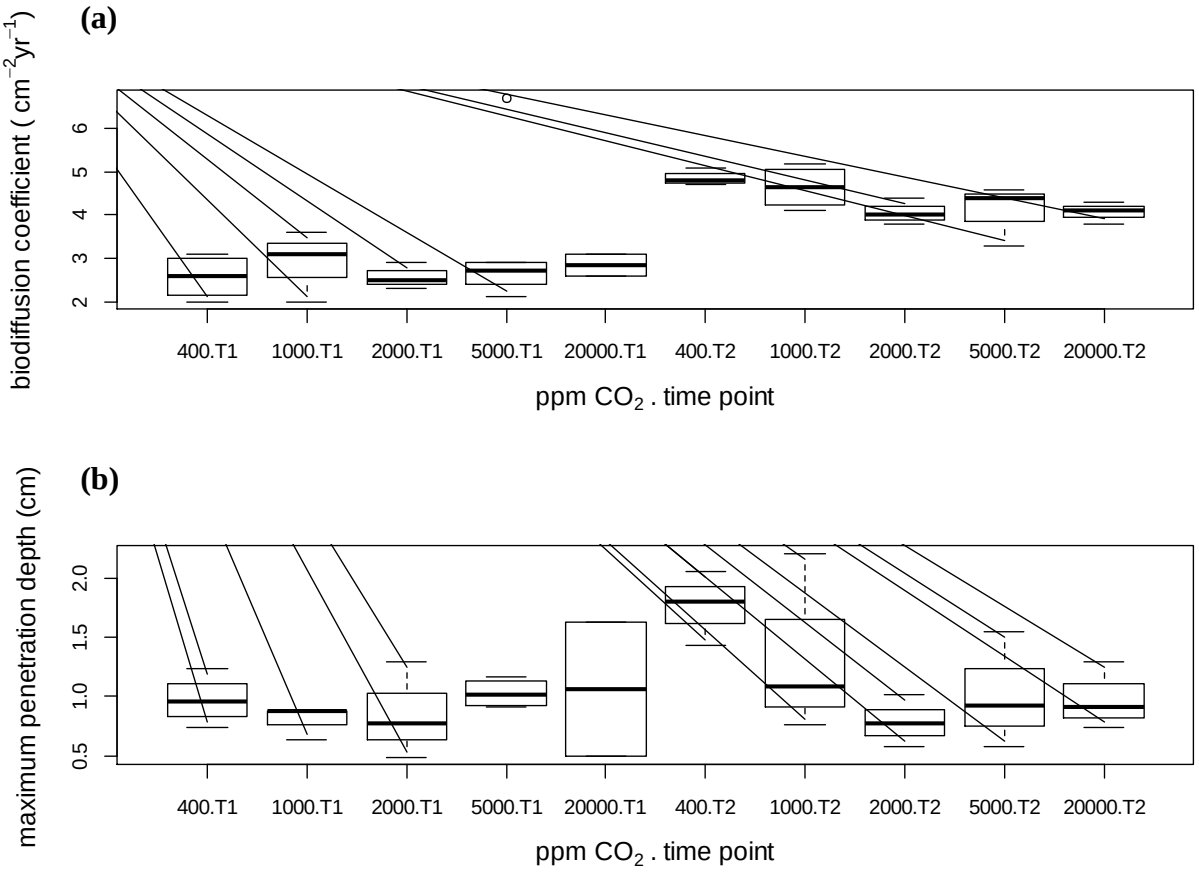

Figure 33: Estimates of bioturbation, made during the high CO_2 experiment. (a) Biodiffusion coefficient; and (b) bioturbation depth.

As there was a suggestion that community structure may have changed after 20 weeks (fig. 32), the finding of shallower burrowing depth and less intense bioturbation with increased CO_2 at 20 weeks suggests that overall, the community bioturbation may have change as a result of a different community structure. Consequentially, the potential effect of these communities on sedimentary geochemistry, through sediment transport, may also have changed in a medium-term exposure scenario, that worsened with the degree of hypercapnia observed. Figure 34 illustrates that the ordination of systems associated with the CO_2 treatments (Euclidean distance) did indeed increase with exposure time (T1 (a) c.f. T2 (b)), once the results from the (normalized) bioturbation measurements, nutrient fluxes (section 3.5.1.2) and ammonia oxidation in the sediment (3.5.1.3) were considered simultaneously. The dissimilarity between systems at twenty weeks shows a gradation associated with CO_2,

which also appeared to reduce system variability. I.e. high CO_2 systems cluster closer than lower CO_2 systems in figure 34b. This effect is generally seen as negative, as variability within natural systems is typically expected to be an insurance against variable environments. The absence of significant findings relating to bioturbation in the short exposure scenario (T1) suggests that the bioturbation activity of these communities (and potential effect on biogeochemistry) may be preserved in in short-lived leakages (fig.34a), although this may be likely dependent on the degree of hypercapnia caused.

The difference in the bioturbation measurement range between T1 and T2, particularly in the controls, is surprising (figure 33), and we can only speculate that it may possibly be related to seasonal effects (Teal, Bulling et al. 2008). Indeed, globally, bioturbation depth is expected to be deeper in winter than in autumn, as observed here (T2 c.f. T1). Our understanding of seasonality in biodiffusion is currently limited (Teal, Bulling et al. 2008).

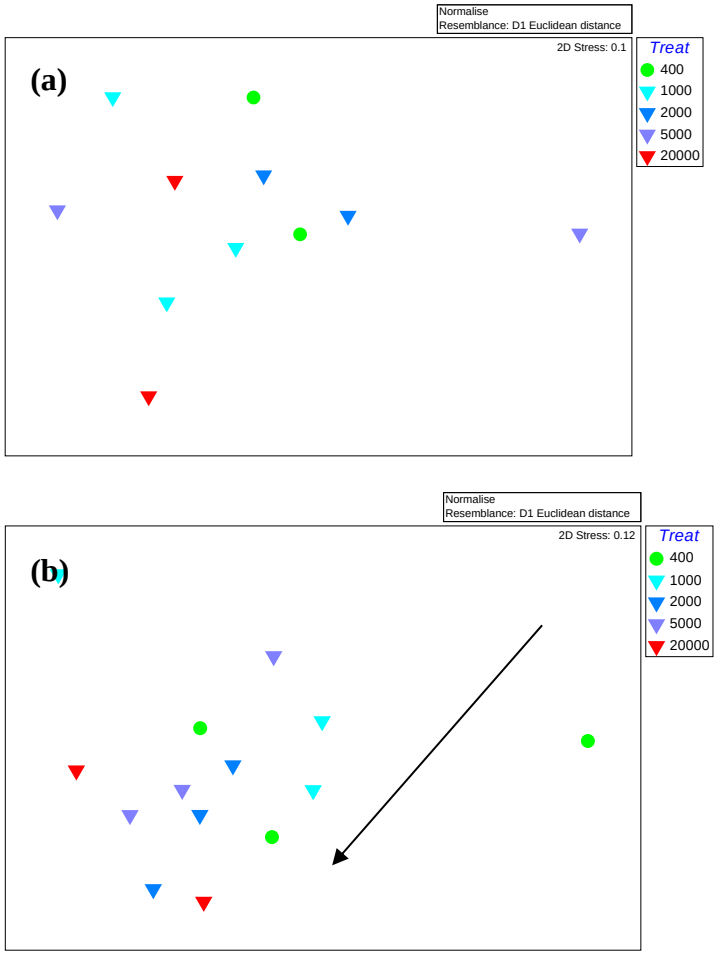

Figure 34: nMDS plot of systems plotted based on distance calculated considered the bioturbation, nutrient fluxes and ammonia odxidation data, together, at 2 weeks of exposure (T1, a), and 200 weeks (T2, b).

3.6.2 Formation water leakage mesocosm experiment

This sections focuses on the measurements of bioturbation carried out during the mescosm experiment: the interpretation of these findings will be improved once the macrofauna (section 3.1.2) and bio-irrigation data become available. Due to time-constrains, in this experiment, bioturbation was quantified using time-lapse set-up (section 2.1.1), but no whole liner assessments were made.

The main finding is that all stressors appeared to change bioturbation significantly, individually and in combination (fig. 35). Both high salinity and hypoxia, individually and in combination, reduced mean bioturbation intensity significantly (generalised least squares model fit allowing for heterogeneous variances between treatments, $p<0.06$), even in the tidal treatment (fig.35a). This finding suggests that the fauna was significantly less active in all treatments in relation to the controls, indicating the occurrence of physiological stress.

This result was also observed in the depth of bioturbation, which was significantly shallower in the hypoxic, high salinity and mixed treatments, than in the controls (fig.35b, generalised least squares model fit allowing for heterogeneous variances between treatments, $p<0.08$). It is noteworthy, however, that in the tidal treatment, the mean of burrowing depth was similar to the controls (fig.35b), and the variance increased. This finding is consistent with observations, during the exposures, of fauna occurring at the surface of the sediments during the mixed water phase of the tidal cycle, and re-burying during the control water phase (see section 2.1.2).

These findings confirm that hypoxia and high salinity, associated with formation water, can cause significant physiological impact on burrowing fauna. But more importantly perhaps, they highlight the importance of tidal and hydrodynamic conditions in general, in modulating the impacts of plumes associated with the release of formation water, as found in QICS project, in relation to high CO_2 plumes. This flushing of the brine plume may thus confer macrofauna organisms with a daily window during which recovery from stress responses may occur, as illustrated by the difference in bioturbation depth between the mixed and the tidal treatments (fig. 35b). However, the significant decrease in bioturbation intensity (fig.35a) suggests that some physiological costs are nevertheless ongoing, and thus that impairment of bioturbation may occur during longer exposures.

The analysis of community and respiration data (ongoing, section 2.1.1. and 2.1.2) will greatly add to the interpretation of these findings.

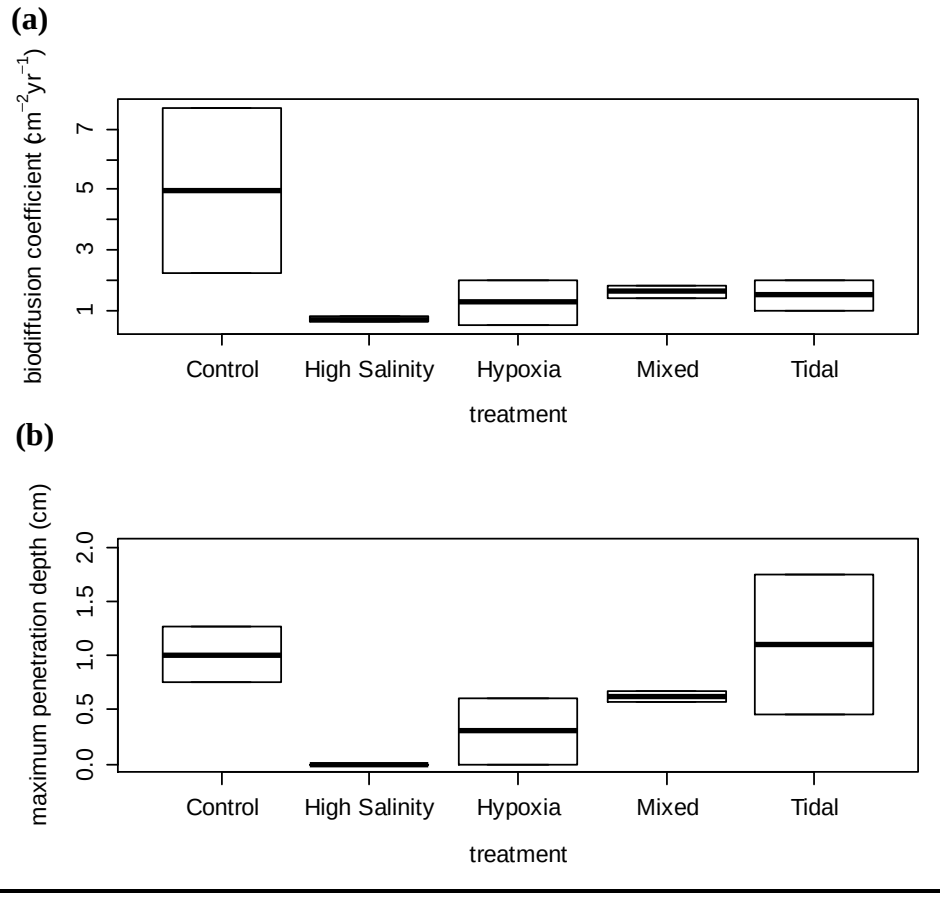

Figure 35: Estimates of bioturbation during the formation water experiment. (a) Biodiffusion coefficient; and (b) bioturbation depth.

With regard to the relation of bioturbation to biogeochemistry, as with the high CO_2 experiment, we plotted the similarity between systems (Figure 36) considering both elements (i.e. bioturbation and nutrient fluxes (section 3.5.2.2), but not ammonia oxidation, as that was measured in cores where we did not measure bioturbation). We found that once bioturbation and biogeochemistry were considered together, the effect of the experimental treatments on the systems was clear (fig.36), with distance to the controls increasing from single to multi-stressor systems, and the tidal system showing the greatest departure overall (figure 36). As before, the effect of the stressors is also visible on a reduction of the natural variability of parameters observed in the controls (one control system in figure 36 is omitted, showing the

greatest distance overall to the others). This effect is also generally seen as negative, as variability within natural systems is typically expected to be an insurance against variable environments.

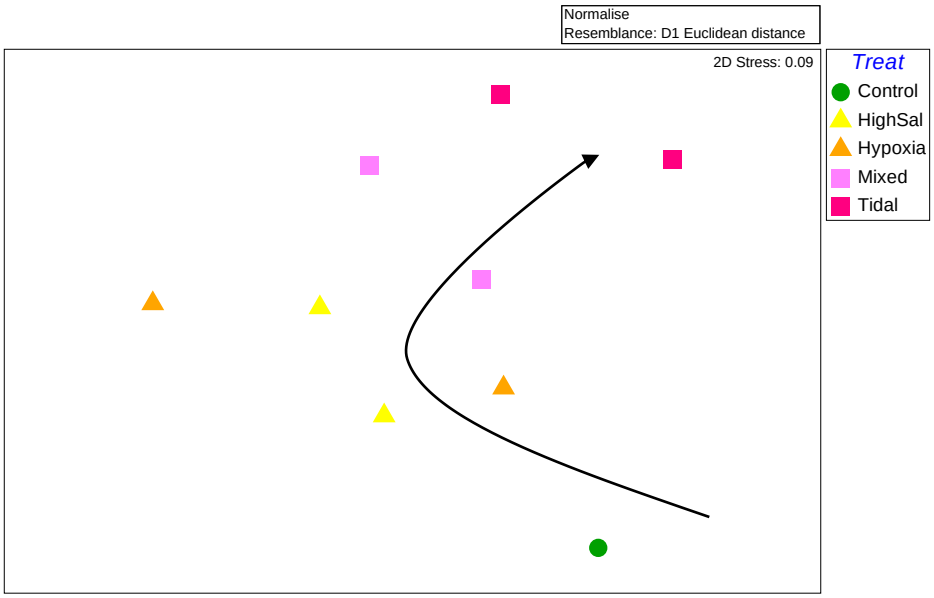

Figure 36: Non-metric multidimensional scaling (nMDS) plot where formation water liners are represented with the distance between them indicating the overall dissimilarity (Euclidean distance), calculated on the (normalized) bioturbation and nutrient flux measurements together. One control system has been removed, which exhibited the highest distance to all other points, to highlight the forcing of the experimental treatments.

3.7 Planktonic communities

All data on planktonic communities came from the Panarea natural seep sites.

The outcomes obtained from different temporal and spatial sampling strategies (long transect–PACO2, short transect-LB and Basiluzzo area) indicate that the effect of CO_2 seeps on the prokaryotic dynamics in the water column varies widely. Microbial abundances displayed higher variability than those previously observed (Karuza et al. 2012). Generally, CO_2 seeps were associated with low PCP (Prokaryotic Carbon Production) and low turnover rates of heterotrophic prokaryotic community. On the contrary, from what was observed during the PaCO2 cruise, mobilisation processes (prokaryotes exoenzymatic activities) seem to be stimulated by gas leakage.

Viral dynamics (production and decay), investigated only during PACO2 cruise, were more intense at the control site (st. P0) relatively to the vent area, and were more pronounced at the surface level where also minor acidification was detected. Viral abundance did not significantly differ between the control site and the vent. Higher burst size (BS) in the control site (BS=37) relative to the CO_2-vent (BS always <12) indicates minor yield of lytic infection in the vent field. The fraction of lysogens in the seep area was up to 60% higher than in the control station (<15%) (Figure 37).

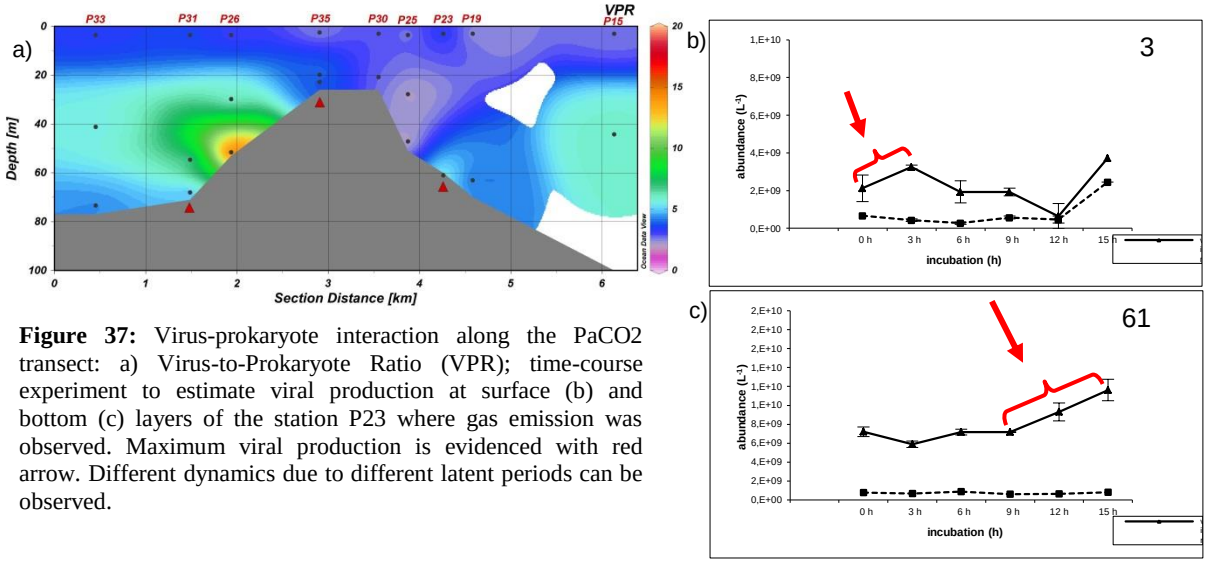

Figure 37: Virus-prokaryote interaction along the PaCO2 transect: a) Virus-to-Prokaryote Ratio (VPR); time-course experiment to estimate viral production at surface (b) and bottom (c) layers of the station P23 where gas emission was observed. Maximum viral production is evidenced with red arrow. Different dynamics due to different latent periods can be observed.

The impact of CO_2 on the abundance and diversity of phytoplankton community was investigated to increase our capability to predict marine ecosystem response to potential CO_2 leakage. Undetermined nanoflagellates were generally the most abundant group, while dinoflagellates were the main taxonomic group in terms of biodiversity. Only in October 2012 and May 2013, near the Basiluzzo island, the community showed a higher number of taxa and a higher biodiversity in relation to the other campaigns and to the other investigated points, with dinoflagellates, diatoms and coccolithophores well represented. From these preliminary results, natural CO_2 emissions in this area do not seem to have any clear influence on phytoplankton community, and community structure appeared, alternatively, to reflect seasonal variability.

As with phytoplankton, preliminary results do not show any significant impact of the CO_2 seeps on the microzooplankton community, and the differences noted seem linked mainly to

seasonal variations. Tintinnids and heterotrophic dinoflagellates were the most abundant organisms in this group, followed by Micrometazoans (mainly copepod nauplii). Aloricate ciliates never reached high values. Foraminifera, Radiolaria and Acantharia were scarce in all stations. In total, 22 genera and 55 species of microzooplankton were identified. Among tintinnids, the most representative species were *Eutintinnus tubulosus*, *Salpingella decurtata*, *Dadayiella ganymedes* and *Dictyocysta mitra* (Figure 38). *Protoperidinium* and *Diplopsalis* were the most representative genera among heterotrophic dinoflagellates. The community of naked ciliates was dominated by Strombidiidae and Strobilidiidae.

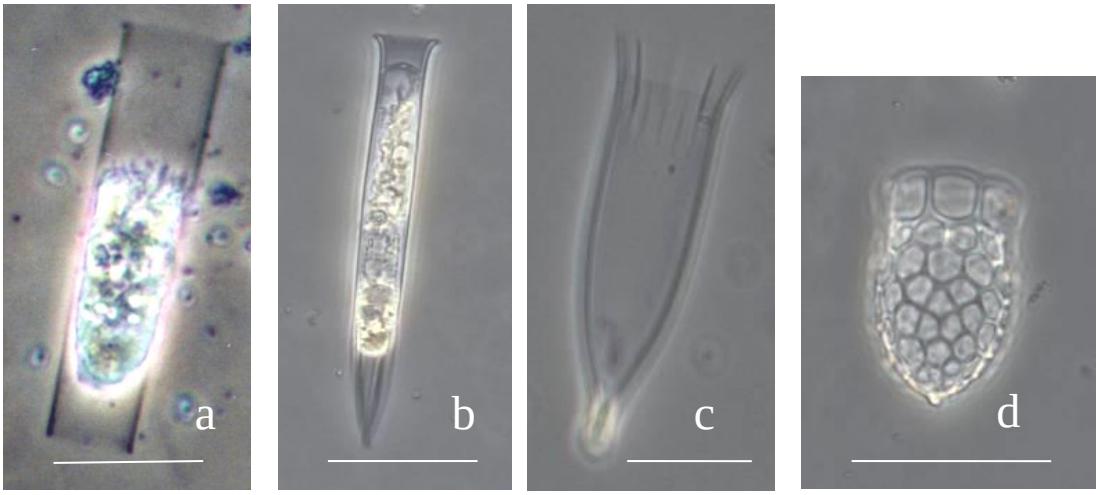

Figure 38: Photos of the most representative species of tintinnids: *Eutintinnus tubulosus* (a), *Salpingella decurtata* (b), *Dadayiella ganymedes* (c) and *Dictyocysta mitra* (d). (Scale bar = 50 µm).

4. Recommendations

- There are currently very few studies published which have exposed whole benthic communities to elevated levels of CO_2. In order to appreciate the full range of responses observed across different benthic habitats and communities, more of these large exposure experiments need to be conducted on a greater variety of benthic systems.

- Experiments need to incorporate more realistic exposure scenarios. The vast majority of CO_2 exposure studies conducted to date have used continuous levels of CO_2 exposure. However, results from both models and observations have shown that, due

to local hydrodynamics such as tides and currents, and seasonality, benthic systems will most likely be exposed to CO_2 levels which can fluctuate and pulse with time. This periodic exposure to high CO_2 could have very different effects on marine organisms and communities and needs to be more adequately characterized.

- The ECO2 project was the first (and currently only) to run an experiment to simulate exposure to high salinity, low oxygen formation water. Given the strong impacts seen in this experiment and the likelihood that CCS activities could displace formation water into the marine environment, more of these experiments are urgently needed. Here too, the modulating effects of hydrodynamics and seasonality need to be adequately characterized.

- The majority of data on high CO_2 impacts currently available have come from experiments that increase the CO_2 content of the overlying water. Whilst this approach is appropriate for stuying the effects of a dense, CO_2 enriched plume, it does not adequately replicate the effects of CO_2 migrating up through the sediment and interacting with the pore waters. A recent controlled, sub-seabed, CO_2-releaase experiment (the QICS project) has been successfully conducted (Blackford et al., 2014) and more such experiments are urgently needed.

5. Acknowledgements

The research leading to these results has received funding from the European Community‘s Seventh Framework Programme ([FP7/2007-2013] under grant agreement n° 265847 for project ECO2: Sub-seabed CO_2 Storage: Impact on Marine Ecosystems.

6. References

Aller, R. C. (1982). The Effects of Macrobenthos on Chemical Properties of Marine Sediment and Overlying Water. Animal-Sediment Relations. the biogenic Alteration of Sediments. P. L. McCall and M. J. S. Tevesz. New York, Plenum Press**:** 53 - 102.

Alve, E. and J. Nagy (1990). "Main features of foraminiferal distribution reflecting estuarine hydrography in Oslo Fjord." Marine Micropaleontology **16**(3): 181-206.

Beccaluva, L., Rossi, P.L., Serri, G. (1982). Neogene to Recent volcanism of the southern Tyrrhenian-Sicilian area: Implications for the geodynamic evolution of the Calabrian arc. Earth Evol. Sci 3: 222-238.

Beman, J. M., C.-E. Chow, et al. (2011). "Global declines in oceanic nitrification rates as a consequence of ocean acidification." Proceedings of the National Academy of Sciences **108**(1): 208-213.

Birchenough, S., R. Parker, et al. (2012). "Combining bioturbation and redox metrics: potential tools for assessing seabed function." Ecological Indicators **12**(1): 8-16.

Blackford, J., H. Stahl, et al. 2014) Detection and impacts of leakage from sub-seafloor Carbon Dioxide Storage. *Nature Climate Change*. doi:10.1038/nclimate2381

Blasutto, O., Cibic, T., et al. (2005). "Microphytobenthic primary production and sedimentary carbohydrates along salinity gradients in the lagoons of Grado and Marano (Northern Adriatic Sea)." Hydrobiologia **550**(1): 47-55

Bligh, E.G. and Dyer W. (1959). "A rapid method for total lipid extraction and purification." Canadian Journal of Biochemistry and Physiology **37**: 911-917.

Brewer, P. and J. Riley (1965). The automatic determination of nitrate in sea water. Deep Sea Research and Oceanographic Abstracts, Elsevier.

Brown, J. H., J. F. Gillooly, et al. (2004). "Toward a metabolic theory of ecology." Ecology **85**(7): 1771-1789.

Buchanan, J. (1984). Sediment analysis. Methods for the study of marine benthos. N. Holme and A. McIntyre, Blackwell Scientific Publications, Oxford**:** 41-65.

Cai, W. J. and C. E. Reimers (1993). "The Development of pH and pCO_2 microelectrodes for studying the carbonate chemistry of pore waters near the sediment-water interface." Limnology and Oceanography **38**: 1762-1773.

Calanchi, N., Romagnoli, C., Rossi, P.L. (1995). Morphostructural features and some petrochemical data from the submerged area around Alicudi and Filicudi volcanic islands (Aeolian Arc, southern Tyrrhenian Sea). Mar.

Geol. 123: 215-238.Capasso, G., and S. Inguaggiato (1998). "A simple method for the determination of dissolved gases in natural waters. An application to thermal waters from Vulcano Island." Applied Geochemistry **13**: 631-642.

Dickson, A.G., C.L. Sabine, J.R. Christian (2007). Guide to best practices for ocean CO_2 measurements." PICES Special Publication **3**, 191 pp.

Dixson, D. L., P. L. Munday, et al. (2010). "Ocean acidification disrupts the innate ability of fish to detect predator olfactory cues." Ecology Letters **13**(1): 68-75.

Dubois, M., Gilles, K. A., et al. (1956). "Colorimetric method for determination of sugars and related substances". Analytical Chemistry **28**(3): 350-356.

Fichez, R. (1991). "Composition and fate of organic matter in submarine cave sediments; implications for the biogeochemical cycle of organic carbon". Oceanological Acta **14**: 369-377.

Fonselius S.H., D. Dyrssen, B. Yhlen (1999). "Determination of hydrogen sulphide." In: Grasshoff, K., K. Kremling, M. Ehrhardt (1999) Methods of Seawater Analysis 3rd Edition, Wiley-VCH, Weinheim, 600 pp.

Gabbianelli, G., Gillot, P.Y., Lanzafame, G., Romagnoli, C., and Rossi, P.L. (1990) Tectonic and volcanic evolution of Panarea (Aeolian Islands, Italy). Mar. Geol. 92: 313-326.

Gerchov, S.M. and Hatcher, P.G. (1972). "Improved technique for analysis of carbohydrates in sediments." Limnology Oceanography **17**: 938-943.

Gerino, M., R. Aller, et al. (1998). "Comparison of different tracers and methods used to quantify bioturbation during a spring bloom: 234-thorium, luminophores and chlorophyll a." Estuarine Coastal and Shelf Science **46**: 531–547.

Grasshoff, K., K. Kremling, et al. (2009). Methods of seawater analysis, John Wiley & Sons.

Guinasso, N. and D. Schink (1975). "Quantitative estimates of biological mixing rates in abyssal sediments." Journal of Geophysical Research **80**(21): 3032-3043.

Hansen H.P. and E. Koroleff (1999). "Determination of nutrients." In: Grasshoff, K., K. Kremling, M. Ehrhardt (1999) Methods of Seawater Analysis, 3rd Edition, Wiley-VCH, Weinheim, 600 pp.

Hartree, E.F. (1972). "Determination of proteins: a modification of the Lowry method that give a linear photometric response." Analytical Biochemistry **48**: 422-427.

Hoffmann, A. A. and C. M. Sgrò (2011). "Climate change and evolutionary adaptation." Nature **470**(7335): 479-485.

Karuza, A., Celussi, M., et al. (2012). "Virioplankton and bacterioplankton in a shallow CO_2-dominated hydrothermal vent (Panarea Island, Tyrrhenian Sea)." Estuarine, Coastal and Shelf Science **97**: 10-18.

Kirkwood, D. (1989). "Simultaneous determination of selected nutrients in sea water." International Council for the Exploration of the Sea (ICES) CM **100**: 29.

Kitidis, V., B. Laverock, et al. (2011). "Impact of ocean acidification on benthic and water column ammonia oxidation." Geophysical research letters **38**(21).

Kristensen, E., G. Penha-Lopes, et al. (2012). "What is bioturbation? The need for a precise definition for fauna in aquatic sciences." Marine Ecology-Progress Series **446**: 285-302.

Krom, M. D. and R. A. Berner (1980). "Adsorption of phosphate in anoxic marine sediments." Limnol. Oceanogr **25**(5): 797-806.

MA (2003). The millenium atlas: petroleum geology of the central and northern North Sea. London, The Geological Society of London.

Mahaut, M. and G. Graf (1987). "A luminophore tracer technique for bioturbation studies." Oceanologica Acta **10**: 323-328.

Mantoura, R. and E. Woodward (1983). "Optimization of the indophenol blue method for the automated determination of ammonia in estuarine waters." Estuarine, Coastal and Shelf Science **17**(2): 219-224.

Marinelli, R. L. (1992). "Effects of polychaetes on silicate dynamics and fluxes in sediments: Importance of species, animal activity and polychaete effects on benthic diatoms." Journal of Marine Research **50**(4): 745-779.

Marsden, I. D. and M. J. Bressington (2009). "Effects of macroalgal mats and hypoxia on burrowing depth of the New Zealand cockle (Austrovenus stutchburyi)." Estuarine Coastal and Shelf Science **81**(3): 438-444.

Marsh, J. B. and Weinstein, D. B. (1966). "Simple charring method for determination of lipids". Journal of Lipid Research **7**: 754-576

McGinnis, D., Beaubien, et al. (2011) "The Panarea natural CO_2 seeps: fate and impact of the leaking gas (PaCO2)"; R/V URANIA, Cruise No. U10/2011, 27 July – 01 August 2011, Naples (Italy) – Naples (Italy) EUROFLEETS Cruise Summary Report . IFM-GEOMAR, Kiel, 55 pp. DOI 10.3289/CR_ECO2_19835.

Murray, F., S. Widdicombe, et al. (2013). "Consequences of a simulated rapid ocean acidification event for benthic ecosystem processes and functions." Marine Pollution Bulletin **73**(2): 435-442.

Pearson, T. H. and R. Rosenberg (1978). "Macrobenthic succession in relation to organic enrichment and pollution of the marine environment." Oceanography and Marine Biology Annual Review **16**: 229-311.

Platon, E., B. K. Sen Gupta, et al. (2005). "Effect of seasonal hypoxia on the benthic foraminiferal community of the Louisiana inner continental shelf: the 20th century record." Marine Micropaleontology **54**(3): 263-283.

Pörtner, H. O. and A. P. Farrell (2008). "Physiology and Climate Change." Science **322**: 690-692.

Pörtner, H. O., M. Langenbuch, et al. (2004). "Biological impact of elevated ocean CO_2 concentrations: lessons from animal physiology and earth history." Journal of Oceanography **60**(4): 705-718.

Presley, B. and G. Claypool (1971). "Techniques for analyzing interstitial water samples." Part **1**: 1749-1755.

Queirós, A. M. (2010). Ecosystem Engineers in Diversity and Ecosystem Process Relationships. PhD, Bangor University.

Queirós, A. M., J. G. Hiddink, et al. (2011). "Context dependence of marine ecosystem engineer invasion impacts on benthic ecosystem functioning." Biological Invasions **13**: 1059-1075.

Queirós, A. M., P. Taylor, et al. (*in review*). "Optical assessment of impact and recovery of sedimentary pH profiles in ocean acidification and carbon capture and storage research." International Journal of Greenhouse Gas Control.

Rice, D.L. (1982). "The detritus nitrogen problem: new observations and perspectives from organic geochemistry." Marine Ecology Progress Series **9**: 153-162.

Schiffers, K., L. R. Teal, et al. (2011). "An Open Source Simulation Model for Soil and Sediment Bioturbation." PLoS ONE **6**: e28028. doi:28010.21371/journal.pone.0028028.

Sharp, J. H. (1974). "Improved analysis for "particulate" organic carbon and nitrogen from sea water." Limnology and Oceanography **19**(6): 984-989.

Solan, M., B. D. Wigham, et al. (2004). "In situ quantification of bioturbation using time-lapse fluorescent sediment profile imaging (f-SPI), luminophore tracers and model simulation." Marine Ecology Progress Series **271**: 1-12.

Somero, G. (2010). "The physiology of climate change: how potentials for acclimatization and genetic adaptation will determine 'winners' and 'losers'." The Journal of experimental biology **213**(6): 912-920.

Teal, L., M. Bulling, et al. (2008). "Global patterns of bioturbation intensity and mixed depth of marine soft sediment." Aquatic Biology **2**: 207-218.

Thomsen, J., I. Casties, et al. (2013). "Food availability outweighs ocean acidification effects in juvenile Mytilus edulis: laboratory and field experiments." Global Change Biology.

Utermöhl, H. (1958). Mitt.-Int. Ver.Theor.Angew.Limnol. **9**: 1-38

Widdicombe, S., S. L. Dashfield, et al. (2009). "Effects of CO_2 induced seawater acidification on infaunal diversity and sediment nutrient fluxes." Marine Ecology Progress Series **379**: 59-75.

Widdicombe, S. and H. Needham (2007). "Impact of CO~ 2-induced seawater acidification on the burrowing activity of Nereis virens and sediment nutrient flux." Marine Ecology Progress Series **341**: 111-122.

Zhang, J.-Z. and J. Chi (2002). "Automated analysis of nanomolar concentrations of phosphate in natural waters with liquid waveguide." Environmental science & technology **36**(5): 1048-1053.

Annex I: *In situ* methods used in fields surveys at the Panarea site (Section 2.2, Table II)

Several in-situ-measuring devices were deployed at the investigated Basiluzzo sedimentary sites to geochemically characterize the respective habitats. In addition, the divers thoroughly documented each site by video and photography.

Timelapse Camera

The gas flow was monitored for several hours during each deployment with the timelapse technique using a Canon EOS D600. These recordings are currently being evaluated by HYDRA. Observations made by the divers under water indicate the potential for considerable differences in seepage intensity during the day that may be caused by wave action, tides or changing currents.

SEAGUARD Recording Current Meter

As during last year's field trip, a SEAGUARD recording current meter (AADI, Norway) was used to monitor current speed and direction, temperature, salinity/conductivity, pressure, turbidity and oxygen concentrations within the water column.

Microsensor Profiler

A microsensor profiler for sediments was equipped with sensors for pH (de Beer et al. 1997) and Microelectrodes Inc., USA], O_2 (Revsbech and Ward 1983), CO_2 (Microelectrodes Inc., USA), ORP (oxidation reduction potential; a Pt wire, exposed tip is 50 µm thick and 0.5 mm long), T (Pt100; UST Umweltsensortechnik GmbH, Geschwenda, Germany), H_2 (Unisense, Denmark) and H_2S (Jeroschwski et al. 1996). It was deployed at all three sedimentary sampling sites. In addition to the recording of high-resolution profiles in the sediment, the unit was also used to assess the spatial heterogeneity of the water column.

RBR Sensors

RBR sensors (RBR-Datalogger XR-420 D; RBR, Ottawa, Canada, www.rbr-global.com) are loggers for pH, O_2, ORP and pressure (tides), here measuring at 2 cm from the sediment surface. Out of 6 loggers, 5 functioned well and revealed strong dynamics of O_2, pH and ORP that were perfectly synchronous to tides. Seepage occurred mainly at low tide, during which anoxic, acidic and reduced substances are emitted into the water column. The reductant could be either H_2S, H_2 or Fe^{2+}.

Gas sampling

The goal was to determine the overall gas composition and to verify again that no methane and no sulfide are emitted at the investigated sites. Sampling and analyses were done in cooperation with Dr. S. Beaubien (UniRoma1, Italy) and Dr. F. Italiano (INGV Palermo, Italy). Gas samples were taken at the CO_2-impacted sites. Sampling was done by holding an exetainer upside down over the seep until it was filled. During surfacing the exetainer had a syringe needle stuck through the septum for the pressure release. The needle was pulled out shortly before surfacing with the samples. The exetainer content was transferred into metal containers on board and analysis was done at UniRoma1 (Italy). From sub-samples out of 2 gas collecting tubes analysis of H_2S were done immediately on board directly after sampling (UniRoma1, Italy). The concentration of H_2S was <1ppm. The sampling for the extended analysis was done with funnels into gas collecting tubes. The containers were closed when full with gas and surfaced without any pressure compensation. The analysis were done INGV Palermo (Italy) and revealed a CO_2 content of ~97-99% at both sites as well as a CH_4 content of <0.001%.

Bacteria abundance and community structure

Natural sediment samples for analyzing bacterial communities were obtained by using segmented push cores (0-2 cm intervals, maximum length up to 15 cm) and sterile Sarstedt tubes (for scooping 0-2 cm surface sediment). Samples were either directly frozen at -20°C for DNA analyses, or were fixed in 4% formaldehyde/seawater for cell counts. Prokaryotic total abundance can be obtained using Acridine Orange (Boetius et al. 1996). We determined the bacterial community structure both by automated ribosomal intergenic spacer analysis (ARISA; for methodological details see e.g. Böer et al. 2009) and by 454 massively parallel

tag sequencing (MPTS; for methodological details see e.g. Gobet et al. 2012). Additional samples were taken for fluorescence in situ hybridization (FISH). These samples were fixed for 3-12 h at 4°C in 4% formaldehyde/seawater. The samples were then washed twice with 1×PBS (phosphate buffered saline; pH 7.4) to remove the fixative before being stored at -20°C in a 1:1 mixture of 1×PBS and EtOH (molecular grade). Once in MPI laboratories the samples were processed with specific probes for Bacteria and Archaea as described by Ishii et al. (2004).

Meiofauna abundance and community structure

At each site five replicate meiofauna samples were taken with plastic cores that were precut in 2 cm slices and taped, and which had an inner diameter of 5 cm (equivalent to 19.6 cm²). After retrieval the cores were sliced, where possible to 10 cm depth, and stored on a 4% formaldehyde-seawater solution. Meiofaunal organisms were retrieved from the sediments after rinsing the sediments with tap water over a 1mm and a 32 µm mesh sieve, and decanting the 32 µm fraction for 3 times. All meiofaunal organisms were identified to higher taxon level under a Leica MZ 12.5 stereomicroscope (8 - 100x magnification), and where possible 50 nematodes per sediment layer were identified at UGent to species level under a compound microscope (1000× magnification).

Macrofauna abundance and community structure

At each site five replicate macrofaunal samples were taken with plexiglass tubes with an inner diameter of 6.4 cm (equivalent to 32.17 cm²). The upper 10 cm of the sediment was stored on a 4% formaldehyde-seawater solution. Afterwards, samples were sieved on a 1 mm sieve and macrofaunal organisms were identified to species level where possible (UGent).

Enzymatic activities

The task was to investigate the microbial extracellular enzyme activity in the surface sediment at all three sedimentary sampling sites. At each site, 4 samples of the surface sediment were obtained. The top 2-3 cm of the sediment were scooped into sterile 50 mL-Sarstedt tubes. In addition, 3 water samples were taken with 50 mL-syringes approx. 10 cm above the sediment surface to set up the experiments. For each site, 3 of the 4 sampling tubes were chosen to set up the essays, while the fourth one was immediately stored at -20°C (backup and for calibration purposes). In total, 4 different substrates were used to set up the

essays, i.e. β-glucoside (β-glucosidase), N-acetyl-glucosamine (chitobiase), Leucine (Leucine-aminopeptidase) and Fluorescein diacetate (esterase). Dublicates were set up in sterile 15 mL-Sarstedt tubes with each substrate by mixing each time 3 mL sediment and 3 mL filter-sterile seawater with 120 µL of the substrate stock solutions (final concentrations 100 µM for all, except 500 µM for Leucine). Essays were mixed well before and inbetween incubation at in situ temperature (16-19°C). Sampling was done after 0.5 h and 1.5 h by taking off 1 mL of the supernatant and directly transferring it to -20°C (storage in cryo-vials). Vials are kept dark until analyses in the MPI home laboratories. The protocol is a modified version of the one described by Boetius & Lochte (1994).

Seagrass survey

The main objectives were to assess the leaf area index, to investigate bacterial and meiofauna community composition, and to determine the presence/absence as well as abundance of epibionts.

Leaf Area Index (LAI). For the assessment of the LAI, the seagrass rhizomes were counted in an area of 0.25 m². At least three counts were conducted per site. From each counted area, ten rhizomes were sampled including the leafs. All leafs were scanned on land in Panarea. In the HYDRA laboratory, the leaf area will be assessed and the LAI will be calculated.

Seagrass Biology: Bacteria. At each site, seagrass leaves were sampled at three different spots. For one sample, 10 outermost leaves were randomly chosen, ripped off and transferred into one sterile plastic bag. Back in the field laboratories, at first the leaf dimensions (length × width) were measured. The top 5 cm of each leaf were cut off and preserved for DNA analyses and cell counts. Three of the 10 leafs were fixed at 4°C in 14.5 mL 4% formaldehyde/seawater. Two of the 10 leafs were frozen (-20°C) as is in sterile 15 mL-Sarstedt tubes (backup). For DNA analyses, the rest of the leafs were each wetted with 1 mL 1 × TE-buffer (molecular grade; Promega Corporation, Madison, WI) before being scraped on both sites with a sterile scalpel. The detached material was then transferred via pipetting (autoclaved tips) into autoclaved plastic vials and stored at -20°C.

In addition to the leaf sampling, the divers also collected seawater samples above and between the seagrass leafs for each of the three different spots per site. For this purpose, 50

mL-syringes were filled and brought back to the field laboratory. Sub-samples were taken for pH measurements and nutrient analyses, DIC and TA.

Seagrass Biology: Meiofauna

At each site, six replicate samples were collected from the natural sea grass beds. The divers collected around 12 to 18 leafs per sample by placing a plastic bag over the leafs and gently cutting of the leafs at the base before closing the bags with elastic bands. The remaining shoots were cut off from the rhizomes and gently transferred into separate plastic bags, with a minimal of transfer through the water column. On land, both leaf and shoot samples were poured on a 32µm sieve to eliminate the water. The material collected on the 32 µm sieve was stored on a 4% formaldehyde-seawater solution. Back at the lab (UGent), the samples were poured on a 1 mm and 32 µm sieve and the meiofauna and nematodes in the 32 µm fraction are currently being studied in a similar way as is done for the organisms inhabiting the sediment. In order to standardize the meiofaunal densities, seagrass leaf surfaces were calculated with the software program ImageJ before they were burned to determine the ash-free dry weight. As for the shoots, their volume was measured by means of submersion, before they were burned to determine their ash-free dry weights.

Seagrass Biology: Epibionts

A thorough assessment of the epibionts was done in the laboratories of HYDRA. For the epibiont samples, the leaves of one rhizome were grabbed at the lowest part and cut off. The leaf bundle was put into one plastic bag. All leaves from one sample were scanned with high resolution on each side for later analysis. The samples were then fixed in 4% formaldehyde/seawater.

Sediment Geochemistry

From the segmented push cores (0-2 cm intervals, maximum length up to 15 cm) several samples were preserved for analyses of methane concentration, porosity, TOC (total organic carbon) and CPE (chloroplastic pigment equivalents), granulometry, TN, TOC and TOM. For methane concentration, 5 mL of sediment were added to 10 mL 2.5% NaOH in glass vials, mixed, stored upside down at 4°C and then analysed with gas chromatography. For porosity, 3-4 mL of each sediment horizon were stored at 4°C in 5 mL-syringes, the porosity was calculatete from weight/volume ratio. For CPE, a 5 mL-syringe was inserted into the core,

thereby preserving the natural vertical structure of the sediment. Each syringe was wrapped in aluminum foil and stored at -20°C. CPE analyzed as described in Böer et al. (2008). Grain size distribution was measured using a Coulter Counter LS 100TM Particle Size Analyser. The 0.06–1000 mm sediment fractions were expressed in volume percentage (vol%) and classified according to Wentworth (1922). For total sedimentary organic carbon (TOC) and nitrogen (TN), samples were lyophilized, homogenized and acidified with 1% HCl and the contents were measured using a Flash EA 1112+ Mas 200 elemental analyzer (detection limit of 0.01%). Total organic matter or ash-free dried weight is determined as the mass loss observed upon the combustion of the dried sample (48h at 60°C) at 500°C for 2h.

Pore-water Geochemistry

To investigate how pH, DIC (dissolved inorganic carbon), TA (total alkalinity), nutrients (NH_4^+, PO_4^{3-}, NO_2^-, NO_3^-/NO_2^-, Si), sulfide concentrations, Fe/Mn concentrations change with depth at the investigated sites, pore-water samples were obtained with the help of the TUBO device and by using Rhizons MOM (19.21.21F, mean pore size 0.15 µm; Rhizosphere Research Products, Wageningen, Netherlands) attached to 10 mL-syringes (Fig. 4a,b). In principle, the TUBO device was pushed into the sediment and then emptied. At each depth, 2 Rhizons were inserted into the sediment at opposite locations. To allow direct comparison with the bacterial samples (0-2 cm intervals), Rhizons were inserted at 1, 3, 5, 7 and 9 cm depth. At each of the investigated sedimentary sites 3 replicate pore-water profiles were taken. Dissolved silicate was photmetrically measured according to Grasshoff et al. (1983). NH_4^+, PO_4^{3-}, NO_2^-, NO_3^- were spectrophotometrically measured with a continuous-flow analyzer (Bran & Lübbe GmbH, Nordestedt, Germany) using a variant of the method of Grasshoff et al. (1983).

Measurements of pH were directly done in the field laboratory with a pH 96 by WTW (WTW Wissenschaftlich-Technische Werkstätten GmbH, Weilheim, Germany) and an InLab Semi-Micro electrode by Mettler Toledo (Gießen, Germany). pH was determined at ambient temperature and values will have to be adjusted to in situ conditions later. Calibration was done with conventional buffer solutions by Mettler Toledo (pH 4.00 and 7.00).

For DIC and TA, 2 mL pore-water were filled headspace-free into glass vials and stored at 4°C. DIC and TA were assessed via flow injection analysis (Hall and Aller, 1992) and two-point tritaion (Edmond 1970), respectively.

Sulfide samples were fixed in plastic vials pre-filled with 0.5 mL 2% ZnAc before being stored at 4°C. In addition to the TUBO-Rhizon strategy, further samples were obtained by using syringes attached to a pore-water lance. The 10 mL-syringes had been pre-filled with 2 mL 2% ZnAc to allow for direct fixation of pore waters under water. Samples were obtained from 5 cm and 10 cm below the sediment surface. In the field laboratory, these samples were transferred to 15 mL-Sarstedt tubes and stored at 4°C. Analyses were done in the MPI home laboratories according to procedure described by Cline (1969). To be able to determine Fe/Mn concentrations in the recovered pore waters, samples were fixed in plastic vials pre-filled with 0.2 mL 1M HCl before being stored at 4°C. Fe and Mn concentrations were assessed by atomic absorption spectrometry.

Seawater microbiology and geochemistry

In order to obtain background information with regard to benthic bacterial community composition and geochemistry, a 5 L-Niskin bottle was used to sample seawater at a height of approx. 30 cm above each of the sedimentary sampling areas. Sub-samples for pH, nutrients concentrations, as well as DIC and TA (but with addition of $HgCl_2$) were processed the same way as pore-water samples. Samples for measuring CH_4 concentration were filled into evacuated and pre-weighed glass containers that contained 2-3 NaOH pellets. Samples for sulfide concentration was fixed in 15 mL-Sarstedt tubes pre-filled with 2 mL 2% ZnAc at 4°C.

To investigate the bacterial community composition, seawater samples were filtered and filters were stored at -20°C for subsequent DNA analyses in the MPI home laboratories. With the help of a portable vacuum pump, 500 mL of seawater were passed through a 0.2 µm GTTP-filter (Merck Millipore, Billerica, MA). A cellulose nitrate filter (0.45 µm; Sartorius, Göttingen, Germany) was used as support filter. Filtrations were repeated at least three times (i.e. finally at least 2 L of seawater had been filtered per site). Part of the seawater was fixed with filter-sterile formaldehyde (final concentration of 1%) over night at 4°C in sterile 50 mL-Sarstedt tubes. Finally, 15 mL were filtered through a 0.2 µm GTTP-filter (Merck

Millipore), while using a 0.45 µm cellulose nitrate filter (Sartorius) as support filter. Filtrations were repeated 5 times to obtain in total 6 replicate filters (stored at -20°C). These samples were used for counting bacterial cell numbers by DAPI-staining and fluorescence in situ hybridization.

Annex I references:

Böer S, Arnosti C, van Beusekom J, Boetius A. (2008). Temporal variations in microbial activities and carbon turnover in subtidal sandy sediments. Biogeosciences 6(7): 1149–1165.

Böer SI, Hedtkamp SIC, van Beusekom JEE, Fuhrman JA, Boetius A, Ramette A. (2009). Time- and sediment depth-related variations in bacterial diversity and community structure in subtidal sands. ISME J 3: 780–791.

Boetius A, Scheibe S, Tselpides A, Thiel H, 1996. Microbial biomass and activities in deep-sea sediements of the Eastern Mediterranean: trenches are benthic hotspots. Deep-sea research I 43(9):1439-1460.

Boetius, A., and Lochte, K. (1994) Regulation of microbial enzymatic degradation of organic matter in deep-sea sediments. Mar. Ecol. Prog. Ser. 104: 299-307.

Cline J.D., (1969) Spectrophotometric determination of hydrogen sulfide in natural waters. Limnol. Oceanogr., 14(3), 1969, 454-458.

de Beer, D., Schramm, A., Santegoeds, C.M., and Kühl, M. (1997) A nitrite microsensor for profiling environmental biofilms. Appl. Environ. Microbiol. 63: 973-977.

Edmond J.M., (1970) High determination of titration alkalinity and total carbon dioxide content of seawater by potentiometric titration. Deep-Sea Res., 17, pp. 737–750.

Gobet A, Boer SI, Huse SM, van Beusekom JEE, Quince C, et al. (2012) Diversity and dynamics of rare and of resident bacterial populations in coastal sands. ISME J 6: 542–553

Grasshoff K., Ehrhardt M., Kremling K., 1983, Methods of seawater analysis, (2nd edn.) Verl. Chem., Weinheim, 419 pp.

Hall, P.O.J. and Aller, R.C. 1992, Rapid, small-volume, flow injection analysis for ΣCO2 and NH4+ in marine and freshwaters, Limnol. Oceanogr. 37 1113-1119.

Ishii K, Mußmann M, MacGregor BJ, Amann R (2004) An improved fluorescence in situ hybridization protocol for the identification of Bacteria and Archaea in marine sediment. FEMS Microbiol Ecol 50:203–212.

Jeroschewski, P., Steuckart, C., and Kühl, M. (1996) An amperometric microsensor for the determination of H2S in aquatic environments. Anal. Chem. 68: 4351-4357.

Revsbech, N.P., and Ward, D.M. (1983) Oxygen microelectrode that is insensitive to medium chemical composition: Use in an acid microbial mat dominated by Cyanidium caldarium. Appl. Environ. Microbiol. 45: 755-759.

Wentworth, C.K., 1922. A scale of grade class terms for clastic sediments. Journal of Geology 30 (5), 377–392.

Deliverable 4.1: Potential impact of CCS leakage on marine communities
WP4; lead beneficiary: Plymouth Marine Laboratory

Annex II: Dissolved oxygen, alkalinity, phosphate, nitrate+nitrite, ammonia, manganese (II) , iron (II), DIC, Ω_{Ar} and Ω_{Ca} pore water profiles, from the mesocosm formation water experiment (Section 3.5.2)

A) Control

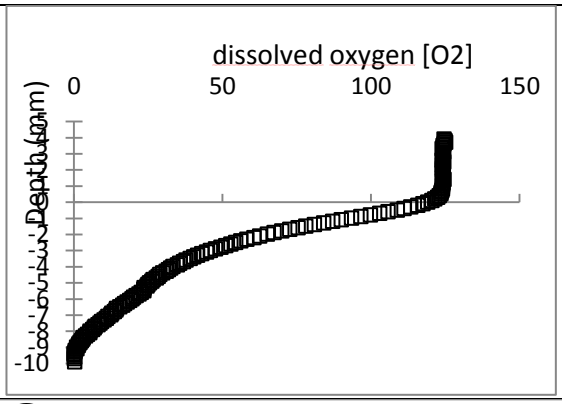

B) Hypersaline

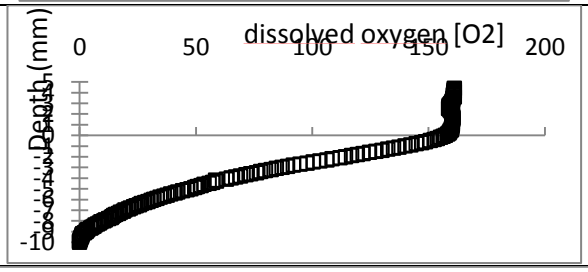

C) Mixed

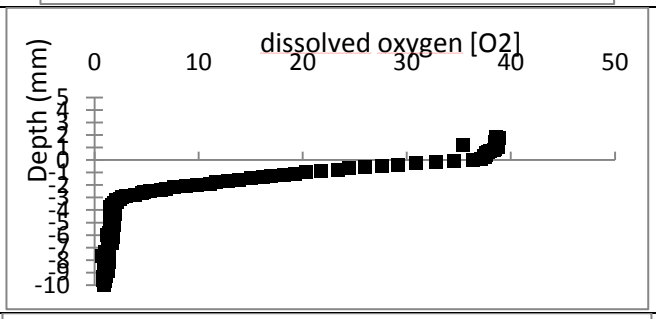

D) Hypoxic

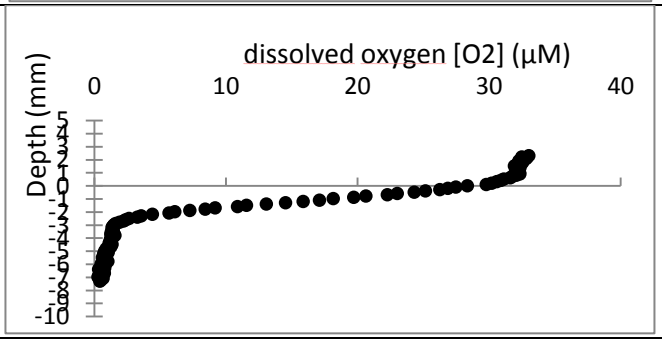

Deliverable 4.1: Potential impact of CCS leakage on marine communities
WP4; lead beneficiary: Plymouth Marine Laboratory

E) Tidal

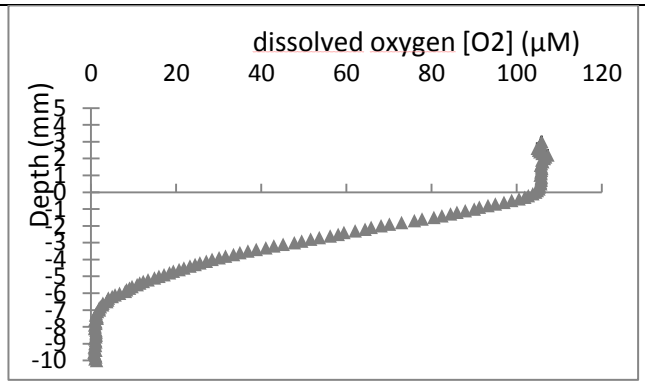

Figure A1: Oxygen profiles. Oxygen concentration in micromolar (µM) forsediment pore water in cores exposed in treatments waters for 1 week: control (A), hypersaline (B), hypoxic +hypersaline (C), hypoxic (D) and tidal (E) water. Sediment depth is given in mm.

A) Control

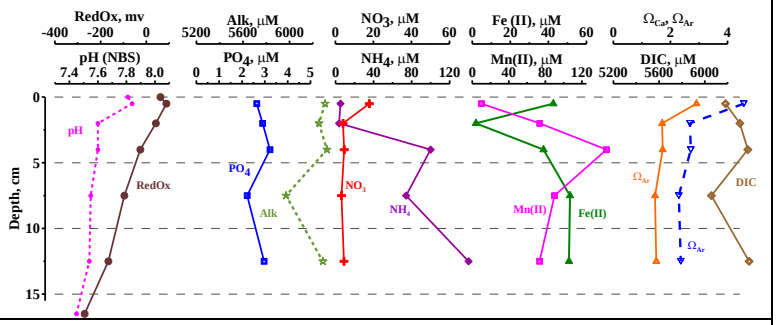

B) Hypersaline

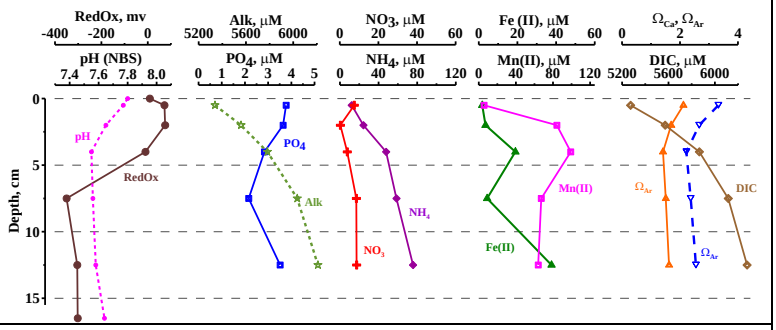

C) Mixed

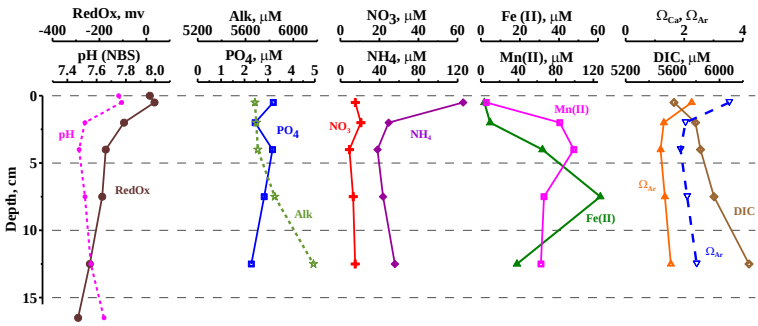

Deliverable 4.1: Potential impact of CCS leakage on marine communities
WP4; lead beneficiary: Plymouth Marine Laboratory

D) Hypoxic

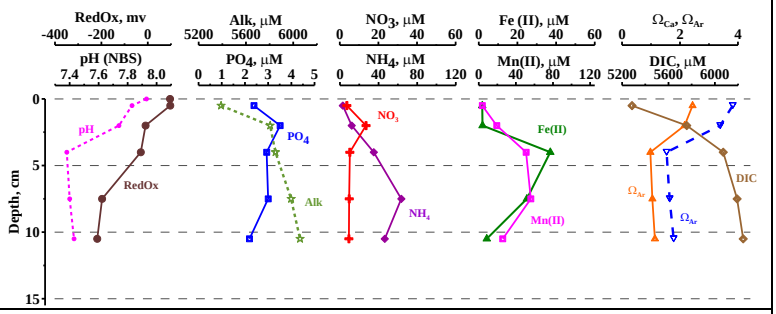

E) Tidal

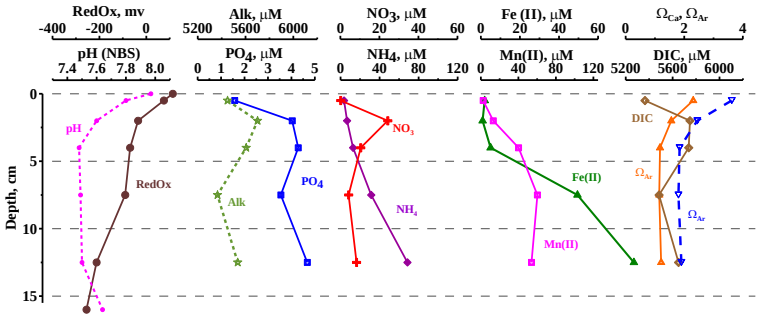

Figure A2: Vertical distributions of pH, redox potential, alkalinity, phosphate, nitrate+nitrite, ammonia, manganese (II) , iron (II), DIC, Ω_{Ar} and Ω_{Ca} in the sediment pore waters for control (A), hypersaline (B), hypoxic +hypersaline (C), hypoxic (D) and tidal (E) water. Sediment depth is given in cm.